UNIVERSITY OF AMSTERDAM

UvA-DARE (Digital Academic Repository)

Measurement of $t\bar{t}$ production in association with additional b-jets in the eμ final state in proton-proton collisions at √s = 13 TeV with the ATLAS detector

The ATLAS collaboration

DOI
10.1007/JHEP01(2025)068

Publication date
2025

Document Version
Final published version

Published in
Journal of High Energy Physics

License
CC BY

Link to publication

Citation for published version (APA):
The ATLAS collaboration (2025). Measurement of *tt̄* production in association with additional *b*-jets in the *eμ* final state in proton-proton collisions at √s = 13 TeV with the ATLAS detector. *Journal of High Energy Physics*, *2025*(1), Article 068. https://doi.org/10.1007/JHEP01(2025)068

General rights
It is not permitted to download or to forward/distribute the text or part of it without the consent of the author(s) and/or copyright holder(s), other than for strictly personal, individual use, unless the work is under an open content license (like Creative Commons).

Disclaimer/Complaints regulations
If you believe that digital publication of certain material infringes any of your rights or (privacy) interests, please let the Library know, stating your reasons. In case of a legitimate complaint, the Library will make the material inaccessible and/or remove it from the website. Please Ask the Library: https://uba.uva.nl/en/contact, or a letter to: Library of the University of Amsterdam, Secretariat, P.O. Box 19185, 1000 GD Amsterdam, The Netherlands. You will be contacted as soon as possible.

UvA-DARE is a service provided by the library of the University of Amsterdam (https://dare.uva.nl)

Download date:07 Sep 2026

Published for SISSA by Springer

Received: *July 19, 2024*
Accepted: *November 21, 2024*
Published: *January 14, 2025*

Measurement of $t\bar{t}$ production in association with additional b-jets in the $e\mu$ final state in proton–proton collisions at $\sqrt{s} = 13$ TeV with the ATLAS detector

The ATLAS collaboration

E-mail: atlas.publications@cern.ch

Abstract: This paper presents measurements of top-antitop quark pair ($t\bar{t}$) production in association with additional b-jets. The analysis utilises 140 fb^{-1} of proton–proton collision data collected with the ATLAS detector at the Large Hadron Collider at a centre-of-mass energy of 13 TeV. Fiducial cross-sections are extracted in a final state featuring one electron and one muon, with at least three or four b-jets. Results are presented at the particle level for both integrated cross-sections and normalised differential cross-sections, as functions of global event properties, jet kinematics, and b-jet pair properties. Observable quantities characterising b-jets originating from the top quark decay and additional b-jets are also measured at the particle level, after correcting for detector effects. The measured integrated fiducial cross-sections are consistent with $t\bar{t}b\bar{b}$ predictions from various next-to-leading-order matrix element calculations matched to a parton shower within the uncertainties of the predictions. State-of-the-art theoretical predictions are compared with the differential measurements; none of them simultaneously describes all observables. Differences between any two predictions are smaller than the measurement uncertainties for most observables.

Keywords: Hadron-Hadron Scattering, Top Physics

ArXiv ePrint: 2407.13473

Open Access, Copyright CERN,
for the benefit of the ATLAS Collaboration.
Article funded by SCOAP^3.

https://doi.org/10.1007/JHEP01(2025)068

JHEP01(2025)068

Contents

1 Introduction **2**

2 ATLAS detector **4**

3 Signal and background simulations **5**
- 3.1 $t\bar{t}$ samples 6
- 3.2 $t\bar{t}b\bar{b}$ samples 7
- 3.3 Background samples 8

4 Detector-level event reconstruction and selection **9**
- 4.1 Detector-level object reconstruction 9
- 4.2 Event selection 12

5 Definitions of fiducial phase space **12**
- 5.1 Particle-level object selections 12
- 5.2 Phase-space definitions 13

6 Observables **13**
- 6.1 Classification of b-jets 16

7 Background estimation **18**
- 7.1 Backgrounds with prompt leptons 19
- 7.2 Background with non-prompt or misidentified leptons 19

8 Extraction of fiducial cross-sections **20**
- 8.1 Data-driven correction factors for flavour composition of additional jets in $t\bar{t}$ events 21
- 8.2 Unfolding 28

9 Statistical and systematic uncertainties **29**
- 9.1 Statistical uncertainties 30
- 9.2 Experimental uncertainties 30
- 9.3 Signal modelling uncertainties 32
- 9.4 Background modelling uncertainties 33

10 Results **34**

11 Conclusion **39**

The ATLAS collaboration **58**

JHEP01(2025)068

1 Introduction

Measurements of the production cross-section of a top–antitop quark pair ($t\bar{t}$) with jets emanating from gluon radiation (additional jets) at the Large Hadron Collider (LHC) provide essential tests of the predictions of quantum chromodynamics (QCD). Among these, the process of $t\bar{t}$ events produced in association with jets originating from b-quarks (b-jets), as shown in figure 1, is of special interest, as it is difficult to predict due to the scale hierarchy between $t\bar{t}$ production and $b\bar{b}$ production from gluon emission and the non-negligible mass of the b-quark. There can be a single gluon emission in the initial or final state producing a pair of b-quarks as shown in figure 1(a) and figure 1(b), or multiple gluon emissions where at least one splits into a pair of b-quarks as shown in figure 1(c), or a b-quark participates in initiating the process leading to a $t\bar{t}$ in association with a final state b-quark as shown in figure 1(d).

Since the discovery of the Higgs boson [1, 2], the measurement of the Higgs boson coupling to the heaviest elementary particle, the top quark, has become an essential test of the Standard Model (SM). Direct measurements of the top quark Yukawa coupling are only possible in events where a Higgs boson is produced in association with one or two top quarks, tH or $t\bar{t}H$ [3, 4]. The production of $t\bar{t}H$ with a subsequent decay of $H \to b\bar{b}$ is shown in figure 2(a). While $H \to b\bar{b}$ has the largest Higgs boson branching fraction, its detection suffers from a large irreducible background from QCD $t\bar{t}$+b-jets production [5, 6]. Similarly, the production of $t\bar{t}Z$ with $Z \to b\bar{b}$ as shown in figure 2(b) faces significant challenges due to large backgrounds, making it crucial to enhance our understanding of QCD $t\bar{t}$+b-jets production. A better understanding of the QCD production of $t\bar{t}$+b-jets as predicted by the SM and improved Monte Carlo (MC) modelling would greatly benefit the $t\bar{t}H$ ($H \to b\bar{b}$) measurements and other analyses with similar final states.

MC simulations of the $t\bar{t}$+b-jets process differ in the treatment of the b-quark mass, the calculation of the b-quark production in the matrix element at next-to-leading order (NLO) or parton shower, and the merging of b-quark production into the inclusive $t\bar{t}$ prediction [7–15]. The predictions vary in the angular distribution of the produced jets, their transverse momenta (p_{T}), mass and energy, requiring a large number of observables to comprehensively probe the various aspects of the $t\bar{t}$+b-jets process. Comparing the predictions with both integrated and differential cross-section measurements of $t\bar{t}$ production with additional b-jets is crucial for improving the MC modelling. State-of-the-art QCD calculations give predictions for the $t\bar{t}$ production cross-section with up to two additional massless partons at NLO in perturbation theory matched to a parton shower algorithm [16]. QCD predictions of $t\bar{t}b\bar{b}$ are also calculated at NLO matched to a parton shower algorithm [13–15].

The ATLAS Collaboration has measured $t\bar{t}$+jets production with 7 TeV [17, 18], 8 TeV [19], and early 13 TeV data [20, 21], as well as $t\bar{t}$+b-jets with 7 TeV [22], 8 TeV [23], and partial 13 TeV data [24]. The data were found to be consistently higher than the MC predictions in the previous $t\bar{t}$+b-jets fiducial inclusive measurements, while the sensitivity of fiducial differential measurements to predictions suffered from a limited amount of data. The CMS Collaboration has also reported measurements of $t\bar{t}$+jets, $t\bar{t}$+b-jets and $t\bar{t}$+c-jets production using a similar amount of data collected at different centre-of-mass energies [25–29]. A new set of $t\bar{t}b\bar{b}$ measurements in the semileptonic $t\bar{t}$ decay channel was recently reported using the full 13 TeV data sample by the CMS Collaboration [30], where the data exceed the predictions from several MC configurations.

JHEP01(2025)068

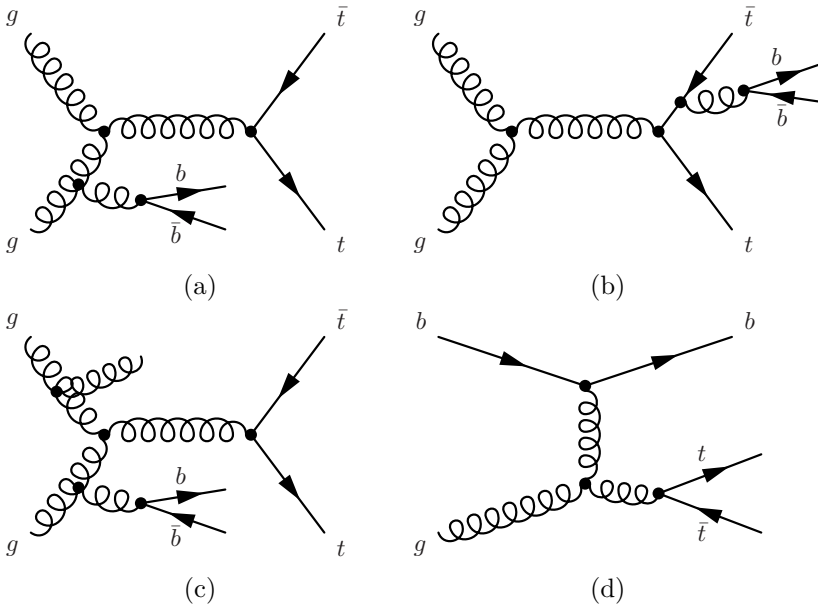

Figure 1. Example Feynman diagrams of QCD processes leading to a $t\bar{t}$+b-jets final state: (a) with additional b-quarks produced from initial-state gluon radiation, (b) with additional b-quarks produced from final-state gluon radiation, (c) the process with more than one gluon emission, where one of them produces a pair of b-quarks, and (d) the process initiated with a b-quark in the initial state.

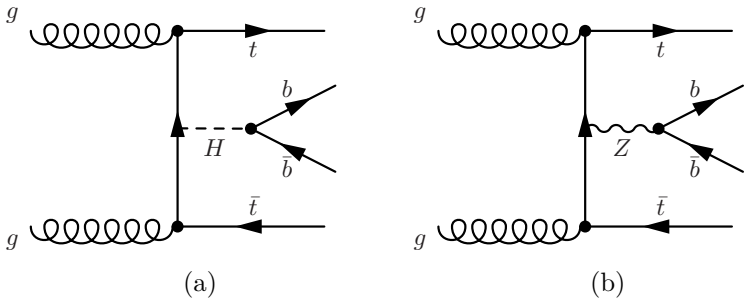

Figure 2. Example Feynman diagrams of electroweak processes leading to a $t\bar{t}$+b-jets final state, (a) the $t\bar{t}H$ ($H \to b\bar{b}$) process and (b) the $t\bar{t}Z$ ($Z \to b\bar{b}$) process.

In this paper, measurements of QCD $t\bar{t}$+b-jets fiducial cross-sections are presented using data recorded with the ATLAS detector during $2015-2018$ in proton–proton (pp) collisions at a centre-of-mass energy $\sqrt{s} = 13$ TeV, corresponding to an integrated luminosity of $140\,\text{fb}^{-1}$. Various fiducial regions are defined at the stable particle level with the criteria as close as possible to the detector-level event selections to minimise the MC modelling uncertainties due to extrapolation to the full phase space. Additionally, fiducial differential measurements are presented as a function of several observables. Since the top quark decays into a b-quark and W boson nearly 100% of the time, $t\bar{t}$ events are usually classified according to how the two W bosons decay. Only the $e\mu$ channel, in which both the W bosons decay leptonically, is considered. This includes events where one W boson decays into an electron and electron neutrino and the other into a muon and muon neutrino, as well as those where one or both

JHEP01(2025)068

W bosons produce a leptonically decaying τ-lepton. The dilepton channel has the advantage of having no contamination from jets coming from the hadronic decay of the W boson, as compared to the single-lepton or all-hadronic channels. Requiring one electron and one muon makes the background composition much simpler than other dilepton channels. The observables measured in $t\bar{t}$+b-jets events in the fiducial phase space include: b-jet multiplicity, p_{T} spectra of the leading four p_{T}-ordered b-jets, p_{T} spectra of the two b-jets originating from the top quark decay, p_{T} spectra of the two highest-p_{T} additional b-jets, dijet mass and angular distribution of the first two additional b-jets ordered in p_{T}. A variable characterising the $t\bar{t}$ invariant mass, i.e. the invariant mass of the electron, the muon, and the two b-jets presumably from the top quark decay, is also measured. The fiducial phase space definitions considered in these differential measurements extend those presented in the previous ATLAS results [24].

This paper is organised as follows. The ATLAS detector is described in section 2. The simulation of signal and background processes and the event reconstruction and selection are discussed in sections 3 and 4, respectively. The definition of the fiducial phase space is presented in section 5. A summary of all measured observables in each fiducial phase space region is detailed in section 6. The estimate of the background processes is summarised in section 7. The extraction of fiducial cross-sections is detailed in section 8. The sources of systematic uncertainties considered in the measurements are described in section 9. The results of the inclusive and differential cross-section measurements are presented in section 10. Finally, a summary of the results is given in section 11.

2 ATLAS detector

The ATLAS detector [31] at the LHC covers nearly the entire solid angle around the collision point.[1] It consists of an inner tracking detector surrounded by a thin superconducting solenoid, electromagnetic and hadronic calorimeters, and a muon spectrometer incorporating three large superconducting air-core toroidal magnets.

The inner-detector system (ID) is immersed in a 2 T axial magnetic field and provides charged-particle tracking in the range $|\eta| < 2.5$. The high-granularity silicon pixel detector covers the vertex region and typically provides four measurements per track, the first hit generally being in the insertable B-layer (IBL) installed before Run 2 [32, 33]. It is followed by the SemiConductor Tracker (SCT), which usually provides eight measurements per track. These silicon detectors are complemented by the transition radiation tracker (TRT), which enables radially extended track reconstruction up to $|\eta| = 2.0$. The TRT also provides electron identification information based on the fraction of hits (typically 30 in total) above a higher energy-deposit threshold corresponding to transition radiation.

The calorimeter system covers the pseudorapidity range $|\eta| < 4.9$. Within the region $|\eta| < 3.2$, electromagnetic calorimetry is provided by barrel and endcap high-granularity

[1] ATLAS uses a right-handed coordinate system with its origin at the nominal interaction point (IP) in the centre of the detector and the z-axis along the beam pipe. The x-axis points from the IP to the centre of the LHC ring, and the y-axis points upwards. Polar coordinates (r, ϕ) are used in the transverse plane, ϕ being the azimuthal angle around the z-axis. The pseudorapidity is defined in terms of the polar angle θ as $\eta = -\ln\tan(\theta/2)$ and is equal to the rapidity $y = \frac{1}{2}\ln\left(\frac{E+p_z c}{E-p_z c}\right)$ in the relativistic limit. Angular distance is measured in units of $\Delta R \equiv \sqrt{(\Delta y)^2 + (\Delta\phi)^2}$.

JHEP01(2025)068

lead/liquid-argon (LAr) calorimeters, with an additional thin LAr presampler covering $|\eta| < 1.8$ to correct for energy loss in material upstream of the calorimeters. Hadronic calorimetry is provided by the steel/scintillator-tile calorimeter, segmented into three barrel structures within $|\eta| < 1.7$, and two copper/LAr hadronic endcap calorimeters. The solid angle coverage is completed with forward copper/LAr and tungsten/LAr calorimeter modules optimised for electromagnetic and hadronic energy measurements respectively.

The muon spectrometer (MS) comprises separate trigger and high-precision tracking chambers measuring the deflection of muons in a magnetic field generated by the superconducting air-core toroidal magnets. The field integral of the toroids ranges between 2.0 and 6.0 T m across most of the detector. Three layers of precision chambers, each consisting of layers of monitored drift tubes, cover the region $|\eta| < 2.7$, complemented by cathode-strip chambers in the forward region, where the background is highest. The muon trigger system covers the range $|\eta| < 2.4$ with resistive-plate chambers in the barrel, and thin-gap chambers in the endcap regions.

The luminosity is measured mainly by the LUCID-2 [34] detector that records Cherenkov light produced in the quartz windows of photomultipliers located close to the beampipe.

Events are selected by the first-level trigger system implemented in custom hardware, followed by selections made by algorithms implemented in software in the high-level trigger [35]. The first-level trigger accepts events from the 40 MHz bunch crossings at a rate below 100 kHz, which the high-level trigger further reduces in order to record complete events to disk at about 1 kHz.

A software suite [36] is used in data simulation, in the reconstruction and analysis of real and simulated data, in detector operations, and in the trigger and data acquisition systems of the experiment.

3 Signal and background simulations

Simulated events were produced using various MC algorithms to estimate contributions from $t\bar{t}b\bar{b}$ signal and background processes, determine detector resolution and acceptance correction factors, and evaluate systematic uncertainties. Additionally, comparisons between unfolded data and theoretical predictions were facilitated using MC generators. All samples were normalised based on the best available theory predictions as indicated in the text below.

The response of the ATLAS detector and trigger were simulated based on the detailed model implemented in the GEANT4 program [37, 38] or, for the estimation of some of the systematic uncertainties, using a faster approach employing parameterised showers in the calorimeter [39]. The effect of multiple pp interactions in each bunch crossing (pile-up) was modelled by overlaying each hard-scattering event with inelastic pp collisions generated using Pythia 8.186 [40] with the `NNPDF2.3LO` set of parton distribution functions (PDFs) [41] and the A3 set of tuned parameters [42]. For all samples of simulated events, except those generated using Sherpa, the EvtGen program [43] was used to model the decays of bottom and charm hadrons. The top quark mass m_{top} was set to 172.5 GeV and the Higgs boson mass was set to 125 GeV. Simulated events were reconstructed and analysed using the same software as the data.

JHEP01(2025)068

3.1 $t\bar{t}$ samples

The $t\bar{t}$ event production was simulated using the PowhegBox v2 heavy-quark (hvq) [7–10] event generator, employing matrix elements calculated at NLO precision in QCD with the `NNPDF3.0NLO` [44] PDF set in the five-flavour scheme (5FS). These events were then interfaced to Pythia 8.230 [45] to simulate the processes for parton showering, hadronisation and the underlying event. Top quark decays, including spin correlations, were modelled at leading-order (LO) precision in QCD. To regulate the p_{T} of the first additional emission beyond the Born configuration, the h_{damp} parameter was set to $1.5m_{\mathrm{top}}$ [46]. Additionally, the renormalisation and factorisation scales defined for the Born process were set to the default scale $\sqrt{m_{\mathrm{top}}^2 + p_{\mathrm{T,top}}^2}$, derived from the top quark mass, m_{top}, and the transverse momentum of the top quark before radiation, $p_{\mathrm{T,top}}$. The $p_{\mathrm{T}}^{\mathrm{hard}}$ parameter [47], which determines the region of phase space vetoed during showering when matched to a parton shower, was set to zero by default. This sample used a recoil scheme where partons recoil against a b-quark. This recoil scheme changes the modelling of second and subsequent gluon emissions from the b-quark produced by the top quark decay, and therefore affects how the momentum is rearranged between the W boson and the b-quark. This sample is referred to as Powheg+Pythia 8. All samples using Pythia 8 for the modelling of parton showering, hadronisation and underlying event used the A14 set of tuned parameters [48] and the `NNPDF2.3LO` set of PDFs. All $t\bar{t}$ samples were normalised to the cross-section prediction at next-to-next-to-leading order (NNLO) in QCD including the resummation of next-to-next-to-leading logarithmic (NNLL) soft-gluon terms calculated using Top++ 2.0 [49–55]. In pp collisions at a centre-of-mass energy of $\sqrt{s} = 13\,\mathrm{TeV}$, this cross-section corresponds to $\sigma(t\bar{t})_{\mathrm{NNLO+NNLL}} = 832 \pm 51\,pb$ using a top quark mass of $m_{\mathrm{top}} = 172.5\,\mathrm{GeV}$. The uncertainties in the cross-section due to the PDF and the strong coupling constant α_{s} were calculated using the PDF4LHC15 prescription [56] with the `MSTW2008NNLO` [57, 58], `CT10NNLO` [59, 60] and `NNPDF3.0NNLO` PDF sets in the 5FS, and were added in quadrature to the scale uncertainty.

Various alternative $t\bar{t}$ samples were generated to assess the uncertainties arising from QCD MC model choices and to compare with unfolded data. Uncertainties due to initial- and final-state radiation were assessed by using event weights to vary the QCD renormalisation and factorisation scales in the matrix element independently by factors of 2.0 and 0.5 from their default values, using the `Var3c` variation of the A14 tune, and by changing the renormalisation and factorisation scales used in the parton shower by factors of 2.0 and 0.625. A higher scaling factor than 0.5 was used for the downward variation to keep the variations of the kinematic variables in the upward and downward directions symmetrical.

Another sample was generated mirroring the nominal $t\bar{t}$ settings, but with the h_{damp} parameter set to $3m_{\mathrm{top}}$, enabling the assessment of the impact of variations in the first QCD emission scale. This sample is referred to as Powheg+Pythia 8 h_{damp}. Furthermore, the uncertainty in the matrix element and parton shower matching is evaluated by utilising an alternative Powheg+Pythia 8 sample. The $p_{\mathrm{T}}^{\mathrm{hard}}$ parameter of Pythia 8 was set to 1 instead of the default value of 0, altering the overlap in the phase space filled by Powheg and Pythia 8. The sample is referred to as Powheg+Pythia 8 $p_{\mathrm{T}}^{\mathrm{hard}}$.

Another sample was generated with identical settings to the nominal $t\bar{t}$ sample, except for a modified recoil scheme. Here, the default gluon recoil, typically recoiling against the b-quark,

JHEP01(2025)068

was replaced by the top quark itself serving as the recoil for the second and subsequent gluon emissions from the b-quark. This sample is referred to as Powheg+Pythia 8 RecoilToTop. A Powheg+Pythia 8 sample, with the same settings as the nominal but replacing the recoil scheme of the initial-state emission by an alternative scheme, was used only for comparison with the measurement. In the alternative scheme, only one final state parton takes the recoil of an emission in contrast to the global recoil. This sample is referred to as Powheg+Pythia 8 dipole.

Additionally, further $t\bar{t}$ samples were generated by replacing Pythia 8 with Herwig 7.1.3 [61] to model the parton showering, hadronisation and underlying event, and are used to evaluate uncertainties. This alternative approach used the Herwig 7.1 default set of tuned parameters [61] and the `MMHT2014LO` [62] PDF set.

Further predictions were computed for comparison with data, including alternative NLO samples of $t\bar{t}$ events produced with MadGraph5_aMC@NLO v2.6.0 [12] interfaced to either Pythia 8.230 or Herwig 7.1.3. These samples are referred to as MadGraph5_aMC@NLO+Pythia 8 and MadGraph5_aMC@NLO+Herwig 7, respectively. Additionally, samples were generated using the Sherpa 2.2.12 generator [11] and OpenLoops [63, 64] using NLO accurate matrix elements for up to one additional parton and LO accurate matrix elements for up to four additional partons. The additional parton emissions were matched and merged with the Sherpa parton shower based on Catani-Seymour dipole factorisation [65, 66] using the MePs@Nlo prescription [67, 68]. Samples were generated using the `NNPDF3.0NNLO` PDF set, along with a dedicated set of tuned parton shower parameters developed by the Sherpa authors. Additional b-quarks were treated as massless. The Sherpa samples include approximate NLO $\mathrm{EW}_{\mathrm{virtual}}$ corrections [69–71]. The scale used for the multijet merging was set to 30 GeV. This sample is referred to as Sherpa $t\bar{t}$. These samples are summarised in table 1.

3.2 $t\bar{t}b\bar{b}$ samples

Dedicated samples focusing on $t\bar{t}b\bar{b}$ events were produced to capture additional b-quarks calculated by the matrix element, ensuring NLO QCD accuracy in the four-flavour scheme (4FS), and interfaced to Pythia 8.230. Using the Powheg Box Res [13] generator alongside OpenLoops, and the four-flavour `NNPDF3.0NLO NF4` [44] PDF set, this set-up incorporated a specialised implementation to take the scale hierarchy into account [13, 72]. This includes setting the factorisation scale to $\frac{1}{2}\Sigma_{i=t,\bar{t},b,\bar{b},j} m_{\mathrm{T},i}$ (where j stands for extra partons), and the renormalisation scale to $\sqrt[4]{\prod_{i=t,\bar{t},b,\bar{b}} m_{\mathrm{T},i}}$, where $m_{\mathrm{T},i} = \sqrt{m_i^2 + p_{\mathrm{T},i}^2}$ is the transverse mass of a given parton. The h_{damp} parameter was set to $\frac{1}{2}\Sigma_{i=t,\bar{t},b,\bar{b}} m_{\mathrm{T},i}$, and the $p_{\mathrm{T}}^{\mathrm{hard}}$ parameter was set to zero. The global recoil scheme, as implemented by default in Pythia 8, was used such that the recoil of the initial-state emission is taken by the whole final state. The parameter h_{bzd} that controls the enhancement in the Born cross-section due to soft and collinear NLO radiative contributions from light jets [13] was set to 5, and the Powheg Box Res hardness criterion (`POWHEG:pTdef`) used in the matching was set to 1 following studies reported in ref. [73]. This sample is referred to as Powheg+Pythia 8 $t\bar{t}b\bar{b}$. Further variations were explored through three additional $t\bar{t}b\bar{b}$ samples. One sample had h_{bzd} set to 2, the second sample had $p_{\mathrm{T}}^{\mathrm{hard}}$ set to 1, and the third sample used a different scheme for the recoil of the initial-state

JHEP01(2025)068

emission such that only one final-state parton took the recoil of an emission and had h_{bzd} set to 2, all other settings were the same as the nominal POWHEG+PYTHIA 8 $t\bar{t}b\bar{b}$ sample. These three samples are referred to as POWHEG+PYTHIA 8 $t\bar{t}b\bar{b}$ h_{bzd}, POWHEG+PYTHIA 8 $t\bar{t}b\bar{b}$ $p_{\text{T}}^{\text{hard}}$, and POWHEG+PYTHIA 8 $t\bar{t}b\bar{b}$ dipole, respectively.

An additional $t\bar{t}b\bar{b}$ (4FS) sample was generated, preserving the POWHEG BOX RES generator settings while substituting PYTHIA 8 with HERWIG 7.1.6. This sample, referred to as POWHEG+HERWIG 7 $t\bar{t}b\bar{b}$, used the HERWIG 7.1 set of tuned parameters and the `MMHT2014LO` PDF set.

Furthermore, a dedicated sample of $t\bar{t}b\bar{b}$ events was generated using SHERPA 2.2.10 in conjunction with OPENLOOPS. Matrix element calculations, performed at NLO accuracy using the COMIX [65] and OPENLOOPS generators, were merged with the SHERPA parton shower [66]. The renormalisation scale was set to $\sqrt[4]{\prod_{i=t,\bar{t},b,\bar{b}} m_{\text{T},i}}$. The factorisation and resummation scales were both set to $\frac{1}{2}\Sigma_{i=t,\bar{t},b,\bar{b},j} m_{\text{T},i}$ where j refers to extra partons. The `NNPDF3.0NNLO NF4` PDF set was used. This sample is referred to as SHERPA $t\bar{t}b\bar{b}$. In all $t\bar{t}b\bar{b}$ (4FS) samples, the mass of the b-quark was set to 4.75 GeV in the matrix element. The MC yields of all $t\bar{t}b\bar{b}$ samples were normalised to the cross-sections computed by the corresponding matrix element generators.

Additionally, the results featuring at least four b-jets were compared to the NLO computation of the $pp \to e\nu_e\mu\nu_\mu b\bar{b}b\bar{b}$ process, encompassing resonant and non-resonant top quark contributions, and all interference effects among them, along with the non-resonant and off-shell effects of the W boson. These calculations were performed using the HELAC-NLO framework [74] by the authors of refs. [75] and [76]. The renormalisation and factorisation scales were set to $\mu_{\text{R}} = \mu_{\text{F}} = \mu_0 = H_{\text{T}}/3$, and employed the `NNPDF3.1NLO` [77] PDF sets. Here, H_{T} represents the scalar sum of the p_{T} of all four b-jets, electron, muon, and the missing transverse momentum from the two neutrinos. The predictions were corrected to account for the effects of non-perturbative contributions such as multiple parton interactions and hadronisation, and the leptonic decays of at least one τ-lepton in the dileptonic $t\bar{t}$ channel yielding the prompt $e\mu$ final state. The POWHEG+PYTHIA8 $t\bar{t}b\bar{b}$ MC samples, as discussed above, were used to derive the corrections. These predictions are denoted by HELAC-NLO (off-shell) $e\mu + 4b$ and are summarised in table 1.

3.3 Background samples

Single-top-quark production processes, namely tW associated production, t-channel, and s-channel production, were simulated using the POWHEG BOX v2 [8–10, 78–80] generator at NLO in QCD interfaced to PYTHIA 8 for the parton showering, hadronisation and the underlying event, using the A14 set of tuned parameters and the `NNPDF2.3LO` set of PDFs. The t-channel process was generated in the 4FS with the `NNPDF3.0NLO NF4` [44] PDF set, while the 5FS was used for tW and s-channel processes. To handle the interference between tW and $t\bar{t}$ production, the diagram removal scheme [81] was employed. An alternative tW sample was generated with the same settings as the nominal one except that the diagram subtraction scheme [81] was used to evaluate the uncertainty due to the treatment of the interference with $t\bar{t}$ production. Additionally, one sample was simulated for tW using the same set-up as the nominal one, but replacing PYTHIA 8 with HERWIG 7.0.4, and another sample

JHEP01(2025)068

was generated at NLO in QCD with MadGraph5_aMC@NLO interfaced to Pythia 8. The single-top MC samples for the t- and s-channels were normalised to cross-sections from NLO predictions [82, 83], while the tW-channel MC sample was normalised to NLO+NNLL [84].

The production of $t\bar{t}H$ events was simulated using the Powheg Box generator at NLO in QCD with the h_{damp} parameter set to $0.75 \times (2m_{\text{top}} + m_H)$, and interfaced to Pythia 8. All possible SM decay modes of the Higgs boson were included and simulated using Pythia 8. Alternative $t\bar{t}H$ samples were generated using Powheg Box with the same settings as the nominal ones, but replacing the parton shower model with Herwig 7. Another sample was generated with MadGraph5_aMC@NLO and interfaced to Pythia 8.

Events for $t\bar{t}Z$, $t\bar{t}W$, tWZ, tWH, $tHbj$, tZ and $t\bar{t}t\bar{t}$ were generated with MadGraph5_aMC@NLO at NLO in QCD. The $t\bar{t}Z$ and $t\bar{t}W$ background processes are collectively labelled as $t\bar{t}V$. The MC yields were normalised to the corresponding cross-sections from the MadGraph5_aMC@NLO computation.

All of these nominal background events generated using Powheg Box or MadGraph5_aMC@NLO, as mentioned above, were interfaced to Pythia 8.230 [45] for the parton showering, hadronisation and the underlying event, using the A14 set of tuned parameters and the `NNPDF2.3LO` set of PDFs.

For V+jets events (where $V = W$ or Z), simulation was carried out using the Sherpa 2.2.1 generator [11] with NLO-accurate matrix elements for up to two partons and LO-accurate matrix elements for up to four partons. The MC yields were normalised to the NNLO cross-sections, computed using Fewz [85] with the `MSTW2008NNLO` PDF set. Additionally, samples of diboson final states were simulated using the Sherpa 2.2.2 generator [11] at NLO in QCD for up to one additional parton and at LO accuracy for up to three additional partons. The samples were normalised according to the cross-sections computed by the generator.

4 Detector-level event reconstruction and selection

4.1 Detector-level object reconstruction

Interaction vertices resulting from pp collisions are reconstructed based on a minimum of two tracks with $p_{\text{T}} > 500$ MeV, demonstrating consistency with originating from the beam collision region in the x–y plane. Of all primary vertex candidates, the one associated with the highest sum of squared p_{T} of its associated tracks is designated as the hard-scatter primary vertex [86].

Electron candidates are reconstructed by using energy clusters in the EM calorimeter, which are then matched to a track in the ID [87]. These candidates must satisfy $p_{\text{T}} > 25$ GeV and pseudorapidity $|\eta_{\text{cluster}}| < 2.47$, excluding the transition region between the endcap and barrel calorimeters ($1.37 < |\eta_{\text{cluster}}| < 1.52$). The selection criteria use tight electron identification working point, characterised by a likelihood discriminant utilising calorimeter, tracking, and combined variables to effectively discriminate between electrons and jets [87].

Muon candidates are reconstructed by combining tracks in the ID with tracks in the MS [88]. The resulting muon candidates undergo a refitting process using comprehensive track information from both detector systems. Selection criteria ensure that these candidates have $p_{\text{T}} > 25$ GeV and $|\eta| < 2.5$ and satisfy the medium muon identification working point (*Medium*) [88].

JHEP01(2025)068

MC sample	Generator	Process	Flavour Scheme (4FS/5FS)	Parton shower	Matching/ Parton shower settings	Tune	Use
Powheg+Pythia8	Powheg Box v2	$t\bar{t}$ NLO	5FS	Pythia 8.230	Powheg h_{damp} =1.5m_{top} $p_{\text{T}}^{\text{hard}}=0$ `globalRecoil` `recoilToColoured`=ON	A14	nom.
Powheg+Pythia8 h_{damp}	Powheg Box v2	$t\bar{t}$ NLO	5FS	Pythia 8.230	Powheg h_{damp} =3m_{top}	A14	syst.
Powheg+Pythia8 $p_{\text{T}}^{\text{hard}}$	Powheg Box v2	$t\bar{t}$ NLO	5FS	Pythia 8.230	Powheg $p_{\text{T}}^{\text{hard}}=1$	A14	syst.
Powheg+Pythia8 RecoilToTop	Powheg Box v2	$t\bar{t}$ NLO	5FS	Pythia 8.230	Powheg `recoilToTop`	A14	syst.
Powheg+Herwig 7	Powheg Box v2	$t\bar{t}$ NLO	5FS	Herwig 7.1.3	Powheg	H7.1-Default	syst.
Powheg+Pythia8 dipole	Powheg Box v2	$t\bar{t}$ NLO	5FS	Pythia 8.230	Powheg `dipoleRecoil` on	A14	comp.
MadGraph5_aMC@NLO+Pythia 8	MadGraph5_ aMC@NLO v2.6.0	$t\bar{t}$ NLO	5FS	Pythia 8.230	MC@NLO	A14	comp.
MadGraph5_aMC@NLO+Herwig 7	MadGraph5_ aMC@NLO v2.6.0	$t\bar{t}$ NLO	5FS	Herwig 7.1.3	MC@NLO	H7.1-Default	comp.
Sherpa	Sherpa 2.2.12	$t\bar{t}$ +0,1 @NLO +2,3,4 @LO	5FS	Sherpa	MEPs@NLO	Author's tune	comp.
Powheg+Pythia8 $t\bar{t}b\bar{b}$	Powheg Box Res	$t\bar{t}b\bar{b}$ NLO	4FS	Pythia 8.230	Powheg Box Res h_{bzd}=5 $p_{\text{T}}^{\text{hard}}=0$ `globalRecoil`	A14	comp.
Powheg+Pythia8 $t\bar{t}b\bar{b}$ $p_{\text{T}}^{\text{hard}}$	Powheg Box Res	$t\bar{t}b\bar{b}$ NLO	4FS	Pythia 8.230	Powheg Box Res $p_{\text{T}}^{\text{hard}}=1$	A14	comp.
Powheg+Pythia8 $t\bar{t}b\bar{b}$ h_{bzd}	Powheg Box Res	$t\bar{t}b\bar{b}$ NLO	4FS	Pythia 8.230	Powheg Box Res h_{bzd}=2	A14	comp.
Powheg+Pythia8 $t\bar{t}b\bar{b}$ dipole	Powheg Box Res	$t\bar{t}b\bar{b}$ NLO	4FS	Pythia 8.230	Powheg Box Res h_{bzd}=2 `dipoleRecoil` on	A14	comp.
Powheg+Herwig 7 $t\bar{t}b\bar{b}$	Powheg Box Res	$t\bar{t}b\bar{b}$ NLO	4FS	Herwig 7.1.6	Powheg Box Res	H7.1-Default	comp.
Sherpa $t\bar{t}b\bar{b}$	Sherpa 2.2.10	$t\bar{t}b\bar{b}$ NLO	4FS	Sherpa	MEPs@NLO	Author's tune	comp.
Helac-NLO (off-shell)	Helac-NLO	$e\mu+4b$ NLO	5FS		–	–	comp.

Table 1. Summary of the MC sample set-ups for modelling the signal processes for the data analysis and for comparison with the measured cross-sections and differential distributions. The different blocks indicate, from top to bottom, the samples used as the nominal MC (nom.), systematic variations (syst.) and for comparison only (comp.). Dashes (–) imply that the corresponding settings are not applicable for the fixed-ordered calculations. The $t\bar{t}b\bar{b}$ simulations are performed in the four-flavour scheme (4FS), where the b-quark is treated as a massive particle in the matrix element. Other simulations employ the five-flavor scheme (5FS), where the b-quark is treated as massless within the matrix element. However, all parton shower models consider the b- and c-quarks to be massive. For details see section 3.

The association of electron (muon) candidate tracks with the primary vertex is achieved by requiring that the significance of their transverse impact parameter, d_0, satisfies $|d_0/\sigma(d_0)| < 5$ (3), where $\sigma(d_0)$ denotes the measured uncertainty in d_0. Furthermore, the longitudinal impact parameter is required to satisfy $|z_0 \sin\theta| < 0.5$ mm.

To mitigate the presence of non-prompt leptons and jets misidentified as leptons, stringent isolation criteria are imposed on lepton candidates in both the tracker and calorimeter. For track-based lepton isolation, the quantity $I_R = \sum p_{\text{T}}^{\text{trk}}$ is computed, summing the transverse momenta of all tracks (excluding the lepton candidate itself) within a cone of size R_{cut} around the lepton's direction. Here, R_{cut} is set to the minimum of r_{min} and 10 GeV/p_{T}^{ℓ}, with r_{min} taking the values 0.2 (0.3) for electron (muon) candidates, and p_{T}^{ℓ} representing the lepton's transverse momentum. The electron selection uses p_{T} and η-dependent thresholds on the I_R/p_{T}^{ℓ} ratio, while all muon candidates must satisfy $I_R/p_{\text{T}}^{\ell} < 0.15$.

JHEP01(2025)068

Moreover, both electrons and muons must satisfy a calorimeter-based isolation requirement that calculates the sum of transverse energy within a cone of $R_{\text{cut}} = 0.2$ around the lepton, after subtracting contributions from pile-up and the lepton's own energy deposition. This sum is required to be below 30% of the muon's transverse momentum, while electron candidates are subject to p_{T} and η-dependent thresholds for this quantity.

Reconstruction, identification and isolation efficiencies of electrons (muons) are corrected to match those observed in data using $Z \to e^+e^-(\mu^+\mu^-)$ events, while the position and width of the observed Z peak is used to calibrate the electron (muon) energy (momentum) scale and resolution [87–89].

Jet reconstruction relies on identifying constituents through a particle flow (PFlow) algorithm that combines measurements from both the ID and the calorimeter [90]. Subsequently, jet candidates are formed from these PFlow objects using the anti-k_t algorithm with a radius parameter of $R = 0.4$ [91, 92]. These candidates undergo calibration using simulation, with corrections derived from in situ techniques applied to data [93]. Only jet candidates with $p_{\text{T}} > 25$ GeV and $|\eta| < 2.5$ are retained. To mitigate pile-up effects, jets with $p_{\text{T}} < 60$ GeV and $|\eta| < 2.4$ are required to satisfy the '*Tight*' working point of the jet vertex tagger (JVT) criteria, ensuring an efficiency of 95%–97% depending on the jet p_{T}, which identifies jets as originating from the selected primary vertex [94]. Additionally, a set of quality criteria is applied to discard events containing jets originating from non-collision sources or detector noise [95].

Jets likely to contain b-hadrons, i.e. weakly decaying hadrons composed of a b-quark, are identified as b-jets using the DL1r algorithm [96], which employs a deep neural network. These identified jets are known as b-tagged jets. The network utilises distinctive features of b-hadrons, such as the impact parameters of tracks and the displaced vertices reconstructed in the ID. Additionally, discriminating variables constructed by a recurrent neural network are included as input, exploiting spatial and kinematic correlations between tracks originating from the same b-hadron. For each jet, a multivariate b-tagging discriminant is computed, and the jet is considered b-tagged if this value exceeds a predefined threshold.

The baseline working point, chosen to define signal regions, corresponds to an approximate 77% tagging efficiency for b-jets in simulated $t\bar{t}$ events. However, the b-tagging efficiency varies with p_{T} and η and is measured using collision data [97] with uncertainties ranging from 1% to 8% depending on the jet p_{T}. The tagging algorithm achieves a rejection factor of about 170 against light-flavoured jets (u-, d-, s-quark, or gluon) and approximately 5 against jets originating from c-quarks. The selected working point is optimised to maximise the signal-to-background ratio, while keeping the number of signal events high.

Ambiguities between selected leptons and jets are resolved using an overlap removal procedure. If a muon shares a track with an electron, indicating possible bremsstrahlung, the electron is not selected. To avoid double-counting electron energy deposits as jets, the closest jet within $\Delta R = 0.2$ of a selected electron is removed. Subsequently, if the nearest surviving jet is within $\Delta R = 0.4$ of the electron, the electron is discarded to reduce non-prompt background contributions. Muons are removed if they are within $\Delta R = 0.4$ of the nearest jet, which helps mitigate background from heavy-flavour decays inside jets. However, if this jet is associated with fewer than three tracks, the muon is retained, and the jet is removed

JHEP01(2025)068

instead. This approach prevents inefficiencies caused by high-energy muons experiencing significant energy loss in the calorimeter.

The missing transverse energy (denoted by $E_{\mathrm{T}}^{\mathrm{miss}}$) is defined as the magnitude of the negative vector sum of the p_{T} of all selected and calibrated objects in the event. This includes a term to accommodate the momentum from soft particles in the event that are not associated with any of the selected objects [98]. The soft term is computed from ID tracks matched to the selected primary vertex, enhancing its resilience to contamination from pile-up interactions.

4.2 Event selection

A data sample of pp collisions at a centre-of-mass energy of $\sqrt{s} = 13$ TeV, collected with the ATLAS detector during the period of 2015–2018, is used in this analysis. This data sample corresponds to an integrated luminosity of $140\,\mathrm{fb}^{-1}$ [99]. Events were only recorded under stable beam conditions and when all components of the ATLAS detector were confirmed to be fully functioning.

The data were collected using a combination of single-electron and single-muon triggers, with requirements on the identification, isolation, and p_{T} of the leptons to maintain high efficiency across the full momentum range while controlling the trigger rates [100, 101]. For electrons the trigger thresholds were $p_{\mathrm{T}} = 26$, 60 and 140 GeV, whereas for muons the thresholds were $p_{\mathrm{T}} = 26$ and 50 GeV.[2] Isolation requirements were applied to the triggers with the lowest p_{T} thresholds of 26 GeV for both electrons and muons [102–105].

To ensure events originate from the hard-scattering process, they are required to contain at least one primary vertex candidate. A sample enriched in $t\bar{t}$ events is pre-selected by requiring events to contain exactly one electron and one muon with a minimum p_{T} of 28 GeV, along with at least two jets tagged as containing b-hadrons using the DL1r b-tagging algorithm at the 77% efficiency working point. The selected leptons are required to have opposite charges and to match the corresponding lepton reconstructed by the single-lepton trigger, with a p_{T} exceeding the trigger p_{T} threshold by up to 2 GeV to ensure they remain at the trigger efficiency plateau. Additionally, the invariant mass of the electron and muon pair is required to be larger than 15 GeV to remove contributions from low-mass $\tau\tau$ Drell-Yan processes with only minimal signal efficiency loss. The $t\bar{t}$+b-jets signal events are selected by requiring at least three b-tagged jets at the 77% efficiency working point.

5 Definitions of fiducial phase space

5.1 Particle-level object selections

Particle-level objects are selected in simulated events using definitions that mirror closely the detector-level objects outlined in section 4.1. These particle-level objects are defined based on stable particles with proper lifetimes greater than 30 ps.

Only prompt electrons and muons that are produced directly from the primary vertex, including those from τ-lepton decays, are considered. To account for final-state photon radiation, the four-momentum of each lepton is adjusted by adding the four-momenta of all

[2] Lower p_{T} thresholds of 24 GeV and 120 GeV for electrons and 20 GeV for muons were applied for 2015 data.

JHEP01(2025)068

photons, not emanating from hadrons, within a $\Delta R = 0.1$ cone around the lepton. Electrons and muons are required to have $p_{\mathrm{T}} > 25$ GeV and $|\eta| < 2.5$.

Jet clustering is performed using the anti-k_t algorithm with a radius parameter of $R = 0.4$. All stable particles are considered for jet clustering except for prompt electrons and muons, along with the associated photons. Neutrinos from W boson decays (prompt neutrinos) are excluded from jet clustering, but neutrinos from hadron decays are included. These jets exclude particles from pile-up events but incorporate those from the underlying event. The decay products of hadronically decaying τ-leptons are included in the jet clustering. Jets are required to have $p_{\mathrm{T}} > 25$ GeV and $|\eta| < 2.5$.

Jets are defined as b-jets, if at least one b-hadron with $p_{\mathrm{T}} > 5$ GeV is associated with the jet via ghost association [106]. In this ghost-association procedure, b-hadrons are included in the jet clustering while their p_{T} is scaled to a negligible value. A similar approach is adopted to define c-jets, with the b-jet definition taking precedence. In other words, a jet containing both a b-hadron and a c-hadron is classified as a b-jet. Jets lacking both b-hadrons and c-hadrons are categorised as light-flavour jets.

Electrons and muons, satisfying the selection criteria outlined above, must have a separation from selected jets of $\Delta R(\text{lepton}, \text{jet}) > 0.4$. This criterion ensures consistency with the detector-level selection described in section 4.1.

5.2 Phase-space definitions

The fiducial phase spaces are defined using particle-level objects with kinematic requirements similar to those applied to the reconstructed objects in the event selections. Fiducial integrated cross-sections and fiducial normalised differential cross-sections are determined by requiring the presence of exactly one electron and one muon, each with $p_{\mathrm{T}} \geq 28$ GeV and opposite charges at the particle level, and with two different criteria for the minimum number of b-jets with $p_{\mathrm{T}} > 25$ GeV. Detailed kinematic requirements can be found in section 5.1. One set of measurements are performed in the particle-level phase space with three or more b-jets accounting for at least one b-jet in addition to the two from the top quark decays, and another set with the requirement of four or more b-jets accounting for at least two additional b-jets. The normalised fiducial differential cross-sections as a function of b-jets multiplicity are measured with two different criteria for the minimum number of b-jets: (i) at least two b-jets, and (ii) at least three b-jets. A few percent of events may contain at least one b-jet from a different parton interaction than the one producing the $t\bar{t}$ pair (referred to as 'multiple parton interactions'), with reduced contribution as the b-jet multiplicity requirement increases. Such b-jets are included in the particle-level event selection.

6 Observables

The normalised differential distributions of various physics quantities are measured in the fiducial phase space as outlined in table 2. These distributions fall into two categories of particle-level observables closely corresponding to their detector-level counterparts. In the first category, b-jets are ordered by p_{T}, while in the second category, b-jets are classified as originating from the top quark decay or additional partons using an algorithm based on the angular distances as described in section 6.1. For each category, the observables are

JHEP01(2025)068

defined independently of any specific generator, probing the kinematics of b-jets produced from the top quark decay, dynamics of additional b-jets and non-b-jets, and overall event characteristics within each region of phase space.

Observables such as the number $N_{b\text{-jets}}$ of b-jets in the event, the scalar sum $H_{\mathrm{T}}^{\mathrm{had}}$ of the p_{T} of each jet, and the scalar sum $H_{\mathrm{T}}^{\mathrm{all}}$ of the p_{T} of each lepton, jet and the $E_{\mathrm{T}}^{\mathrm{miss}}$ represent the overall event properties. These observables are sensitive to matrix elements and parton shower modelling. Additionally, variables such as the average angular distance $\Delta R_{\mathrm{avg}}^{bb}$ between any two b-jets and the maximum separation $\Delta\eta_{\mathrm{max}}^{jj}$ in η between any two jets are indicative of additional QCD emissions. Further measurements include the p_{T} and η observables of up to four leading b-jets, as listed in table 2, where the b-jets are labelled as b_1, b_2, b_3, and b_4 according to their rank in descending order of their p_{T}. These variables encapsulate contributions from both the top quark decay products and the additional jets, with the leading b-jets kinematics dominantly reflecting the top quark. The invariant mass $m(e\mu b_1 b_2)$ of the system of electron, muon, and two leading b-jets, as well as the invariant mass $m(b_1 b_2)$, transverse momentum $p_{\mathrm{T}}(b_1 b_2)$, and angular distance $\Delta R(b_1, b_2)$ of the system of two leading b-jets have sensitivity to the dynamics of top quark decay products. Moreover, the additional b-jet activity is explored through distributions of the angular distance $\min\Delta R(bb)$, invariant mass $m(bb^{\min\Delta R})$, and transverse momentum $p_{\mathrm{T}}(bb^{\min\Delta R})$ of the two closest b-jets. The $N_{b\text{-jets}}$ distributions are measured separately in phase spaces with $\geq 2b$ and $\geq 3b$, while all other differential observables are measured in $\geq 3b$ and $\geq 4b$ phase spaces, where $2b$, $3b$ and $4b$ refer to the number of b-jets.

In the second category, p_{T} and η distributions are obtained after assigning b-jets as originating from top quarks (b_1^{top} and b_2^{top}) using the reconstruction algorithm to better probe the kinematics of the top quark, where the subscripts 1 and 2 indicate the leading- and sub-leading b-jets assigned to the top quarks, respectively. Similarly, the p_{T} and η distributions of the leading additional b-jet (b_1^{add}) assigned using the reconstruction algorithm are measured. The invariant mass $m(e\mu bb^{\mathrm{top}})$ of the system of electron, muon, and two b-jets from top quarks, and the invariant mass $m(bb^{\mathrm{top}})$ and transverse momentum $p_{\mathrm{T}}(bb^{\mathrm{top}})$ of the system of two b-jets assigned to top quarks are studied. Another interesting observable is the angular distance between the leading additional b-jet and the system of electron, muon, and two b-jets from the top quarks, which is sensitive to the recoil momentum distribution shared by final-state partons. These observables are measured in $\geq 3b$ and $\geq 4b$ phase spaces. Additionally, the p_{T} and η distributions of the sub-leading additional b-jet (b_2^{add}), invariant mass $m(bb^{\mathrm{add}})$, and transverse momentum $p_{\mathrm{T}}(bb^{\mathrm{add}})$ of two additional b-jets system are measured in the $\geq 4b$ phase space.

Additional non-b-jets (denoted by l/c-jets), defined as those not containing any ghost-matched b-hadron, can occur in the dileptonic events only via QCD radiation. This is only partially predicted by the matrix element with limited accuracy in QCD. The production rate of additional l/c-jets are sensitive to both the matrix element and the parton shower models. The activity of those jets is measured in terms of the multiplicity $N_{l/c\text{-jets}}$ of additional l/c-jets in the $\geq 3b$ and $\geq 4b$ phase spaces, the p_{T} and η variables of the leading additional l/c-jet (l/c-jet$_1$), the scalar difference $p_{\mathrm{T}}(l/c\text{-jet}_1) - p_{\mathrm{T}}(b_1^{\mathrm{add}})$ in the transverse momenta of the leading additional l/c-jet and the leading additional b-jet, and the angular separation

JHEP01(2025)068

Observable	Description	Phase spaces				
		$\geq 2b$	$\geq 3b$	$\geq 3b \geq 1l/c$	$\geq 4b$	$\geq 4b \geq 1l/c$
σ^{fid}	Fiducial total cross-section		✓	✓	✓	✓
$N_{b\text{-jets}}$	Number of b-jets	✓	✓			
$N_{l/c\text{-jets}}$	Number of light- or c-jets		✓		✓	
$H_{\text{T}}^{\text{had}}$	Scalar sum of p_{T} of all jets		✓		✓	
$H_{\text{T}}^{\text{all}}$	Scalar sum of p_{T} of charged leptons, jet and missing E_{T}		✓		✓	
$\Delta R_{\text{avg}}^{bb}$	Average angular distance in ΔR of b-jet pairs		✓		✓	
$\Delta\eta_{\text{max}}^{jj}$	Maximum absolute difference in η between any pair of jets		✓		✓	
$p_{\text{T}}(b_1)$	p_{T} of the hardest b-jet		✓		✓	
$p_{\text{T}}(b_2)$	p_{T} of second-hardest b-jet		✓		✓	
$p_{\text{T}}(b_3)$	p_{T} of third-hardest b-jet		✓		✓	
$p_{\text{T}}(b_4)$	p_{T} of fourth-hardest b-jet				✓	
$\eta(b_1)$	η of hardest b-jet		✓		✓	
$\eta(b_2)$	η of second-hardest b-jet		✓		✓	
$\eta(b_3)$	η of third-hardest b-jet		✓		✓	
$\eta(b_4)$	η of fourth-hardest b-jet				✓	
$p_{\text{T}}(l/c\text{-jet}_1)$	p_{T} of the hardest light- or c-jet			✓		✓
$\eta(l/c\text{-jet}_1)$	η of the hardest light- or c-jet			✓		✓
$m(b_1b_2)$	Invariant mass of two hardest b-jets in p_{T}		✓		✓	
$\Delta R(b_1, b_2)$	ΔR between two hardest b-jets		✓		✓	
$p_{\text{T}}(b_1b_2)$	p_{T} of two hardest b-jets		✓		✓	
$m(bb^{\text{min}\Delta R})$	Invariant mass of two closest b-jets in ΔR				✓	
$p_{\text{T}}(bb^{\text{min}\Delta R})$	p_{T} of the closest b-jets pair				✓	
$\text{min}\Delta R(bb)$	Closest angular distance in ΔR among b-jets				✓	
$m(e\mu b_1b_2)$	Invariant mass of electron, muon and two hardest b-jets		✓		✓	
$p_{\text{T}}(b_1^{\text{top}})$	p_{T} of the hardest b-jet assigned to top quark		✓		✓	
$p_{\text{T}}(b_2^{\text{top}})$	p_{T} of the second-hardest b-jet assigned to top quark		✓		✓	
$p_{\text{T}}(b_1^{\text{add}})$	p_{T} of the hardest additional b-jet		✓		✓	
$p_{\text{T}}(b_2^{\text{add}})$	p_{T} of the second-hardest additional b-jet				✓	
$\eta(b_1^{\text{top}})$	η of the hardest b-jet assigned to top quark		✓		✓	
$\eta(b_2^{\text{top}})$	η of the second-hardest b-jet assigned to top quark		✓		✓	
$\eta(b_1^{\text{add}})$	η of the hardest additional b-jet		✓		✓	
$\eta(b_2^{\text{add}})$	η of the second-hardest additional b-jet				✓	
$m(bb^{\text{top}})$	Invariant mass of a pair of b-jets assigned to top quarks		✓		✓	
$p_{\text{T}}(bb^{\text{top}})$	p_{T} of a pair of b-jets assigned to top quarks		✓		✓	
$m(bb^{\text{add}})$	Invariant mass of a pair of additional b-jets				✓	
$p_{\text{T}}(bb^{\text{add}})$	p_{T} of a pair of additional b-jets				✓	
$m(e\mu bb^{\text{top}})$	Invariant mass of $e\mu$ and the b-jets pair assigned to top quarks		✓		✓	
$\Delta R(e\mu bb^{\text{top}}, b_1^{\text{add}})$	ΔR between the direction of the system of $e\mu$ and b-jet pair assigned to top and the direction of the hardest additional b-jet		✓		✓	
$\Delta R(e\mu bb^{\text{top}}, l/c\text{-jet}_1)$	ΔR between the direction of the system of $e\mu$ and b-jet pair assigned to top and the direction of the hardest light- or c-jet			✓		✓
$p_{\text{T}}(l/c\text{-jet}_1) - p_{\text{T}}(b_1^{\text{add}})$	Difference in p_{T} between the hardest l/c-jet and the additional b-jet			✓		✓

Table 2. Summary of all measured observables in each fiducial phase space region. The availability of an observable is indicated by ✓ in the last five columns. The first half of the table lists the global event variables and the kinematics of b-jets ordered in p_{T}, whereas the second half lists the quantities specific to the b-jets assigned to top quark decays or to extra $b\bar{b}$ system as well as those related to the additional light- or c-jets (l/c-jets).

$\Delta R(e\mu bb^{\text{top}}, l/c\text{-jet}_1)$ between the leading l/c-jet and the direction of the system of electron, muon and b-jets assigned to the top quarks in the $\geq 3b \geq 1l/c$ and $\geq 4b \geq 1l/c$ phase spaces, as listed in table 2.

All of these observables are also constructed in a similar way at the detector level, where the b-tagged jets are considered as a proxy for the b-jets. The b-tagged jets are ordered in p_{T} at the detector-level unless mentioned otherwise. Similary, the additional l/c-jets at the detector-level refer to all those reconstructed jets that are not b-tagged.

JHEP01(2025)068

6.1 Classification of b-jets

In events with three or more b-jets, ambiguity arises regarding whether these b-jets originate from top quark decays or gluon radiation. An empirical algorithm is developed to better identify the origins of representative b-jets and compare their kinematics with particle-level predictions from various MC generators. This approach aims to improve the understanding of b-jets sources and enhance the accuracy of kinematic measurements.

The discriminating kinematic variables are investigated in the simulated events after attaching 'truth' labels to b-jets to indicate their true origin in the MC. The particle-level b-jets originating from top quark decay are classified based on the origin of hadrons, a method used in this study as described in ref. [6]. This approach involves mapping the original heavy hadrons to the b-quarks that are closest in ΔR. Subsequent heavy hadrons from decay chains are excluded from this mapping. Those hadrons associated with a b-quark originating from the top quark decay are denoted by b-hadrons derived from a top quark. Correspondingly, the selected particle-level b-jet that is ghost-associated with such b-hadrons is designated as a b-jet from top, while the remaining b-jets are labelled as additional b-jets.

The algorithm uses angular separations, as defined in section 2, between two physics objects and is applied to both detector-level and particle-level events. Key metrics such as the minimum distance $\Delta R_{\ell 1b}^{\min}$ between the leading lepton and any b-jet, the minimum distance $\Delta R_{\ell 2b}^{\min}$ between the sub-leading lepton and any b-jet, the maximum distance $\Delta R_{bb}^{\max}$ between two b-jets, and the minimum distance $\Delta R_{bb}^{\min}$ between two b-jets, are essential for discriminating between b-jets from top quark decays and additional b-jets, as illustrated in figure 3. In most of the $t\bar{t}$+b-jets MC events, leptons are closer to the b-jet originating from top quark decays, as shown in figures 3(a) and 3(b). Additionally, two b-jets not originating from top quark decays often show the smallest angular distance among any b-jet pairs as shown in figure 3(c). In instances where one of the b-jets fails the fiducial requirement, the angular separation between a b-jet from a top quark and an additional b-jet may be larger than that of any other b-jet pair combination, as shown in figure 3(d).

At the particle level, the algorithm is restricted to four input b-jets ordered in p_{T}. If four b-jets are not available, it uses only three b-jets per event. Events featuring fewer than three b-jets are not classified relative to the b-jets. The b-jets are arranged into a number of permuted sets depending on the b-jet multiplicity, with the first two b-jet positions in the set representing the b-jets from top quarks, and the remaining b-jets representing the additional b-jets. The chosen permutation among these sets is the one that minimises $-\ln w$, defined in terms of the sum of squares of the differences between the ΔR values of the lepton-b-jet pairs relative to the global quantities $\Delta R_{\ell 1b}^{\min}$ or $\Delta R_{\ell 2b}^{\min}$, and of the differences between the ΔR values of b-jet pairs in a given permutation relative to $\Delta R_{bb}^{\max}$ or $\Delta R_{bb}^{\min}$. The full expression is:

$$-\ln w = \begin{cases} \left(\Delta R_{\ell 1 b1} - \Delta R_{\ell 1b}^{\min}\right)^2 + \left(\Delta R_{\ell 2 b2} - \Delta R_{\ell 2b}^{\min}\right)^2 + \left(\max(\Delta R_{b1b3}, \Delta R_{b2b3}) - \Delta R_{bb}^{\max}\right)^2 \\ \qquad\qquad\qquad\qquad\qquad\qquad\qquad\qquad\qquad\qquad \text{if } N_{b\text{-jets}} = 3, \\ \left(\Delta R_{\ell 1 b1} - \Delta R_{\ell 1b}^{\min}\right)^2 + \left(\Delta R_{\ell 2 b2} - \Delta R_{\ell 2b}^{\min}\right)^2 + \left(\Delta R_{b3b4} - \Delta R_{bb}^{\min}\right)^2 \\ \qquad\qquad\qquad\qquad\qquad\qquad\qquad\qquad\qquad\qquad \text{if } N_{b\text{-jets}} \geq 4, \end{cases}$$

where $\Delta R_{\ell 1b1}$ ($\Delta R_{\ell 2b2}$) represents the angular distance between the leading (sub-leading)

JHEP01(2025)068

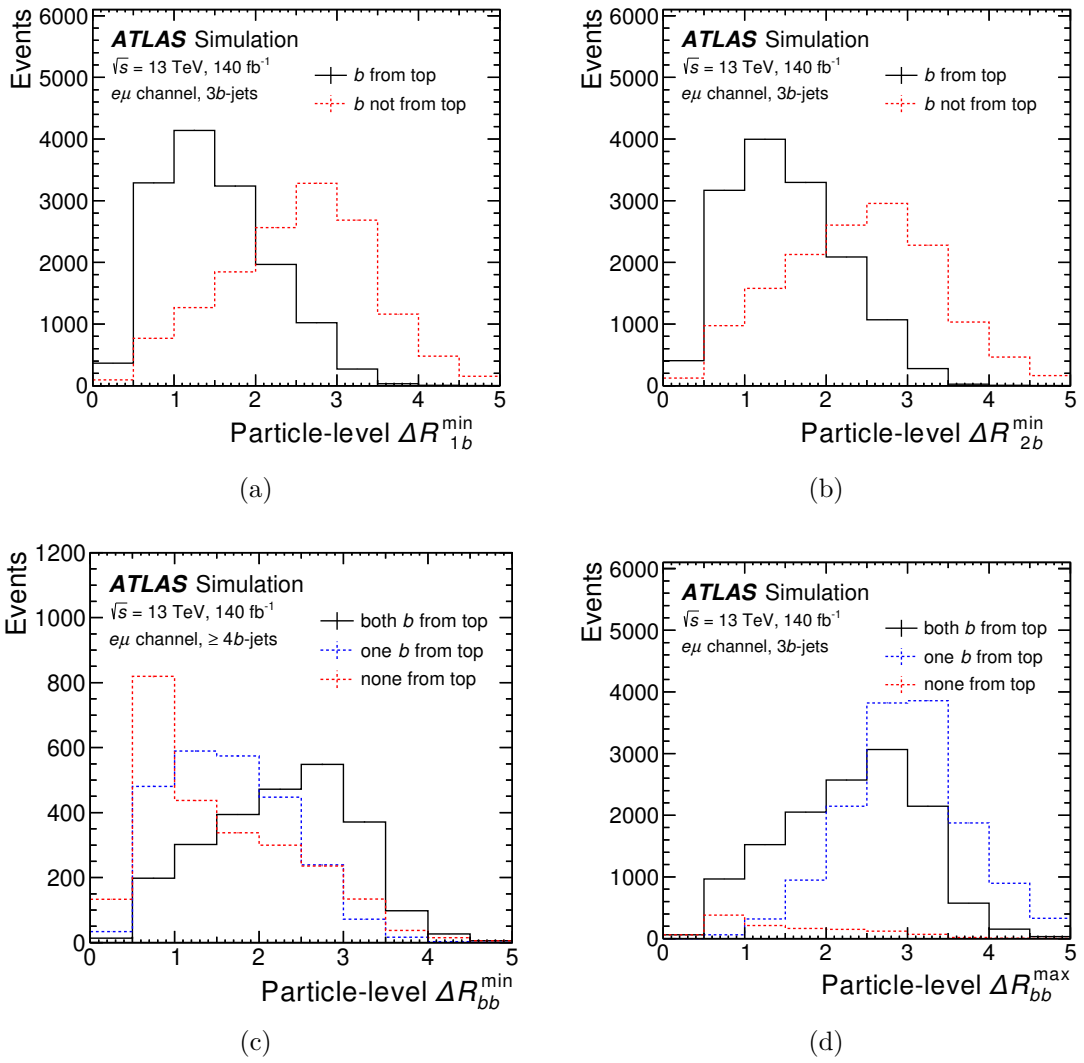

Figure 3. Distributions of discriminating variables at the particle-level used in the reconstruction algorithm are compared for the b-jets originating from top quark (b from top) and those originating from the gluon system (b not from top): (a) $\Delta R^{\min}_{\ell 1b}$, (b) $\Delta R^{\min}_{\ell 2b}$ in the fiducial phase space with one electron, one muon, and exactly three b-jets; (c) $\Delta R^{\min}_{bb}$ in the fiducial phase space with one electron, one muon, and at least four b-jets; and (d) $\Delta R^{\max}_{bb}$ in the fiducial phase space with one electron, one muon, and exactly three b-jets.

lepton in the event and the first (second) b-jet of a given set, ΔR_{b1b3} (ΔR_{b2b3}) refers to the angular distance between first (second) and third b-jet of the set, and ΔR_{b3b4} represents the angular distance between the third and fourth b-jet in a given permutation. Each variable entering in the squared sum in the expression is assigned the same weight for simplicity. The $N_{b\text{-jets}}$ is the number of b-jets in the event. The set that gives the smallest value of $-\ln w$ is finally chosen to classify its first two b-jets as belonging to the top quark, and the remaining b-jets are assigned as additional b-jets. At the detector level, the same algorithm is applied to reconstructed leptons and b-tagged jets, after taking only up to four b-tagged jets into account. If there are more than four b-tagged jets present, then the first four ordered in p_{T} are taken.

JHEP01(2025)068

The purities of b-jet classifications according to this algorithm are evaluated using 'truth' labels to b-jets in simulated events, as discussed above. This is done solely to assess the performance of the algorithm, it is not integral to the definitions of the measured observables. According to this definition of 'truth' b-jet origin, the typical fraction of QCD $t\bar{t}$+b-jets simulated events wherein the two highest-p_{T} particle-level b-jets originate from top quarks amounts to 42% (27%) in events containing at least three (four) b-jets. The fractions of particle-level events where two b-jets are correctly assigned to top quarks according to this technique are found to be 53% (56%) in the selected sample of simulated $t\bar{t}$+b-jets events containing three (four) b-jets. Slightly lower (by 1%–2%) purities are obtained with the corresponding reconstructed events where the b-tagged jets are geometrically matched to the particle-level b-jets. The probabilities of correct assignment of b-jet (two or more b-jets in case of kinematic observable defined with multiple b-jets) in a given bin of the measured observable ranges from 50% to 85% (40% to 75%). The reconstruction algorithm is not optimal for signal events that have at least one of the b-jets from $t\bar{t}$ decay outside the fiducial volume ($< 10\%$ fraction of events with three or more b-jets), and hence the correct assignments of b-jets cannot be made to both top quarks.

7 Background estimation

The $t\bar{t}$+jets candidate events are pre-selected with a prompt electron and a prompt muon of opposite charge and two or more b-tagged jets ($\geq 2b$@77%), as detailed in section 4. The $t\bar{t}$+b-jets signal events consist of a prompt electron and a prompt muon from W decays, have three or more b-tagged jets ($\geq 3b$@77%), and at least three or more particle-level b-jets. The preselection of events with two or more b-tagged jets yields a sample primarily dominated by $t\bar{t}$ production with minimal contributions from other processes. The background events in this sample can be categorised into two main types. Firstly, there are events with genuine prompt leptons originating from top, W, and Z decays, including those arising from leptonic τ-lepton decays, which are elaborated upon in section 7.1. Secondly, there are events where at least one reconstructed lepton candidate is non-prompt or misidentified as a different object. These can be a non-prompt lepton from the decay of a b- or c-hadron, an electron from a photon conversion, hadronic jet activity misidentified as an electron, or a muon from an in-flight decay of a pion or kaon. The estimation of this second type of background involves a combination of data-driven and simulation-based approach, detailed in section 7.2.

The signal event category $t\bar{t}$+b-jets (also denoted as $t\bar{t}b$) refer to events in the $t\bar{t}$ MC sample consisting of three or more particle-level b-jets. Events that contain less than three b-jets but have at least one c-jet are categorised as $t\bar{t}$+c-jets ($t\bar{t}c$), and all remaining events are defined as $t\bar{t}$+light-jets ($t\bar{t}l$). The events with three or more b-tagged jets contain substantial background from $t\bar{t}l$ or $t\bar{t}c$ where c-jets or light jets are mis-identified as b-jets by the b-tagging algorithm. The MC yields of these background processes before any corrections are given in table 3. These backgrounds are estimated simultaneously with the extraction of fiducial cross-sections, as discussed in section 8.

JHEP01(2025)068

7.1 Backgrounds with prompt leptons

The estimation of various background processes with the presence of oppositely charged prompt electrons and muons in the final state is primarily performed using the MC simulation. The $t\bar{t}H$ process constitutes the primary irreducible background, contributing approximately 1% to 6% of the total expected event yields in the $3b$@77% and $\geq 4b$@77% regions, with its contribution increasing as the number of required b-tagged jets increases. The $t\bar{t}V$ production yields a similar contribution as $t\bar{t}H$ production in the $3b$@77% region, and nearly half the size of $t\bar{t}H$ in the $\geq 4b$@77% region. The $t\bar{t}Z$ production dominates the $t\bar{t}V$ process; the $t\bar{t}W$ background is about 30% (1%) of the total $t\bar{t}V$ yield in $3b$@77% ($\geq 4b$@77%) regions.

The single-top-quark production contributes approximately 3% to the expected event yields, decreasing with the number of selected b-tagged jets. Contributions from Z/γ^*+jets and diboson processes are found to be minimal. Other rare SM processes such as $t\bar{t}t\bar{t}$, tZ, tWZ, tWH, and $tHbj$ are also included in the total background estimate, all of which are estimated from MC simulations.

7.2 Background with non-prompt or misidentified leptons

The contribution of non-prompt or misidentified leptons (referred to as 'non-prompt lepton background') is estimated using a data-driven approach, relying on the data events where the electron and muon have the same electric charges. This method, detailed in ref. [107], is based on the assumption that jets misidentified as electrons or muons yield a comparable number of events with opposite-charge (opposite-sign, OS) and same-charge (same-sign, SS) $e\mu$ pairs in the $t\bar{t}$ sample, particularly in instances where at least one W boson decays hadronically. This estimate includes the non-prompt and misidentified leptons produced not only in the $t\bar{t}$ events, but also in other processes such as W+jets. Events are pre-selected with the same baseline criteria for the electron and muon as for the signal except for the requirements on their charges, and that they contain at least two or more b-tagged jets. Known sources of same-sign prompt leptons contribution estimated from the signal and background MC simulation are subtracted from the data distribution of the same-sign events, and the non-prompt lepton background in each bin is extracted by scaling the remaining data events by the lepton-p_{T} dependent and b-tagged jets multiplicity dependent asymmetry factor R.

$$N_{i,\mathrm{non-prompt}} = R \cdot (N_{i,\mathrm{SS}}^{\mathrm{Data}} - N_{i,\mathrm{SS-prompt}}^{\mathrm{MC}}),$$

where $N_{i,\mathrm{SS}}^{\mathrm{Data}}$ is the number of observed data events with same-sign $e\mu$ pair in the ith bin of the observable, and $N_{i,\mathrm{SS-prompt}}^{\mathrm{MC}}$ is the MC simulated yield of the prompt same-sign events in that bin. The factor R, which scales the non-prompt lepton background from the same-sign region to the opposite-sign signal region, is determined using Powheg+Pythia 8 $t\bar{t}$ events where at least one of the leptons originates from the hadronically decaying W boson and is hence misidentified. It is defined as:

$$R = \frac{N_{\mathrm{OS-non-prompt}}^{\mathrm{MC}}}{N_{\mathrm{SS-non-prompt}}^{\mathrm{MC}}},$$

where $N_{\mathrm{OS-non-prompt}}^{\mathrm{MC}}$ and $N_{\mathrm{SS-non-prompt}}^{\mathrm{MC}}$ are the non-prompt lepton background event yields estimated from the MC simulation in the opposite-sign and same-sign events, respectively.

JHEP01(2025)068

Process	$\geq 2j$, $2b$@77%	$\geq 3j$, $3b$@77%	$\geq 4j$, $\geq 4b$@77%
$t\bar{t}$ +b-jets	4100 ± 790	3550 ± 650	474 ± 99
$t\bar{t}c$	11600 ± 2200	2190 ± 430	57 ± 15
$t\bar{t}l$	263000 ± 33000	2080 ± 440	25 ± 15
Wt	9100 ± 1800	227 ± 94	14 ± 11
$t\bar{t}V$	740 ± 230	94 ± 30	16.3 ± 5.1
$t\bar{t}H$	180 ± 22	108 ± 13	37.2 ± 5.3
Non-prompt lepton	340 ± 210	37 ± 20	10.9 ± 6.1
Z/γ^*+jets	96 ± 38	3.4 ± 1.4	0.15 ± 0.09
Diboson	85 ± 43	3.0 ± 1.5	0.11 ± 0.07
Others	41 ± 20	16.4 ± 8.2	6.4 ± 2.9
Total predicted	290000 ± 35000	8300 ± 1300	640 ± 120
Observed	281213	10235	798

Table 3. Predicted and observed event yields for the events pre-selected with two or more reconstructed jets ($\geq 2j$) and further categorised in exactly $2b$@77%, exactly $3b$@77% and $\geq 4b$@77% selections before any flavour composition scale factors are applied to $t\bar{t}$ events. Predicted events in the $t\bar{t}$ sample are split into three categories, with $t\bar{t}$ +b-jets referring to the signal events consisting of at least three particle-level b-jets, and $t\bar{t}c$ ($t\bar{t}l$) referring to background events consisting of less than three particle-level b-jets but more than one (no) c-jets. The background with non-prompt or misidentified leptons is denoted by non-prompt lepton. The quoted errors are symmetrised and indicate total statistical and systematic uncertainties in the predictions due to experimental and theoretical sources.

It is determined as a function of lepton p_{T} in the $2b$@77% events, while it is evaluated inclusively in lepton p_{T} in the $\geq 3b$@77% events due to the very low background and limited MC statistics. The values of R range from 1.98 ± 0.52 to 2.38 ± 0.74 across the lepton-p_{T} bins in $2b$@77% events, while it is 1.65 ± 0.45 for inclusive $\geq 3b$@77% events, where the quoted error represents the uncertainty due to limited MC statistics and the MC modelling uncertainty, with the latter being the dominant component. The MC modelling uncertainty includes the uncertainty in the matrix element and the uncertainty in the modelling of the parton shower, hadronisation and underlying event. Table 3 presents the total estimated background yields in various bins of b-tagged jet multiplicity.

8 Extraction of fiducial cross-sections

The particle-level distributions for different observables in the fiducial phase space defined in section 5.2 are extracted from the data distributions obtained after the event selections described in section 4.2. The number of events meeting the baseline selection criteria with two or more b-tagged jets, primarily comprising $t\bar{t}$ events, agrees well with the predictions, as detailed in table 3. However, there is about a 20% underestimate of the number of events featuring three or more b-tagged jets. This discrepancy, while noticeable in figure 4, is not significant given the large systematics uncertainties in the b-tagged jet multiplicity distribution in figure 4(a). The data distributions of the scalar sum of the p_{T} of charged

JHEP01(2025)068

leptons and jets, the p_{T} of the b-tagged jets assigned to the top quark, and the p_{T} of the additional b-tagged jets show deviations from the predictions. The measurement of $t\bar{t}$+b-jets production is dependent on the estimate of background originating from other $t\bar{t}$ processes, such as the mis-tagged jets in $t\bar{t}c$ and $t\bar{t}l$ events that give substantial background contributions. To address this discrepancy, data-driven scale factors are derived to simultaneously adjust the predictions of additional c-jet or light jet backgrounds alongside the additional b-jets in the $t\bar{t}$ MC simulation, as outlined in section 8.1. The number of background events produced by $t\bar{t}H$, $t\bar{t}V$, and non-$t\bar{t}$ processes and the non-prompt lepton background described in section 7 are subtracted from the data. The data are then unfolded using the corrected MC simulation as described in section 8.2.

8.1 Data-driven correction factors for flavour composition of additional jets in $t\bar{t}$ events

The mis-tagging of jets in $t\bar{t}c$ and $t\bar{t}l$ events contributes significantly to the background in the $t\bar{t}$+b-jets process. For example, only about 50% of simulated events selected at detector level with at least three b-tagged jets contain at least three true b-jets at the particle level in the fiducial phase space. The remaining events include at least one c-jet or light-flavour jet that is misidentified as a b-tagged jet. Moreover, the $t\bar{t}c$ production cross-sections have not yet been precisely measured [29]. To account for these significant background contributions, a template fit to data is performed to simultaneously extract the normalisation factors for $t\bar{t}$+b-jets, $t\bar{t}c$ and $t\bar{t}l$ particle-level event categories and subsequently correct their compositions in $t\bar{t}$ simulated samples. This is done to reduce the impact of systematic uncertainties in $t\bar{t}c$ and $t\bar{t}l$ background estimates.

The template fit is performed using a binned maximum-likelihood approach, with the likelihood function modeled as a Poisson distribution:

$$\mathcal{L}(\vec{\alpha}|x_1,\ldots,x_n) = \prod_k^n \frac{\mathrm{e}^{-\nu_k(\vec{\alpha})}\nu_k(\vec{\alpha})^{x_k}}{x_k!}\,, \tag{8.1}$$

where x_k represents the number of events in bin k from the data template, and $\nu_k(\vec{\alpha})$ is the expected number of events, which depends on a set of free parameters, $\vec{\alpha}$. Only the statistical uncertainty in the data is considered in the fit. Three fit parameters, α_b^s, α_c^s and α_l^s, are used in the maximum-likelihood fit, such that the expected number of events in bin k of region s is

$$\nu_k(\alpha_b^s,\alpha_c^s,\alpha_l^s) = \alpha_b^s N_{t\bar{t}b}^{k,s} + \alpha_c^s N_{t\bar{t}c}^{k,s} + \alpha_l^s N_{t\bar{t}l}^{k,s} + N_{\text{non-}t\bar{t}}^{k,s}\,, \tag{8.2}$$

where $N_{t\bar{t}b}^{k,s}$, $N_{t\bar{t}c}^{k,s}$, $N_{t\bar{t}l}^{k,s}$ and $N_{\text{non-}t\bar{t}}^{k,s}$ are the numbers of events in bin k and in the region s, denoted $\geq 3j \geq 2b$@77%, of the $t\bar{t}b$, $t\bar{t}c$, $t\bar{t}l$ and non-$t\bar{t}$ background templates, respectively.

Templates are created for each category using the third-highest b-tagging discriminant score in the event. This variable is a proxy for the flavour of an additional jet and helps discriminate between the $t\bar{t}$+b-jets, $t\bar{t}c$ and $t\bar{t}l$ processes. Figure 5 shows the shape comparisons of these templates. Two fitting approaches are considered:

1. *Global fit*: normalisation factors for the $t\bar{t}$+b-jets, $t\bar{t}c$ and $t\bar{t}l$ templates are fitted in the inclusive region. This is the nominal approach and is used to correct the normalisation of these components.

JHEP01(2025)068

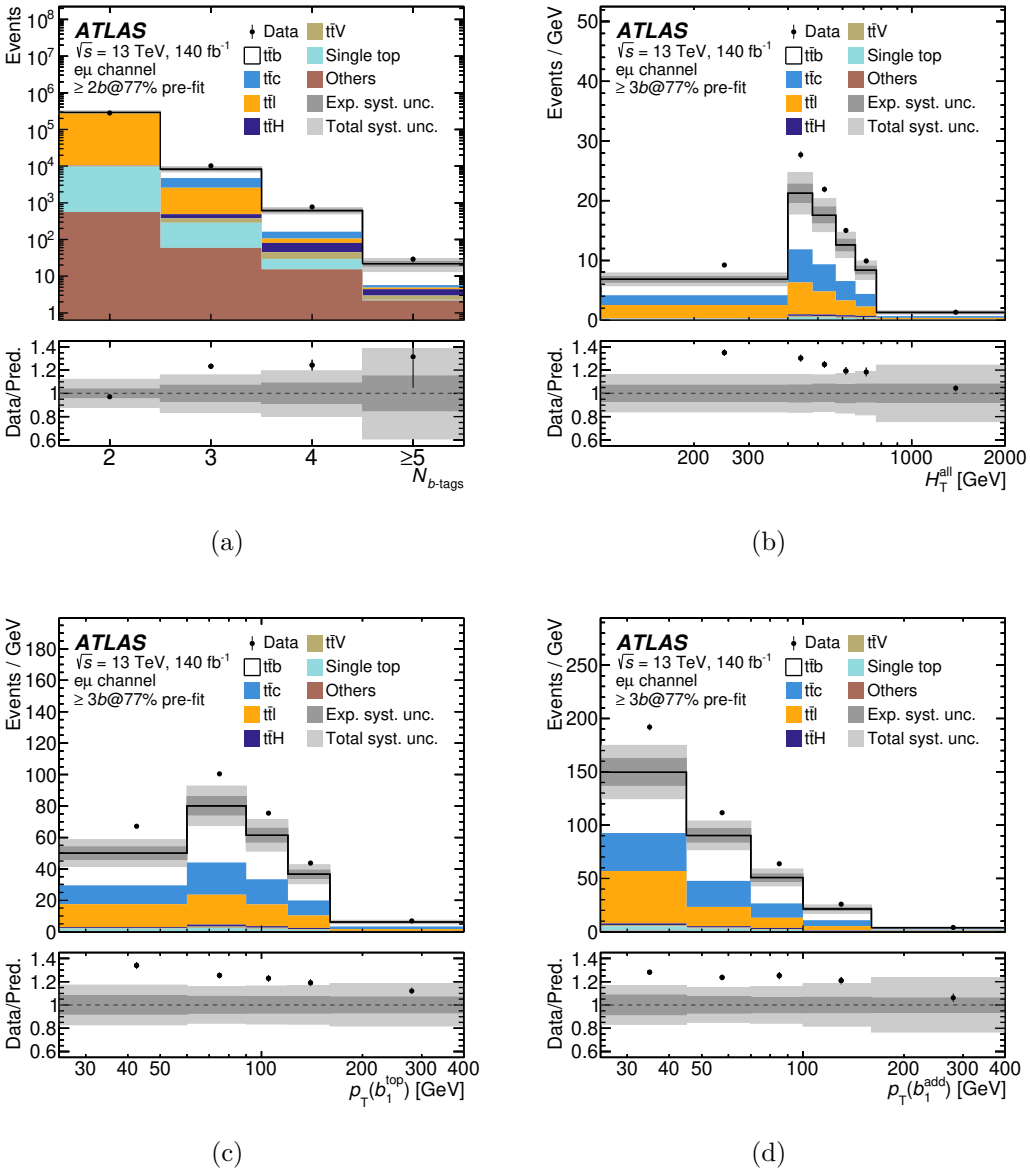

Figure 4. Comparison of data and predictions for the distribution of (a) the number of b-tagged jets for events with at least two b-tagged jets ($N_{b-\text{tags}}$), (b) $H_{\text{T}}^{\text{all}}$, (c) p_{T} (b_1^{top}), and (d) p_{T} (b_1^{add}) in reconstructed events with three or more b-tagged jets before the global scale factors are applied for different event categories as discussed in the text (see section 8.1). The entries in each bin are divided by the bin width in (b), (c) and (d). The lower panels show the ratios of the data to the predictions. The inner band includes the uncertainties due to limited MC statistics and due to various detector effects such as the jet energy scale and resolution, and the b-tagging, while the outer band also includes the theoretical uncertainties in the signal and background modelling. The last bin includes the overflow.

JHEP01(2025)068

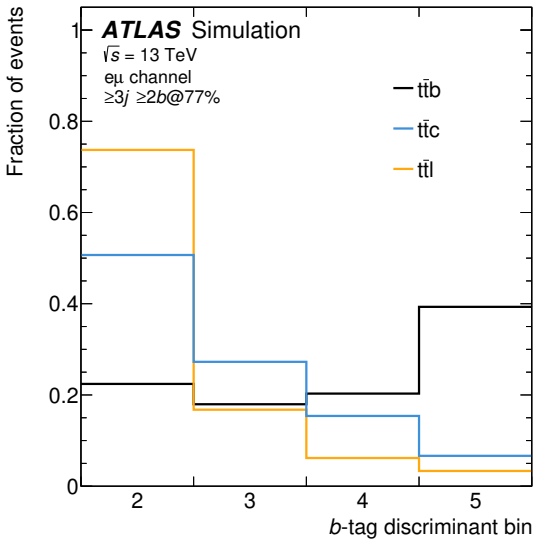

Figure 5. Templates of $t\bar{t}$+b-jets, $t\bar{t}c$, and $t\bar{t}l$ processes in the inclusive detector-level region with $\geq 3j \geq 2b$@77%, as considered in the fit. For each category, they depict the distribution of the third-highest b-tagging discriminant score among selected jets in the event. The score ranging from 2 to 5, correspond to a certain range of b-tagging efficiencies defined by the working points: 85%–77%, 77%–70%, 70%–60%, and < 60%, respectively.

2. *Kinematic-dependent fit*: normalisation factors are fitted in specific regions based on jet multiplicity and the p_{T} of the third-hardest jet in the reconstructed events. This approach is used only to assess the shape uncertainty of the $t\bar{t}c$ and $t\bar{t}l$ backgrounds.

The *Global fit* is chosen as the nominal approach because it improves the modelling of the $t\bar{t}c$ and $t\bar{t}l$ backgrounds while maintaining correlations between the normalisation factors for the $t\bar{t}$+b-jets and $t\bar{t}c$ and $t\bar{t}l$ processes. Figure 6(a) shows the template distributions both before and after applying the best-fit scale factors, with the results summarised in the first row of table 5, where the quoted uncertainties are statistical only. This method ensures that the signal efficiency and acceptance corrections derived from simulation remain intact. On the other hand, the *Kinematic-dependent fit* can improve both the normalisation and shape of the $t\bar{t}c$ and $t\bar{t}l$ backgrounds but may introduce biases into the unfolding corrections. Therefore, the *Kinematic-dependent fit* is used only for evaluating shape uncertainties.

In the case of the *Global fit* approach, events are selected with at least three reconstructed jets, at least two of which are b-tagged. This region labelled as $\geq 3j \geq 2b$@77% and listed in table 4 is used to derive the nominal scale factors. The templates are created for MC events in three different particle-level categories, labelled as $t\bar{t}b$, $t\bar{t}c$, and $t\bar{t}l$ and described in table 4 for the $\geq 3j \geq 2b$@77% region, using the b-tagging discriminant value of the jet with the third-highest b-tagging discriminant. A small fraction ($\sim 5\%$) of events in the signal templates contain at least one additional c-jet and at least one additional b-jet. Likewise, the signal templates contain a relatively small fraction ($\sim 8\%$) of events where at least one of the two b-jets originating from a top quark is outside of the fiducial volume. The fiducial

JHEP01(2025)068

	Inclusive region *Global* approach	Regions in terms of jet multiplicity and third-highest-p_{T} jet-p_{T} *Kinematic-dependent* approach		
	(nominal)	(systematic)		
Category	$\geq 3j \geq 2b$@77% ≥ 25 GeV	$3j \geq 2b$@77% 25–35 GeV	35–50 GeV	≥ 50 GeV	$\geq 4j \geq 2b$@77% 25–50 GeV	50–75 GeV	≥ 75 GeV
$t\bar{t}b$	$\geq$3 b-jets	$\geq$3 b-jets		–		
$t\bar{t}b_{\mathrm{ex}}$	–	–		exactly 3 b-jets		
$t\bar{t}b\bar{b}$	–	–		$\geq$4 b-jets		
$t\bar{t}c$	<3 b-jets and ≥ 1 c-jet	<3 b-jets and ≥ 1 c-jet		<3 b-jets and ≥ 1 c-jet		
$t\bar{t}l$	events that do not meet above criteria	events that do not meet above criteria		events that do not meet above criteria		

Table 4. Truth categorisations, defined using particle level information, of the reconstructed events in the regions with selections $\geq 3j \geq 2b$@77%, $3j \geq 2b$@77%, and $\geq 4j \geq 2b$@77% of the $t\bar{t}$ MC samples. The $3j \geq 2b$@77% and $\geq 4j \geq 2b$@77% regions are sub-divided in terms of the p_{T} of the third-leading p_{T} reconstructed jet. Reconstructed events in each region and sub-region are categorised based on the particle-level selections of the number of b-jets, c-jets and light-flavour jets. All particle-level categories are listed in the first column and their definitions are given in the following columns under the respective reconstruction-level region. The dashes (–) imply that the corresponding event category is not present for that region.

cross-section measurements remain largely unaffected by the choice of 'truth'-heavy-flavour classifications of individual templates considered in the nominal fit, due to the common fiducial definition used in the scale factor evaluation and the cross-section measurement. One additional template is created from the sum of all non-$t\bar{t}$ backgrounds described in section 7.

A selected jet in the analysis can be sorted into one of five possible bins (labelled 1 to 5 in the following) that correspond to a certain range of b-tagging efficiencies defined by the working points: 100%–85%, 85%–77%, 77%–70%, 70%–60%, and $<60\%$ respectively. The bin with 100%–85% efficiency contains only untagged jets mainly coming from the $t\bar{t}l$ category, and is hence not used in the fit. The remaining bins with substantial contributions from the $t\bar{t}c$ and $t\bar{t}b$ categories are considered in the *Global fit* approach.

The *Global fit* procedure for fitting the normalisation factors in the $\geq 3j \geq 2b$@77% region is repeated for each individual uncertainty considered in the analysis. The corresponding scale factors for each uncertainty are then propagated to the unfolding step as discussed in section 8.2.

Figure 7 compares the data with predictions for b-tagged jet multiplicity in events with at least two b-tagged jets and the $H_{\mathrm{T}}^{\mathrm{all}}$, p_{T} (b_1^{top}), and p_{T} (b_1^{add}) spectra in events with three or more b-tagged jets. The *Global fit* scale factors, derived from the $\geq 3j \geq 2b$@77% region, are applied to the reconstructed events for the corresponding $t\bar{t}c$, $t\bar{t}l$ and $t\bar{t}b$ event categories, depending on the observables. The uncertainty band includes the uncertainties from various experimental sources and the theoretical modelling uncertainties. Compared to the pre-fit distributions shown in figure 4, the post-fit predictions show significantly improved agreement with the data after corrections to the individual components.

For the evaluation of *Kinematic-dependent fit* scale factors, the selected events are further split into multiple orthogonal regions depending on the number of reconstructed jets and the p_{T} of the third-highest-p_{T} jet in the event, as summarised in table 4. Three p_{T} sub-regions

JHEP01(2025)068

Regions	Fitted values of scale factors					Type
	α^s_b	$\alpha^s_{b_{\text{ex}}}$	α^s_{bb}	α^s_c	α^s_l	
$\geq 3j \geq 2b$; ≥ 25 GeV	1.20 ± 0.03	–	–	1.62 ± 0.09	0.92 ± 0.04	*Global*
$3j \geq 2b$; (25–35) GeV	1.40 ± 0.15	–	–	1.99 ± 0.42	0.98 ± 0.08	
$3j \geq 2b$; (35–50) GeV	1.30 ± 0.11	–	–	1.74 ± 0.27	0.77 ± 0.11	
$3j \geq 2b$; ≥ 50 GeV	1.26 ± 0.12	–	–	1.05 ± 0.27	1.09 ± 0.15	*Kinematic-*
$\geq 4j \geq 2b$; (25–50) GeV	–	1.31 ± 0.10	1.15 ± 0.14	1.93 ± 0.11	0.92 ± 0.01	*dependent*
$\geq 4j \geq 2b$; (50–75) GeV	–	1.10 ± 0.09	1.20 ± 0.10	1.64 ± 0.09	0.86 ± 0.01	
$\geq 4j \geq 2b$; ≥ 75 GeV	–	1.10 ± 0.10	1.09 ± 0.10	1.25 ± 0.10	0.83 ± 0.02	

Table 5. Best-fit values of the $t\bar{t}b$, $t\bar{t}b_{\text{ex}}$, $t\bar{t}b\bar{b}$, $t\bar{t}c$, and $t\bar{t}l$ scale factors determined from dedicated fit regions. The quoted uncertainties are statistical only.

are chosen with sufficient and similar numbers of events. A total of 21 templates for the multiple binned scenario are created for the region with exactly three reconstructed jets ($3j \geq 2b$@77%) using the third-highest b-tagging discriminant score, and for the region with four or more reconstructed jets ($\geq 4j \geq 2b$@77%) using the b-tagging discriminant values of the third- and fourth-highest score in the event. The $3j \geq 2b$@77% detector-level region has three particle-level categories: $t\bar{t}b$, $t\bar{t}c$, and $t\bar{t}l$, while the $\geq 4j \geq 2b$@77% region has four particle-level categories: $t\bar{t}b_{\text{ex}}$, $t\bar{t}b\bar{b}$, $t\bar{t}c$, and $t\bar{t}l$ with the same definitions for the $t\bar{t}c$ and $t\bar{t}l$ background categories in all regions, as described in table 4. The $t\bar{t}b_{\text{ex}}$ category contains exactly three particle-level b-jets, while the $t\bar{t}b$ ($t\bar{t}b\bar{b}$) category includes three (four) or more particle-level b-jets. One-dimensional templates with four bins are formed starting from bin 2 for the jet with the third highest b-tagging discriminant value in $3j \geq 2b$@77% detector-level regions, while in the $\geq 4j \geq 2b$@77% detector-level regions two-dimensional templates are created using the third- and fourth-highest b-tagging discriminant values in the full range for the two jets.

In the $3j \geq 2b$@77% detector-level region, three fit parameters, α^s_b, α^s_c and α^s_l, are used in the maximum-likelihood fit following eq. (8.1) and eq. (8.2) for each of sub-region s given in table 4. In the $\geq 4j \geq 2b$@77% regions, four fit parameters $\alpha^s_{b_{\text{ex}}}$, α^s_{bb}, α^s_c and α^s_l are used, such that the expected number of events in bin k of a given sub-region s defined in table 4 is

$$\nu_k(\alpha^s_{b_{\text{ex}}}, \alpha^s_{bb}, \alpha^s_c, \alpha^s_l) = \alpha^s_{b\text{ex}} N^{k,s}_{t\bar{t}b_{\text{ex}}} + \alpha^s_{bb} N^{k,s}_{t\bar{t}b\bar{b}} + \alpha^s_c N^{k,s}_{t\bar{t}c} + \alpha^s_l N^{k,s}_{t\bar{t}l} + N^{k,s}_{\text{non-}t\bar{t}},$$

where $N^{k,s}_{t\bar{t}b_{\text{ex}}}$ and $N^{k,s}_{t\bar{t}b\bar{b}}$ are the numbers of events in bin k and each sub-region s of the $t\bar{t}b_{\text{ex}}$ and $t\bar{t}b\bar{b}$ templates, respectively. The fit is performed in each sub-region listed in table 4.

The result of the *Kinematic-dependent* scale factor fits in some regions are presented in figure 6, and the fit values are summarised in table 5 for each fit set-up, where the quoted uncertainties are statistical only. The values of α^s_b, $\alpha^s_{b\text{ex}}$, and α^s_{bb} extracted from various regions suggest 10%–30% level corrections to the POWHEG+PYTHIA 8 predictions. On the other hand the $t\bar{t}c$ background components have scale factors of up to two extracted from the fit and they tend to decrease with the p_{T} of third-highest-p_{T} jet in the event.

The $t\bar{t}c$ +$t\bar{t}l$ background estimation using the *Kinematic-dependent fit* gives up to 5% shape variations relative to that obtained from the *Global fit* estimation method, and this is accounted for as the shape uncertainty of this background.

JHEP01(2025)068

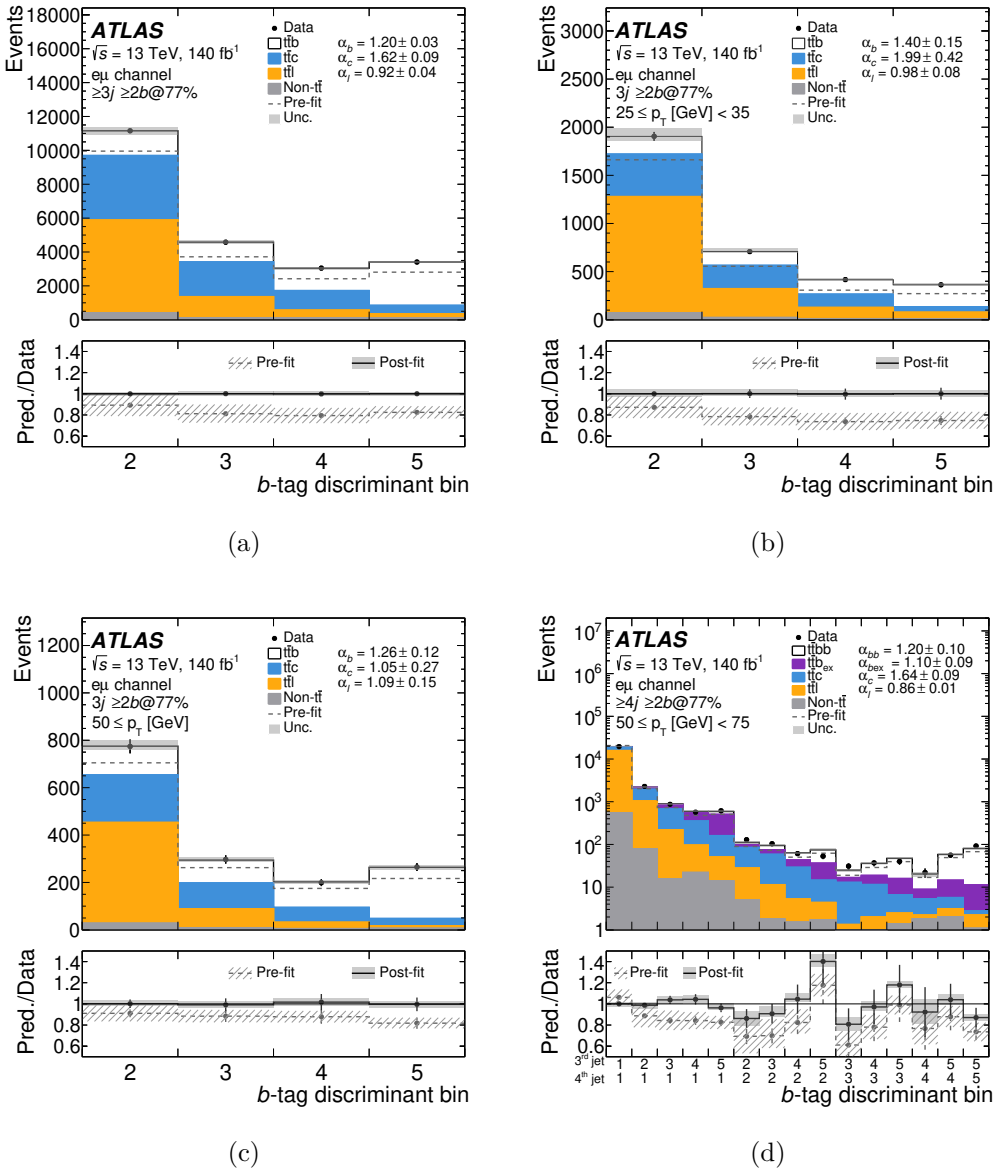

Figure 6. Comparison of data and predictions for the b-tagging discriminant score distributions in (a) the inclusive detector-level $\geq 3j \geq 2b$@77% region considered for the *Global* fit. The score ranging from 1 to 5, correspond to a certain range of b-tagging efficiencies defined by the working points: 100%–85%, 85%–77%, 77%–70%, 70%–60%, and $< 60\%$, respectively. (b), (c) and (d) show the distributions of discriminant score in the multiple binned sub-regions used for *Kinematic-dependent* fit in the p_{T} ranges of the third highest-p_{T} jet in the event. (b) 25–35 GeV and (c) > 50 GeV for the jet p_{T} sub-regions in the $3j \geq 2b$@77% region, and (d) for the jet p_{T} between 50–75 GeV in the region $\geq 4j \geq 2b$@77%. The two dimensional $\geq 4j \geq 2b$@77% templates representing the third and fourth b-tagging discriminant-ranked jet are flattened into one dimension. The dashed lines in the upper panel show the pre-fit total predictions, and the stacked histograms show the contributions scaled according to the results of the fit. The ratio of total predictions before and after the fit to the data are shown in the lower panel. The vertical bars in each ratio represents only the statistical uncertainty, and the shaded bands represent the total error including the systematic uncertainties from experimental sources. The extracted scale factors α_l, α_c, α_b and α_{bb} are given considering only statistical uncertainties.

JHEP01(2025)068

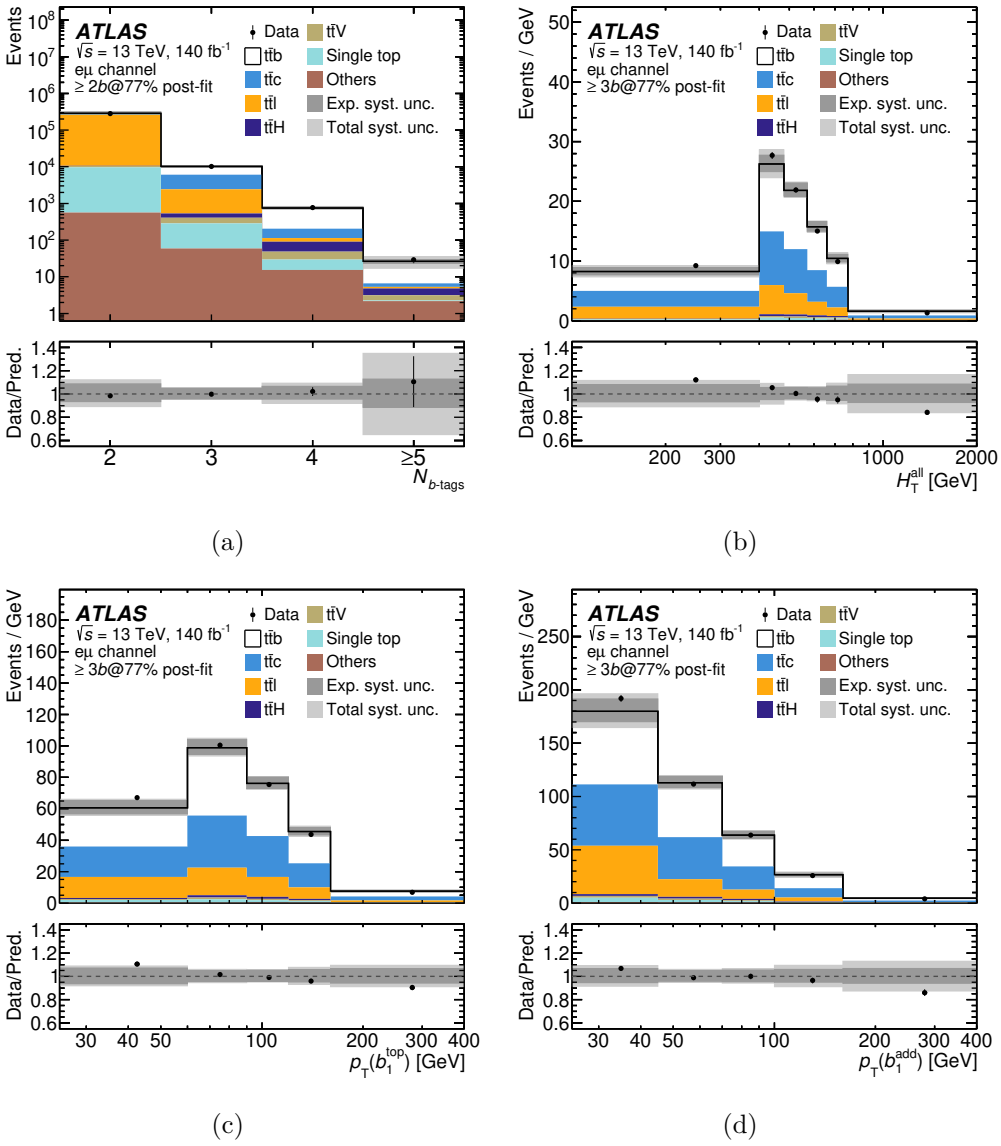

Figure 7. Comparison of data and predictions for the distribution of (a) the number of b-tagged jets for events with at least two b-tagged jets ($N_{b-\text{tags}}$), (b) $H_{\text{T}}^{\text{all}}$, (c) p_{T} (b_1^{top}), and (d) p_{T} (b_1^{add}) in reconstructed events with three or more b-tagged jets after the *Global* scale factors are applied for different event categories as discussed in text (see section 8.1). The entries in each bin are divided by the bin width in the (b), (c) and (d) distributions. The lower panels show the ratios of the data to the predictions. The inner band includes the uncertainties due to limited MC statistics and due to various detector effects such as the jet energy scale and resolution, the b-tagging, and the fit method, while the outer band also includes the theoretical uncertainties in the signal and background modelling. The last bin includes the overflow.

JHEP01(2025)068

8.2 Unfolding

The measured distributions at the detector level are unfolded to the stable particle level. The unfolding procedure corrects for resolution effects and for detector efficiencies and acceptances. An iterative Bayesian unfolding technique [108], as implemented in the RooUnfold software package [109], is used.

First, for each of the observable distributions, the number of non-$t\bar{t}$, $t\bar{t}V$, $t\bar{t}H$ and other rare background events in bin k (N^k_{bkg}), as described in section 7, are subtracted from the data distribution at the detector level (N^k_{data}). This retains a mixture of signal and mis-tagged $t\bar{t}c$ and $t\bar{t}l$ background events. A series of corrections are then applied, with all corrections derived from nominal simulated $t\bar{t}$ events after the $t\bar{t}c$, $t\bar{t}l$ and $t\bar{t}b$ event categories are scaled using the *Global* scale factors as described in section 8.1. These correction factors are determined separately for the $t\bar{t}b$ and $t\bar{t}b\bar{b}$ categories of the fiducial definitions. The background-subtracted data are first corrected for the mis-tagged $t\bar{t}c$ and $t\bar{t}l$ background events by applying the correction ($f^k_{t\bar{t}b}$) for the mis-tagged $t\bar{t}c$ and $t\bar{t}l$ background events defined as

$$f^k_{t\bar{t}b} = \frac{\mathcal{S}^k_{t\bar{t}b,\text{reco}}}{\mathcal{S}^k_{t\bar{t}b,\text{reco}} + \mathcal{B}^k_{t\bar{t}b,\text{reco}}},$$

where $\mathcal{S}^k_{t\bar{t}b,\text{reco}}$ is the number of detector-level events belonging to the $t\bar{t}b$ category, and $\mathcal{B}^k_{t\bar{t}b,\text{reco}}$ is the number of detector-level $t\bar{t}c$ and $t\bar{t}l$ events in bin k as predicted by the MC simulation after the global scale factors are applied. Next, an acceptance correction, f^k_{accept}, is applied, which corrects for the fiducial acceptance and is defined as the probability of a $t\bar{t}b$ event satisfying the detector-level selection in a given bin k ($\mathcal{S}^k_{t\bar{t}b,\text{reco}}$) to also fall within the fiducial particle-level phase space ($\mathcal{S}^k_{t\bar{t}b,\text{reco}\wedge\text{part}}$). It is estimated as

$$f^k_{\text{accept}} = \frac{\mathcal{S}^k_{t\bar{t}b,\text{reco}\wedge\text{part}}}{\mathcal{S}^k_{t\bar{t}b,\text{reco}}}$$

with values ranging from 0.97 to 1.

The remaining part of the unfolding procedure consists of inverting the migration matrix $\mathcal{M}$ to correct for the resolution effects and subsequently correcting for detector inefficiencies. The matrix, $\mathcal{M}$, represents the probability for a particle-level event in bin i to be reconstructed in bin k. The chosen binning is optimised for each distribution to have a migration matrix with a large fraction ($\sim 60\%$) of events on the diagonal and a sufficient number of events in each bin. The Bayesian unfolding technique performs the effective matrix inversion, $\mathcal{M}^{-1}_{ik}$, iteratively. Four iterations are used for all measured distributions.

Finally, the factor f^i_{eff} corrects for the reconstruction efficiency and is defined as

$$f^i_{\text{eff}} = \frac{\mathcal{S}^i_{t\bar{t}b,\text{part}\wedge\text{reco}}}{\mathcal{S}^i_{t\bar{t}b,\text{part}}},$$

where $\mathcal{S}^i_{t\bar{t}b,\text{part}}$ is the number of events from $t\bar{t}b$ category passing the particle-level selection in bin i and $\mathcal{S}^i_{t\bar{t}b,\text{part}\wedge\text{reco}}$ is the number of events from $t\bar{t}b$ category in bin i that also satisfy the detector-level selection. This efficiency factor ranges from 20% to 25% (10% to 20%) for the observables defined in phase space with at least three (four) b-jets.

JHEP01(2025)068

The unfolding procedure for an observable X at particle level can be summarised by the following expression

$$N^i_{\text{unfold}} = \frac{1}{f^i_{\text{eff}}} \sum_k \mathcal{M}^{-1}_{ik}\, f^k_{\text{accept}}\, f^k_{t\bar{t}b}\, (N^k_{\text{data}} - N^k_{\text{bkg}}), \tag{8.3}$$

where N^i_{unfold} is the number of events in bin i of the unfolded distribution, and the summation runs over the bin k of the reconstructed distribution. The total fiducial cross-sections (σ^{fid}) are obtained from the expression for N^i_{unfold} with the bin i taken as the entire fiducial region and dividing this by intergrated luminosity $\mathcal{L}$. Results from the unfolded distributions are presented in terms of a normalised differential cross-section given by

$$\frac{1}{\sigma^{\text{fid}}} . \frac{\mathrm{d}\sigma^{\text{fid}}}{\mathrm{d}X^i} = \frac{N^i_{\text{unfold}}}{\Delta X^i \sum_i N^i_{\text{unfold}}},$$

where ΔX^i is the bin width.

The terms f^i_{eff}, $\mathcal{M}^{-1}_{ik}$, f^k_{accept}, $f^k_{t\bar{t}b}$ and N^k_{bkg} are different for the different systematic variations discussed in section 9. The nominal distributions of unfolding corrections, namely f^i_{eff}, $\mathcal{M}^{-1}_{ik}$, f^k_{accept} and $f^k_{t\bar{t}b}$, are obtained using the nominal $t\bar{t}$ MC samples after the *Global* scale factors as given in table 5 are applied, which do not bias the efficiency and acceptance corrections or the migration matrix. The *Kinematic-dependent* scale factors given in table 5 are applied only as a systematic variation on the $t\bar{t}l$ and $t\bar{t}c$ background estimates due to the fit method. The *Global* method is used to re-derive the scale factors for each systematic uncertainty component considered, and the uncertainties in the unfolded results are evaluated as discussed in section 9.

Various tests are performed to check for any biases due to the choice of the nominal unfolding matrix. The pseudo-data distributions are generated after reweighting the distributions from the nominal $t\bar{t}$ sample to the alternative distributions. Three different reweighting scenarios are considered, and the pseudo-data distributions obtained after the reweighting are unfolded using the nominal response matrix. In the first case, the weight functions are derived from the ratio of the detector-level distributions in the data to the nominal $t\bar{t}$ sample, and the weights are applied to the nominal $t\bar{t}$ events depending on the particle-level variables. In the second case, the weights are obtained after taking the ratio of Sherpa $t\bar{t}$ to the Powheg+Pythia 8 $t\bar{t}$ predictions as a function of the observable in question and applied to the nominal $t\bar{t}$ events as a function of particle-level variable. In the third case, an alternative kinematic variable, unrelated to the distribution being unfolded, is selected, and the weights are derived from the ratio of data and MC simulated distribution of this variable. The events in the nominal sample are then reweighted using these weights to produce reweighted distributions. The differences in each bin of the resulting unfolded distribution are found to be compatible with the corresponding expectations within systematic uncertainties, hence validating that the unfolding model does not introduce any biases in the measurements.

9 Statistical and systematic uncertainties

Various sources of uncertainties affecting the measurements are described in this section. The effects of finite numbers of data and MC events are evaluated after generating pseudo-

JHEP01(2025)068

experiments as described in section 9.1. Experimental sources of uncertainties are described in section 9.2, sources of uncertainties in $t\bar{t}$ modelling are described in section 9.3, and the uncertainties in the background estimates are described in section 9.4.

9.1 Statistical uncertainties

The impact of the statistical uncertainty in the data is evaluated after generating 1000 pseudo-experiments by fluctuating the data in each bin i of the reconstructed distribution based on a Poisson distribution $P(N^i_{\text{obs}})$ with a mean value of N^i_{obs}, which represents the observed number of events in bin i. The reconstructed distribution obtained from each pseudo-experiment is unfolded using the nominal unfolding matrix, and the standard deviation in each bin of the resulting particle level distributions is taken as the statistical uncertainty in that bin. A similar procedure is used to estimate the effect of the statistical uncertainties in the MC simulation-based quantities in eq. (8.3), where the predictions in each bin are fluctuated according to a Gaussian distribution to generate the pseudo-experiments.

9.2 Experimental uncertainties

As discussed in section 4.1, the efficiencies of physics object reconstruction and identification may differ between data and the MC simulation. The uncertainties in the scale factors to correct for the efficiency differences between data and simulation in lepton trigger [100, 101], reconstruction, identification and isolation [87, 89] are taken into account by varying the scale factors within their uncertainties. These efficiencies are estimated in data using a tag-and-probe technique in $Z \to e^+e^-$ and $Z \to \mu^+\mu^-$ events. The electron (muon) momentum scale and resolution are determined using the measurement of the position and width of the Z boson peak in $Z \to e^+e^-(\mu^+\mu^-)$ events. The lepton-related uncertainties are considerably smaller than the jet energy scale and flavour-tagging efficiency uncertainties discussed below.

Jets are calibrated using a series of simulation-based corrections and in situ techniques [93]. The uncertainties due to the jet energy scale (JES) are estimated by using a combination of simulation, test-beam data and in situ measurements. Contributions from the jet-flavour composition, η-intercalibration, leakage of the hadron showers beyond the extent of the hadronic calorimeters (punch-through), single-particle response, calorimeter response to different jet flavours, and pile-up are taken into account, resulting in 30 independent uncertainty components. The total uncertainty due to the JES is one of the dominant uncertainties in this analysis.

The jet energy resolution (JER) is measured using both data and simulation [93]. First, the resolution in the simulation is determined by comparing the particle-level and reconstructed jet p_{T} in simulation as a function of the jet p_{T} and η. Second, an in situ measurement of the JER is made using the *dijet balance* method in dijet data events. The resolution in data and simulation are compared and the energies of jets in the simulation are smeared to match the resolution observed in data. In total eight independent uncertainty components are used. The uncertainties in the JER stem from uncertainties in both the MC modelling of the JER and the data-driven method.

The JVT is calibrated using $Z(\to \mu\mu)$+jet events where the jet balances the p_{T} of the Z boson. Scale factors binned in jet p_{T} are applied to each event to correct for small

JHEP01(2025)068

differences in the JVT efficiency between the data and simulation. The uncertainty in the efficiency to satisfy the JVT requirement is evaluated by varying the scale factors within their uncertainties [94].

Differences in the b-tagging efficiencies between the data and simulation are corrected using scale factors derived from events containing two leading jets in the dilepton $t\bar{t}$ enriched sample [97] as a function of jet p_{T}. The c-jet mistagging efficiency calibration is derived from lepton+jets $t\bar{t}$ [110] as a function of jet p_{T} with uncertainties in the range of 12%–19%. A negative tag method is used to calibrate mis-tagged light-flavour jets with a precision of 18%–31% [111]. The scale factors are measured for different efficiency working points. The associated flavour-tagging uncertainties, including the high-p_{T} extrapolations, are computed by varying the scale factors within their uncertainties. In total, there are 49 components related to the b-tagging efficiencies and 22 (24) components related to the mis-tag rates of c-jets (light-flavour jets).

The uncertainty in the pile-up reweighting of the reconstructed events in the simulation is estimated by comparing the distribution of the number of primary vertices in the simulation with the one in the data as a function of the instantaneous luminosity. Differences between these distributions are adjusted by scaling the mean number of pp interactions per bunch crossing in the simulation and the ± 1 standard deviation (s.d.) uncertainties are assigned to these scaling factors. The pile-up weights are recalculated after varying the scale factors within their uncertainties.

The uncertainty in the combined 2015-2018 integrated luminosity is 0.83% [99], obtained using the LUCID-2 detector [34] for the primary luminosity measurements, complemented by measurements using the inner detector and calorimeters.

All experimental uncertainties affecting the backgrounds (N^k_{bkg}), the corresponding fitted values of $t\bar{t}b$, $t\bar{t}c$ and $t\bar{t}l$ scale factors, and the unfolding correction factors (f^i_{eff}, $\mathcal{M}^{-1}_{ik}$, f^k_{accept}, $f^k_{t\bar{t}b}$) are propagated to the unfolded results after repeating the fitting and reweighting procedure for each systematic variation. Various methods are explored for the evaluation of the impact of dominant uncertainty components, such as the JES, to the unfolded results, and the outcomes are compared with the well established approach, where the data distribution is unfolded using eq. (8.3) with varied simulation-based quantities and where the uncertainty is taken as the difference between the result and the nominal unfolded distribution. In the end, a technically convenient approach is taken for each experimental uncertainty component without affecting the estimated size of its impact on the unfolded results. The detector-level pseudo-data distribution constructed from the predicted signal and estimated background with a varied uncertainty component is unfolded using the nominal unfolding distributions, and the result is compared to the corresponding particle-level distribution ($\mathcal{S}^i_{t\bar{t}b,\mathrm{part}}$) of the reweighted signal sample, and the relative difference is taken as an uncertainty.

The statistical uncertainties in the $t\bar{t}b$, $t\bar{t}c$ and $t\bar{t}l$ global scale factors fits are taken into account as ± 1 s.d. variations in those scale factors as given in table 5. Individual components of reconstruction- and particle-level distributions of the nominal MC sample are reweighted with varied scale factors. The detector-level distribution from that reweighted sample is unfolded with the nominal unfolding corrections as described in section 8.2, and the result is compared with the particle-level distribution from the corresponding reweighted

JHEP01(2025)068

sample. The relative difference in each bin is taken as the systematic uncertainty. Additional uncertainties are attributed to the shape differences of the $t\bar{t}c$ and $t\bar{t}l$ background estimates where the alternative fit set-up depending on the jet p_{T} and multiplicity, as presented in table 5, is used. These are evaluated as the relative difference between the nominal unfolded data distribution and the unfolded distribution obtained when the $t\bar{t}c$ and $t\bar{t}l$ background estimates are taken from the alternative fit set-up.

9.3 Signal modelling uncertainties

Uncertainties due to the choice of the $t\bar{t}$ MC generator settings affecting the $t\bar{t}c$ and $t\bar{t}l$ background predictions and the signal modelling are evaluated as follows. Individual components in each alternative $t\bar{t}$ sample are first fit to data using the procedure described in section 8.1, the corresponding samples are then reweighted according to their corresponding fitted scale factors following the same procedure as applied to the nominal Powheg+Pythia 8 sample. Unless stated otherwise, the uncertainties in the results are evaluated after unfolding the detector-level pseudo-data distributions from alternative $t\bar{t}$ samples, described in section 3, using the nominal unfolding set-up as described in section 8.2. The unfolded distributions are then compared with the particle-level distributions from the alternative sample and the relative difference in each bin is taken as the systematic uncertainty.

Uncertainties related to the QCD scale variations in the matrix element predictions are evaluated by varying the renomalisation (μ_{R}) and factorisation (μ_{F}) scale settings in the Powheg+Pythia 8 sample by a factor of 0.5 or 2 independently. The momentum scale, $\mu_{\mathrm{R}}^{\mathrm{ISR}}$, for the initial-state radiation produced by parton shower is varied using the `var3cUp` / `var3cDown` parameter settings in the A14 Pythia 8 tune. The uncertainties in the tuning of final-state radiation in the parton shower are obtained by changing the momentum scale settings of $\mu_{\mathrm{R}}^{\mathrm{FSR}}$ associated with this radiation in Pythia 8 by a factor of 0.625 or 2 relative to the nominal scale. A higher scaling factor than 0.5 is used for the downward variation to avoid spurious generator weights and to keep the upward and downward variations symmetrical. All of these variations are obtained using internal MC generator weights available in the nominal Powheg+Pythia 8 sample, leading to eight alternative models of Powheg+Pythia 8 with independently varied hard-scatter QCD scales in the matrix element and the parton shower scales of the initial- and final-state radiation. The maximum uncertainty of the up or down variations is taken for each model and then added in quadrature.

The uncertainty in the modelling of first hard emission at the matrix element is evaluated using the Powheg+Pythia 8 sample with the h_{damp} parameter set to twice its nominal value. Uncertainties due to the choice of parton shower, hadronisation and underlying-event model are evaluated using the Powheg+Herwig 7 sample. The uncertainty in the choice of matching between matrix element and parton shower is evaluated using the alternative Powheg+Pythia8 $p_{\mathrm{T}}^{\mathrm{hard}}$ sample. The uncertainty in the modelling of second and subsequent gluon radiation from b-quarks in $t \to bW$ decay is evaluated by using the Powheg+Pythia8 `recoilToTop` sample that predicts slightly different energy clustering around the b-jets. The uncertainty due to the choice of PDF is evaluated following the PDF4LHC prescription [56].

An additional uncertainty is assigned due to discrepancies in the simulated top and anti-top quark p_{T} and $m_{t\bar{t}}$ spectra of Powheg+Pythia8 relative to the predictions from the

JHEP01(2025)068

NNLO QCD + NLO EW theory calculations [112]. The POWHEG+PYTHIA8 events are first reweighted iteratively to match the parton-level distributions of the p_{T} of top and anti-top quark and the $m_{t\bar{t}}$ distribution, and then the flavour composition scale factors are extracted using the nominal fit set-up as discussed in section 8.1. The data distributions are unfolded using these reweighted and corrected distributions, the results are then compared to the nominal unfolded data distributions and the relative difference is taken as the uncertainty.

9.4 Background modelling uncertainties

The uncertainties associated with the background estimations are propagated to the unfolded distributions. These are evaluated by independently varying the estimates upward or downward by their uncertainties before subtracting them from the data distributions. The unfolded distribution obtained from the varied background-subtracted detector-level data distribution is compared with the nominal unfolded data distribution and the relative difference in each bin of the distribution is taken as the systematic uncertainty.

The uncertainty in the number of single-top-quark events due to the interference between $t\bar{t}$ and tW amplitudes is evaluated by comparing the nominal tW background prediction (diagram-removal scheme) with an alternative sample generated with the diagram-subtraction scheme [81]. The uncertainties due to QCD scales μ_{R} and μ_{F} dependence in the matrix elements and due to the scale dependence of the initial- and final-state radiation predicted by the parton shower model is taken into account. The uncertainties in parton shower and hadronisation models are evaluated by comparing the nominal estimate to that obtained using the POWHEG+HERWIG 7 sample. The matching uncertainty in the matrix element prediction is evaluated by comparing the nominal estimate to that obtained from MG5_aMC@NLO+PYTHIA8.

The uncertainties in $t\bar{t}H$ predictions are evaluated by independently varying the μ_{R} and μ_{F} scales in the matrix element by factors of 0.5 and 2. The $\mu_{\mathrm{R}}^{\mathrm{ISR}}$ scale for the initial-state radiation produced by the parton shower is varied using the `Var3c` variations. The $\mu_{\mathrm{R}}^{\mathrm{FSR}}$ scale uncertainty for the final-state radiation in the parton shower is evaluated by varying this scale by 0.625 or 2. The parton shower, hadronisation and underlying-event uncertainties are taken from comparisons with the POWHEG+HERWIG 7 sample and the NLO matrix element matching uncertainty is evaluated using MG5_aMC@NLO+PYTHIA8. Additionally, the 10% theoretical uncertainty in the inclusive cross-section [113], is taken into account.

A normalisation uncertainty of 12% due to theoretical uncertainty in the inclusive cross-section calculations of $t\bar{t}V$ processes is considered similar to that reported in ref. [114–116]. The μ_{R} and μ_{F} QCD scales in matrix element are varied by factors of 0.5 and 2 to evaluate the shape uncertainty in kinematic distributions. An additional conservative uncertainty of 30% is applied due to the modelling of the matrix element matching with the parton shower algorithm based on the comparisons of different MC generator predictions in various kinematics distributions as given in ref. [114, 115, 117].

The uncertainty in the non-prompt lepton background is obtained by varying the transfer factor, as discussed in section 7.2, by 25%–30% depending on the leading lepton p_{T} and the multiplicity of b-jets to account for the effects of showering, hadronisation model and matrix-element matching. Furthermore, the modelling uncertainty in the same-sign prompt

JHEP01(2025)068

event yields are evaluated by comparing the nominal MC prediction with those from the alternative MC samples. An additional 6% uncertainty is attributed to the same-sign prompt lepton estimate from the simulation, which is significantly affected by the electron charge misidentification. This uncertainty is estimated from the overall discrepancy in the data distribution of the same-sign events as compared to the MC estimate.

A 35% uncertainty is attributed to the very small background contribution from Z+jets. This uncertainty is based on the estimates of the normalisation factor of this background in various phase space regions involving heavy-flavour jets. The normalisation factors differ by 15% to 35% from unity, and a conservative estimate of 35% is taken as an uncertainty in the MC prediction of Z+jets background with negligible impact on the measurements [118, 119]. The uncertainty due to the backgrounds from diboson and other rare processes is evaluated by independently varying their estimates by conservative uncertainties of 50%. These uncertainties have no impact on the results.

10 Results

The unfolded results in this section are presented as fiducial cross-sections and as normalised fiducial differential cross-sections at the particle level as a function of the b-jet multiplicity, additional l/c-jet multiplicity, global event properties, and kinematic variables. Table 6 lists the measured fiducial cross-sections for $t\bar{t}$+b-jets production in the phase space with three b-jets ($\geq 3b$), at least three b-jets and one or more l/c-jet ($\geq 3b \geq 1l/c$), at least four b-jets ($\geq 4b$) and least four b-jets with one or more l/c-jet ($\geq 4b \geq 1l/c$). Table 7 lists the contributions to the uncertainty in fiducial cross-sections, among which the most precise measurement in the $\geq 3b$ fiducial phase space has an uncertainty of 8.5%. The uncertainties are predominantly systematic, stemming mainly from b-tagging, JES, and $t\bar{t}$ modelling. The precision of the results presented here surpasses that of previous fiducial measurements of $t\bar{t}$+b-jets production using partial 13 TeV ATLAS data [24]. This improvement is due to increased number of data events and a significant reduction in uncertainties related to parton shower, hadronisation, and underlying event models as implemented in Pythia 8 and Herwig 7. Additionally, the updated matrix element uncertainty recommendations, as detailed in refs. [120–122], and improved luminosity calibrations [99] have contributed to this enhancement. The largest gain in precision results from the upgrade in the MC modelling leading to a reduction in the parton shower, hadronisation and underlying event modelling uncertainty by a factor of two. The relative size of the uncertainties due to experimental sources such as the JES and b-tagging are comparable to those in the previous ATLAS results. The measured values of fiducial cross-sections are not fully comparable due to slight differences between the particle-level lepton p_{T} thresholds.

The achieved precision in the fiducial measurements is better than the current uncertainties in the theoretical predictions of fiducial cross-sections, which typically range from 20% to 50%. The results are summarised in figure 8, and compared with $t\bar{t}b\bar{b}$ NLO MC predictions from Powheg+Pythia 8 $t\bar{t}b\bar{b}$, Powheg+Herwig 7 $t\bar{t}b\bar{b}$, Sherpa $t\bar{t}b\bar{b}$, and the Helac-NLO $e\mu + 4b$ calculations including the offshell effects, as well as with the $t\bar{t}$ NLO MC predictions from Powheg+Pythia 8, Powheg+Herwig 7, MadGraph5_aMC@NLO+Pythia 8, MadGraph5_aMC@NLO+Herwig 7, and Sherpa. Predictions that calculate the $t\bar{t}$

JHEP01(2025)068

Fiducial phase space	Fiducial cross-sections [fb]			
	$\geq 3b$	$\geq 3b \geq 1l/c$	$\geq 4b$	$\geq 4b \geq 1l/c$
Measured	143 ±1 (stat) ±12 (syst)	87 ±1 (stat) ±8 (syst)	22 ±1 (stat) ±3 (syst)	14 ±1 (stat) ±2 (syst)
Powheg+Pythia 8 $t\bar{t}b\bar{b}$ (4FS)	132	78	23	14
Powheg+Pythia 8 $t\bar{t}b\bar{b}$ h_{bzd} (4FS)	129	74	21	13
Powheg+Pythia 8 $t\bar{t}b\bar{b}$ dipole (4FS)	128	71	22	13
Powheg+Pythia 8 $t\bar{t}b\bar{b}$ $p_{\mathrm{T}}^{\mathrm{hard}}$ (4FS)	129	68	21	12
Powheg+Herwig 7 $t\bar{t}b\bar{b}$ (4FS)	130	77	22	14
Sherpa $t\bar{t}b\bar{b}$ (4FS)	135	90	21	15
Helac-NLO (off-shell) $e\mu + 4b$	–	–	20	–
Powheg+Pythia 8 $t\bar{t}$ (5FS)	120	74	18	11
Powheg+Herwig 7 $t\bar{t}$ (5FS)	128	75	18	11
MG5_aMC@NLO+Pythia8 $t\bar{t}$ (5FS)	122	72	18	11
MadGraph5_aMC@NLO+Herwig 7 $t\bar{t}$ (5FS)	110	66	13	8
Sherpa 2.2.12 $t\bar{t}$ (5FS)	124	73	16	10

Table 6. Measured and predicted fiducial cross-section results for additional b-jet production in four phase-space regions. The dashes (–) indicate that the predictions are not available. The differences between the various MC generator predictions are smaller than the size of theoretical uncertainties (20%–50%, not presented here) in the predictions.

production matrix element at NLO, but rely on the parton shower for the high jet multiplicities (Powheg+Pythia 8, Powheg+Herwig 7, MadGraph5_aMC@NLO+Pythia 8, MadGraph5_aMC@NLO+Herwig 7) show slightly lower rates of events with three or four b-jets as compared to those where the additional massive b-quarks are included in the matrix element calculations and all the additional radiations are produced at LO accuracy in the parton shower model (Powheg+Pythia 8 $t\bar{t}b\bar{b}$, Powheg+Herwig 7 $t\bar{t}b\bar{b}$, Sherpa $t\bar{t}b\bar{b}$). The Sherpa (5FS), which models the $t\bar{t}$ pair with one parton at NLO accuracy and up to four additional partons at LO accuracy, also gives a relatively low rate of events with three or four b-jets. The differences between the MC generator predictions are smaller than the theoretical uncertainties in the predictions.

The $t\bar{t}b\bar{b}$ (4FS) predictions (Powheg+Pythia 8 $t\bar{t}b\bar{b}$, Powheg+Herwig 7 $t\bar{t}b\bar{b}$, Sherpa $t\bar{t}b\bar{b}$) describe the data very well in the $\geq 4b$ phase spaces. Slightly smaller cross-sections are predicted by Powheg+Pythia 8 $t\bar{t}b\bar{b}$ and Powheg+Herwig 7 $t\bar{t}b\bar{b}$ models in the $\geq 3b$ fiducial phase spaces as shown in figure 8, however, they are still consistent within the measurement uncertainties. The Helac-NLO $e\mu + 4b$ fixed order parton-level cross-section calculations that includes off-shell effects are compared after correcting for the non-perturbative effects such as multiple parton interactions, beam remnants and hadronisation. These corrections are evaluated by comparing the generator level distribution obtained from the Powheg+Pythia 8 $t\bar{t}b\bar{b}$ MC between set-ups with or without turning off the non-perturbative effects. The size of these corrections reach the level of 10% depending on the observable values.

JHEP01(2025)068

Source	Fiducial cross-section phase space			
	$\geq 3b$ Unc. [%]	$\geq 3b \geq 1l/c$ Unc. [%]	$\geq 4b$ Unc. [%]	$\geq 4b \geq 1l/c$ Unc. [%]
Data statistical uncertainty	1.0	1.2	3.9	4.8
Luminosity	0.8	0.8	0.8	0.8
Jet	3.4	5.2	6.6	8.5
b-tagging	5.1	4.9	6.5	6.4
Lepton and trigger	1.4	1.4	1.2	1.2
Pile-up	0.9	0.7	0.6	0.3
$t\bar{t}c/t\bar{t}l$ fit variation	1.7	1.7	0.8	0.8
$t\bar{t}c/t\bar{t}l$ shape variation	0.2	0.5	0.3	1.6
$t\bar{t}H/t\bar{t}V$ and non-$t\bar{t}$ background	1.1	1.1	2.2	2.4
Detector+background total syst.	6.7	7.6	9.7	11.2
Parton shower and hadronisation	2.9	3.5	1.5	3.6
μ_{R} and μ_{F} scale variations	0.7	0.6	0.2	0.3
Matrix element matching ($p_{\mathrm{T}}^{\mathrm{hard}}$)	1.3	1.1	4.8	7.0
h_{damp}	1.8	1.5	2.9	3.2
ISR	0.1	0.4	0.2	0.3
FSR	3.1	3.6	3.3	3.1
RecoilToTop	1.8	1.9	2.4	3.4
PDF	0.2	0.2	0.1	0.1
NNLO reweighting	0.6	0.5	0.5	0.5
MC statistical uncertainty	0.2	0.2	0.5	0.6
$t\bar{t}$ modelling total syst.	5.2	5.7	7.2	9.7
Total syst.	8.5	9.6	12.1	14.8
Total	8.5	9.6	12.7	15.5

Table 7. Main systematic uncertainties in percentage for particle-level measurement of fiducial cross-sections in the $\geq 3b$, $\geq 3b \geq 1l/c$, $\geq 4b$, and $\geq 4b \geq 1l/c$ phase space.

The central values of the measured fiducial cross-sections remain unaffected if the $\geq 3b$ particle-level events in the Powheg+Pythia 8 (5FS) $t\bar{t}$ sample are replaced by those in the Powheg+Pythia 8 $t\bar{t}b\bar{b}$ (4FS) sample for the unfolding corrections. The precision of the measurements depends significantly on the modelling of misidentified background from $t\bar{t}$+jets events. With the improvement in the background MC modelling, various uncertainties arising from the relative flavour composition corrections in the MC samples are reduced. Theoretical developments in the modelling of $t\bar{t}$+jets for all additional-jet flavours at the higher orders in QCD will benefit future measurements.

Figure 9 shows the measured fiducial normalised distribution of the b-jet multiplicity in the phase space with at least two b-jets and the comparisons with various $t\bar{t}$ (5FS) predictions.

JHEP01(2025)068

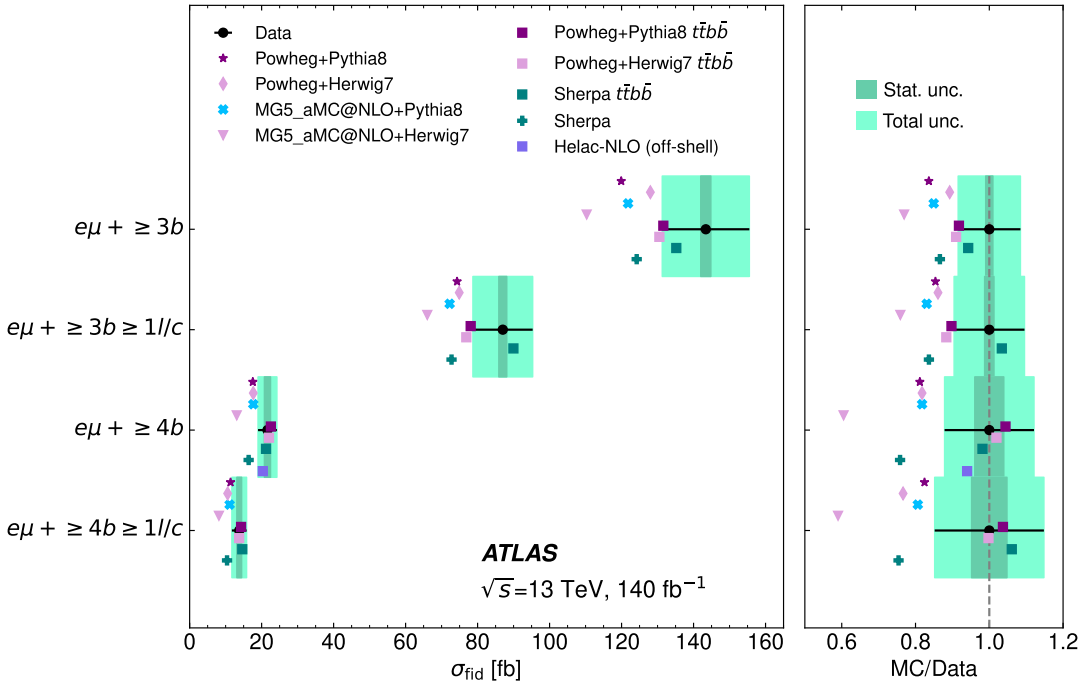

Figure 8. Measured fiducial cross-sections for $e\mu+ \geq 3b$, $e\mu+ \geq 3b \geq 1l/c$, $e\mu+ \geq 4b$, and $e\mu+ \geq 4b \geq 1l/c$ compared with the central values of $t\bar{t}b\bar{b}$ NLO predictions from Powheg+Pythia 8 $t\bar{t}b\bar{b}$, Powheg+Herwig 7 $t\bar{t}b\bar{b}$, Sherpa $t\bar{t}b\bar{b}$, and the Helac-NLO (off-shell) calculations. Comparisons with $t\bar{t}$ NLO MC predictions from Powheg+Pythia 8, Powheg+Herwig 7, MadGraph5_aMC@NLO+Pythia 8, MadGraph5_aMC@NLO+Herwig 7, and Sherpa are also made. The right hand panel shows the ratios of the MC predictions to the data. The inner uncertainty band (dark) is the statistical uncertainty in the data and the outer band (light) includes all uncertainties due to the instrumental and theoretical sources. The differences between the various MC generator predictions are smaller than the size of theoretical uncertainties (20%–50%, not shown) in the predictions.

This observable indicates the relative fractions of the $t\bar{t}$+b-jets rate with zero, one, two or three additional b-jets relative to the total $t\bar{t}$+jets rate in the fiducial phase space. All models are consistent with the data for events with exactly two b-jets, but they face challenges in accurately describing the additional b-jets production in events with three or more b-jets. Figure 10 shows the measured normalised cross-sections as a function of the b-jet and l/c-jet multiplicities, $H_{\text{T}}^{\text{had}}$, and $\Delta R_{\text{avg}}^{bb}$ variables, the distributions are normalised to the fiducial cross-section in the phase space with at least three b-jets. The distributions are compared with various MC predictions obtained at the particle level, and their ratios relative to the measurements are displayed in the lower panels. The large uncertainties due to scale variations in the matrix elements are expected to largely cancel in the normalised predictions in fiducial phase space with three or more b-jets. The $t\bar{t}b\bar{b}$ predictions from Powheg+Herwig 7 $t\bar{t}b\bar{b}$ describes the $H_{\text{T}}^{\text{had}}$ and jet multiplicities reasonably well. The Sherpa $t\bar{t}b\bar{b}$ yields a slightly higher number of events with additional l/c-jets. Distributions such as $\Delta R_{\text{avg}}^{bb}$ show different levels of agreement with data between $t\bar{t}b\bar{b}$ simulations using the 4FS and the 5FS. Although

JHEP01(2025)068

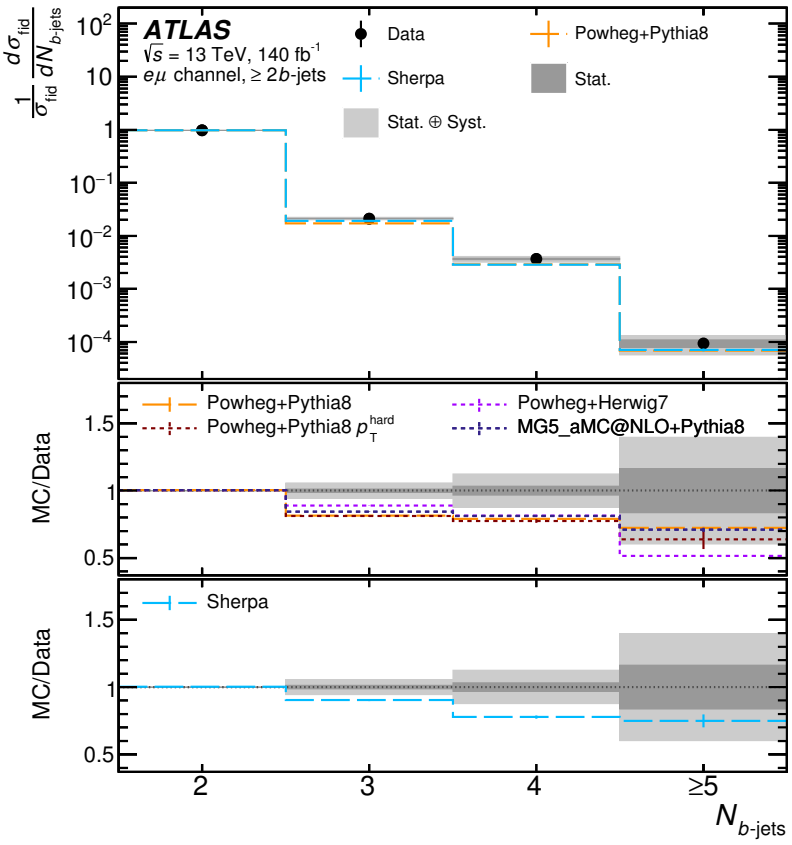

Figure 9. Measured normalised differential cross-section in the phase space with at least two b-jets as a function of the number of b-jets compared with predictions. The lower panels show the ratios of various predictions to the data. The shaded regions show the statistical (dark) and total uncertainties (light) in the measurement. The vertical line on the MC predictions represents the statistical uncertainty. The last bin contains the overflow.

the jets generated by the matrix element generally have higher p_{T} compared to those produced by the parton shower, the matching treatment between the matrix element and the parton shower results in a significant difference.

Figures 11–12 show the kinematics of three leading-p_{T} b-jets and of the b-jets either assigned to the top quarks or to the additional gluon, which are well predicted by MadGraph5_aMC@NLO+Pythia 8, Sherpa and Powheg+Herwig 7 $t\bar{t}b\bar{b}$. Other predictions give varying degrees of consistency with the data distributions within the measurement uncertainties. Figure 13 shows the invariant mass and p_{T} of the system of two leading-p_{T} b-jets or of the b-jet pair assigned to top quark, where the predictions from Powheg+Herwig 7 $t\bar{t}b\bar{b}$ matrix element and MadGraph5_aMC@NLO+Pythia 8 and Sherpa $t\bar{t}$ predictions are closer to the data. Figures 14(a) and 14(b) show the distributions of angular distance in ΔR of the additional b-jet and additional l/c-jet, respectively, relative to the momentum direction of the $e\mu bb$ system. Most predictions agree reasonably with the data in the $\Delta R(e\mu bb^{\mathrm{top}}, b_1^{\mathrm{add}})$ distribution. The $\Delta R(e\mu bb^{\mathrm{top}}, l/c\text{-jet}_1)$ variable probing the dynamics of additional partons in the parton shower, is not so well described by the various MC set-ups. Further compatibility

JHEP01(2025)068

of parton shower models predicting the additional l/c-jets p_{T} and η distributions can be seen in figures 14(c) and 14(d), where various parton shower models have either slightly softer or harder p_{T} spectra than the data. The best agreement is found with the Sherpa $t\bar{t}$ model. A comparison of the relative p_{T} of the leading additional b-jet and the leading additional l/c-jet is made between data and predictions, as shown in figure 14(d), indicating that the additional l/c-jets are typically softer than the leading-p_{T} additional b-jet in the Powheg $t\bar{t}b\bar{b}$ predictions. On the other hand the MadGraph5_aMC@NLO+Pythia 8 $t\bar{t}$, Sherpa $t\bar{t}$, and Sherpa $t\bar{t}b\bar{b}$ give good descriptions of the data for this variable.

The measurements of normalised distributions of the invariant mass and the p_{T} of the two closest b-jets system in the phase space with at least four b-jets are compatible with various predictions as shown in figures 15(a)and 15(b), respectively. The invariant mass and the p_{T} distributions of the two additional b-jets pair as presented in figures 15(c) and 15(d) give similar pictures as expected, because the b-jets with smallest angular separation make significant contributions to the b-jet assignment scheme.

A quantitative assessment of the level of agreement between data and the various predictions is performed by calculating a χ^2 value for each prediction. The χ^2 value is defined as

$$\chi^2 = S_b^T \; V^{-1} \; S_b \,,$$

where V^{-1} is the inverse of the covariance matrix V, calculated for each variable including all statistical and systematic uncertainties that affect the measurements and S_b is a vector of the differences between the measured and predicted cross-sections being tested. The resulting value of the χ^2 calculation is converted into a p-value using the number of degrees of freedom for each variable, which is the number of bins minus one in the case of the normalised differential cross-sections to reflect the normalisation constraint. The uncertainties associated with the MC predictions being tested are not taken into account while computing the p-values.

In the case of normalised distributions, one element of S_b is discarded in the calculation along with the corresponding row and column of the covariance matrix. The resulting χ^2 does not depend on the element of S_b or the row and column of the covariance matrix that is discarded. The p-values summarised in figure 16 (figure 17) for the observables measured in phase space with at least three (four) b-jets give a comprehensive overview of the compatibility of a wide range of measured observables to various predictions. As discussed above, the quantities measured in the phase space with four or more b-jets generally show good agreement with various predictions, but the measurements suffer from the limited amount of data. On the other hand, the difference between any two predictions is relatively larger in the phase space with three or more b-jets; however, the comparisons with data are consistent within the measurement uncertainties for most observables. To facilitate the comparisons with any future MC generator predictions, all measurements together with the correlation matrices will be published in HEPData [123].

11 Conclusion

The fiducial and normalised differential cross-sections of $t\bar{t}$ production in association with b-jets are measured in pp collisions at $\sqrt{s} = 13$ TeV using a data sample corresponding to an

JHEP01(2025)068

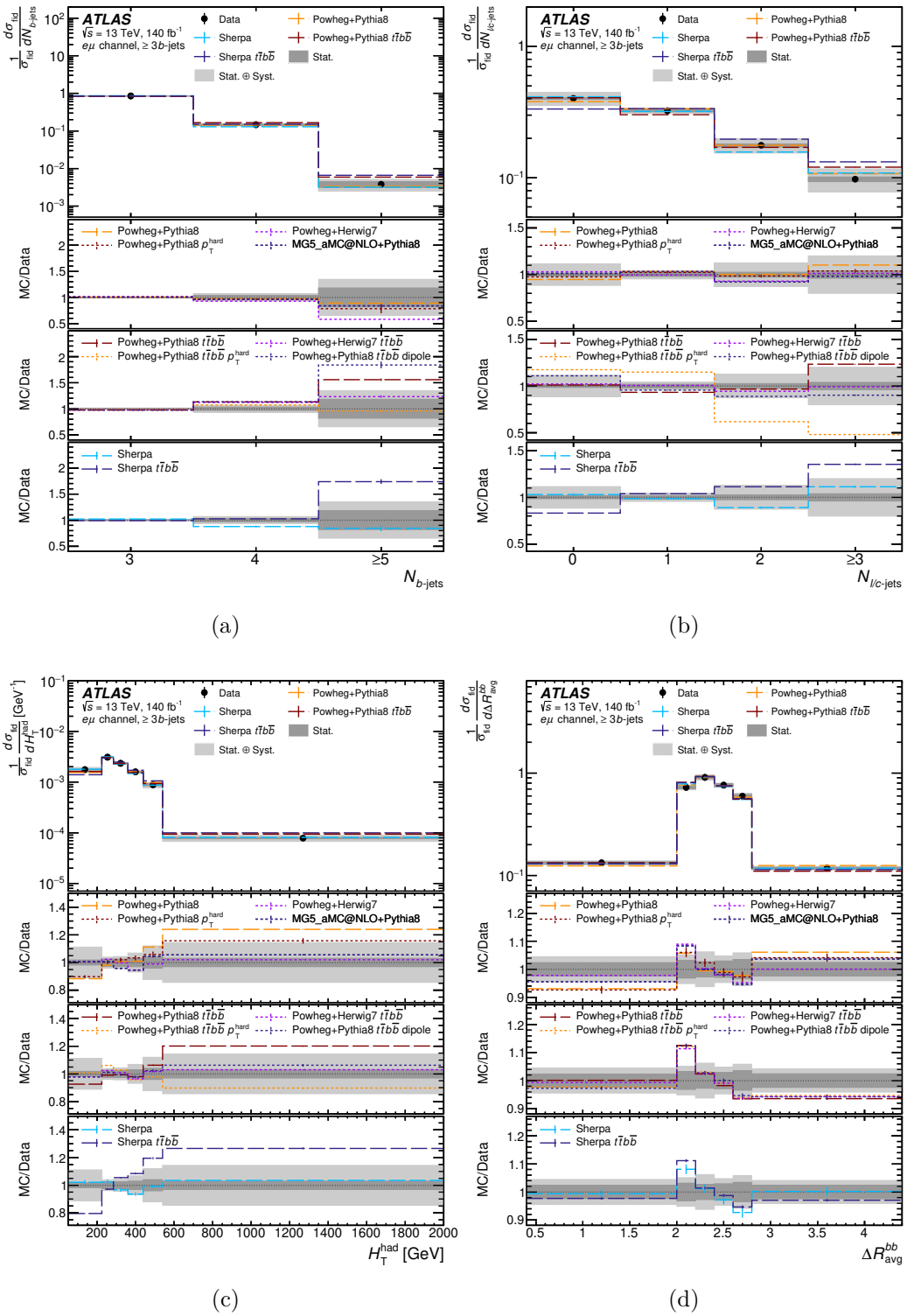

Figure 10. Measured normalised differential cross-section in the phase space with at least three b-jets as a function of (a) b-jet multiplicity, (b) l/c-jet multiplicty, (c) $H_{\mathrm{T}}^{\mathrm{had}}$, and (d) $\Delta R_{\mathrm{avg}}^{bb}$ compared with predictions. The lower panels show the ratios of various predictions to the data. The shaded regions show the statistical (dark) and total uncertainties (light) in the measurement. The vertical line on the MC predictions represents the statistical uncertainty. The last bin contains the overflow.

JHEP01(2025)068

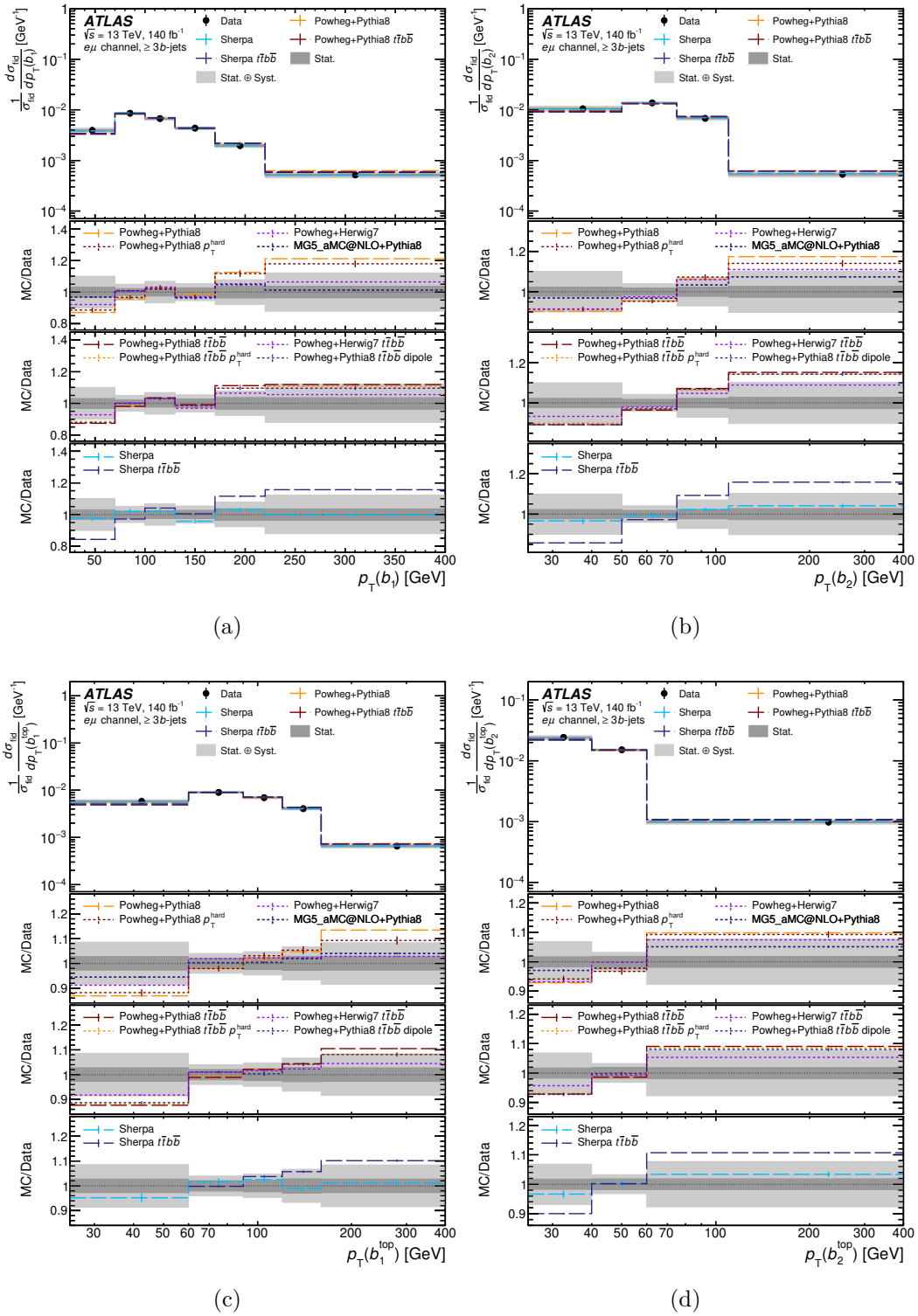

Figure 11. Measured normalised differential cross-section in the phase space with at least three b-jets as a function of (a) $p_{\mathrm{T}}(b_1)$, (b) $p_{\mathrm{T}}(b_2)$, (c) $p_{\mathrm{T}}(b_1^{\mathrm{top}})$, and (d) $p_{\mathrm{T}}(b_2^{\mathrm{top}})$ compared with predictions. The lower panels show the ratios of various predictions to the data. The shaded regions show the statistical (dark) and total uncertainties (light) in the measurement. The vertical line on the MC predictions represents the statistical uncertainty. The last bin contains the overflow.

JHEP01(2025)068

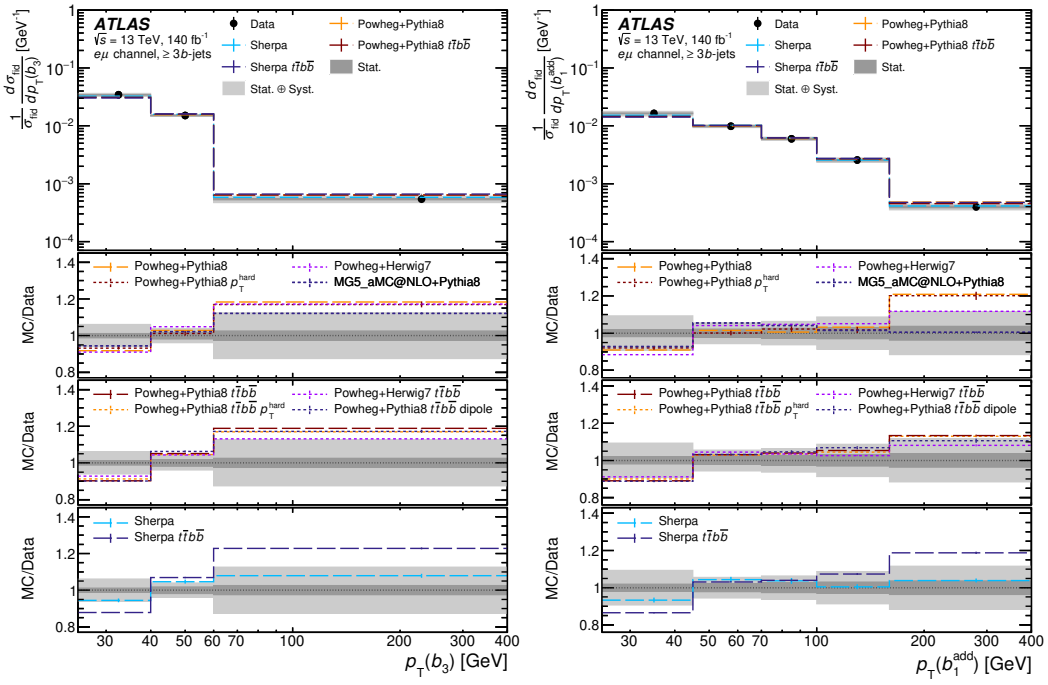

(a) (b)

Figure 12. Measured normalised differential cross-section in the phase space with at least three b-jets as a function of (a) $p_{\mathrm{T}}(b_3)$, and (b) $p_{\mathrm{T}}(b_1^{\mathrm{add}})$ compared with predictions. The lower panels show the ratios of various predictions to the data. The shaded regions show the statistical (dark) and total uncertainties (light) in the measurement. The vertical line on the MC predictions represents the statistical uncertainty. The last bin contains the overflow.

integrated luminosity of 140 fb^{-1} collected by the ATLAS detector at the LHC. The results are presented in the $e\mu$ channel within fiducial phase spaces at the stable particle-level. The fiducial inclusive cross-sections are measured in four phase spaces depending on the number of b-jets and l/c-jets. The measurement precision reaches 8.5% for the $\geq 3b$ phase space, 13% for the $\geq 4b$ phase space, 10% for the $\geq 3b \geq 1l/c$ phase space and 16% for the $\geq 4b \geq 1l/c$ phase space, which are the best to date in the $e\mu$ channel and also better than the theoretical precision of the $t\bar{t}b\bar{b}$ predictions at NLO. Dominant sources of uncertainties are b-tagging, jet energy scale and $t\bar{t}$ modelling uncertainties. The measured fiducial cross-sections are compared with various theoretical predictions, and are found to have good compatibility with $t\bar{t}b\bar{b}$ matrix element (4FS) predictions particularly in the regions with at least four b-jets.

The large variety of variables helps in probing the MC simulations in a comprehensive way. The normalised fiducial differential cross-sections presented as a function of several kinematic variables and global event properties are measured with precisions of 4%–10% (10%–20%) in the $\geq 3b$ ($\geq 4b$) phase space. The b-jets have been assigned to the top decay or gluon radiation, with probabilities of correct assignment varying between 40% and 85%. Most observables are generally well described by the majority of MC predictions. While all models show good agreement with the data for events containing exactly two b-jets, they fail to accurately represent the additional b-jets production in events with three

JHEP01(2025)068

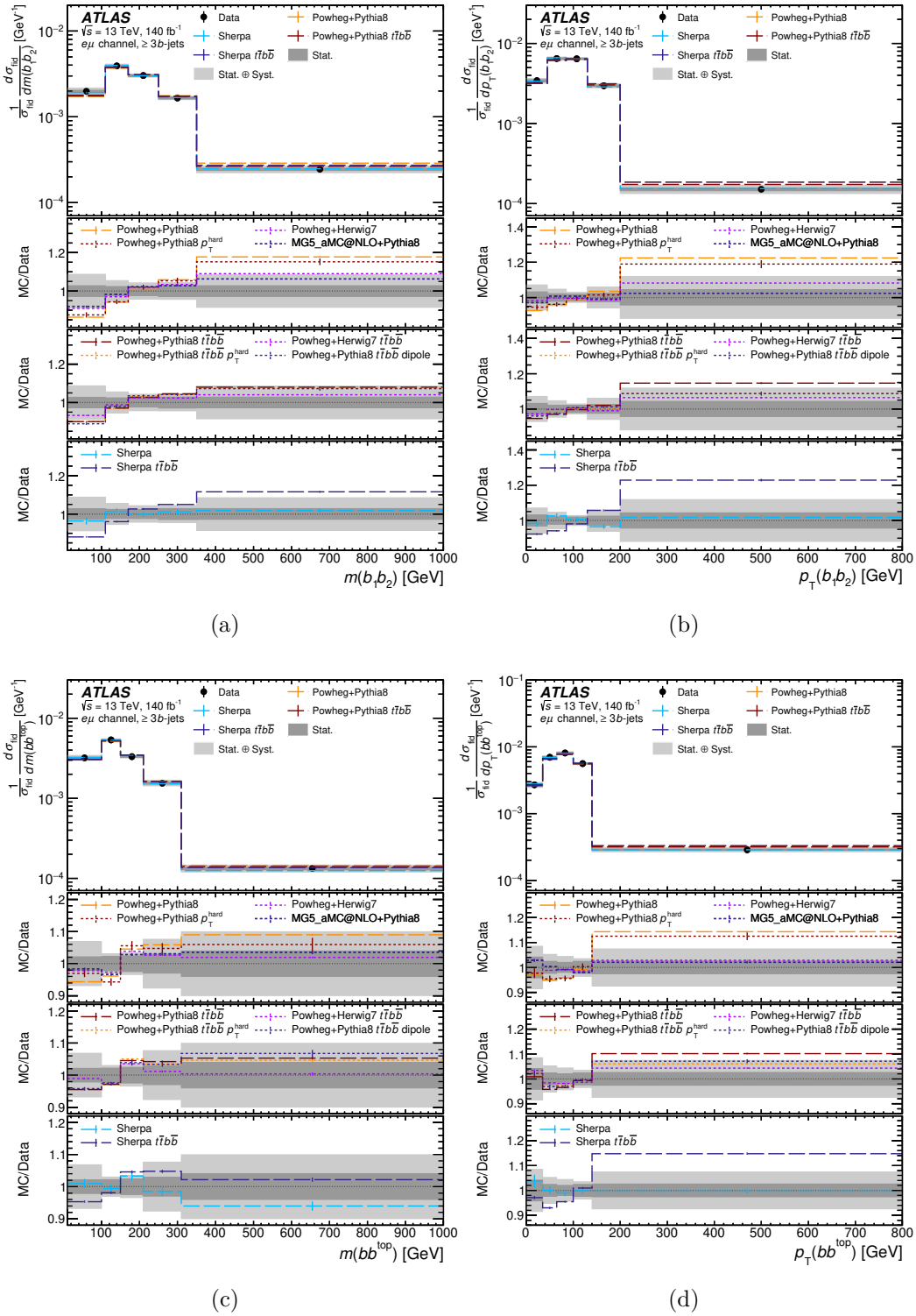

Figure 13. Measured normalised differential cross-section in the phase space with at least three b-jets as a function of (a) $m(b_1b_2)$, (b) $p_{\mathrm{T}}(b_1b_2)$, (c) $m(bb^{\mathrm{top}})$, and (d) $p_{\mathrm{T}}(bb^{\mathrm{top}})$ compared with predictions. The lower panels show the ratios of various predictions to the data. The shaded regions show the statistical (dark) and total uncertainties (light) in the measurement. The vertical line on the MC predictions represents the statistical uncertainty. The last bin contains the overflow.

JHEP01(2025)068

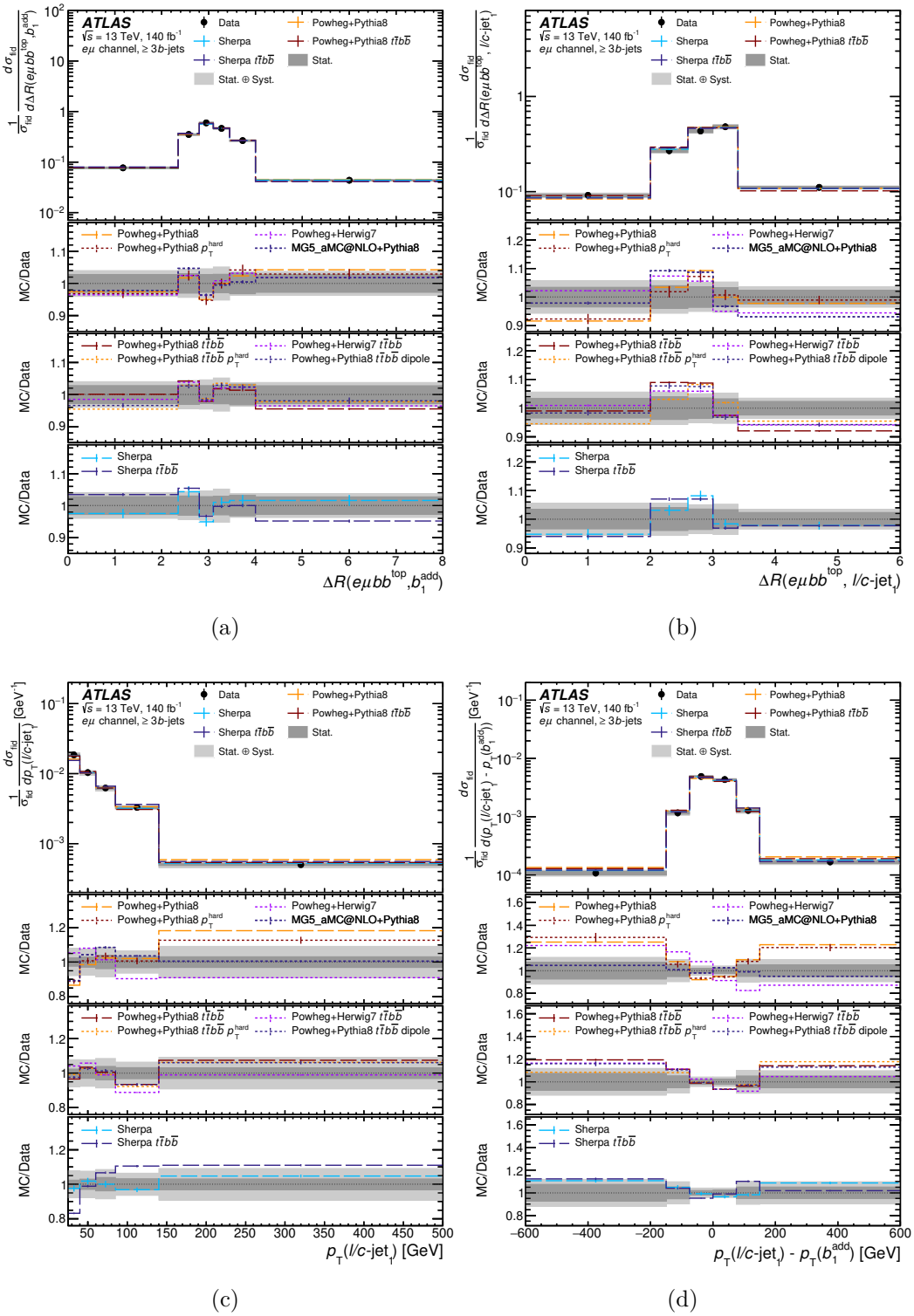

Figure 14. Measured normalised differential cross-section in the phase space with at least three b-jets as a function of (a) $\Delta R(e\mu bb^{\text{top}}, b_1^{\text{add}})$, (b) $\Delta R(e\mu bb^{\text{top}}, l/c\text{-jet}_1)$, (c) $p_{\text{T}}(l/c\text{-jet}_1)$, and (d) $p_{\text{T}}(l/c\text{-jet}_1) - p_{\text{T}}(b_1^{\text{add}})$ compared with predictions. The lower panels show the ratios of various predictions to the data. The shaded regions show the statistical (dark) and total uncertainties (light) in the measurement. The vertical line on the MC predictions represents the statistical uncertainty. The last bin contains the overflow.

JHEP01(2025)068

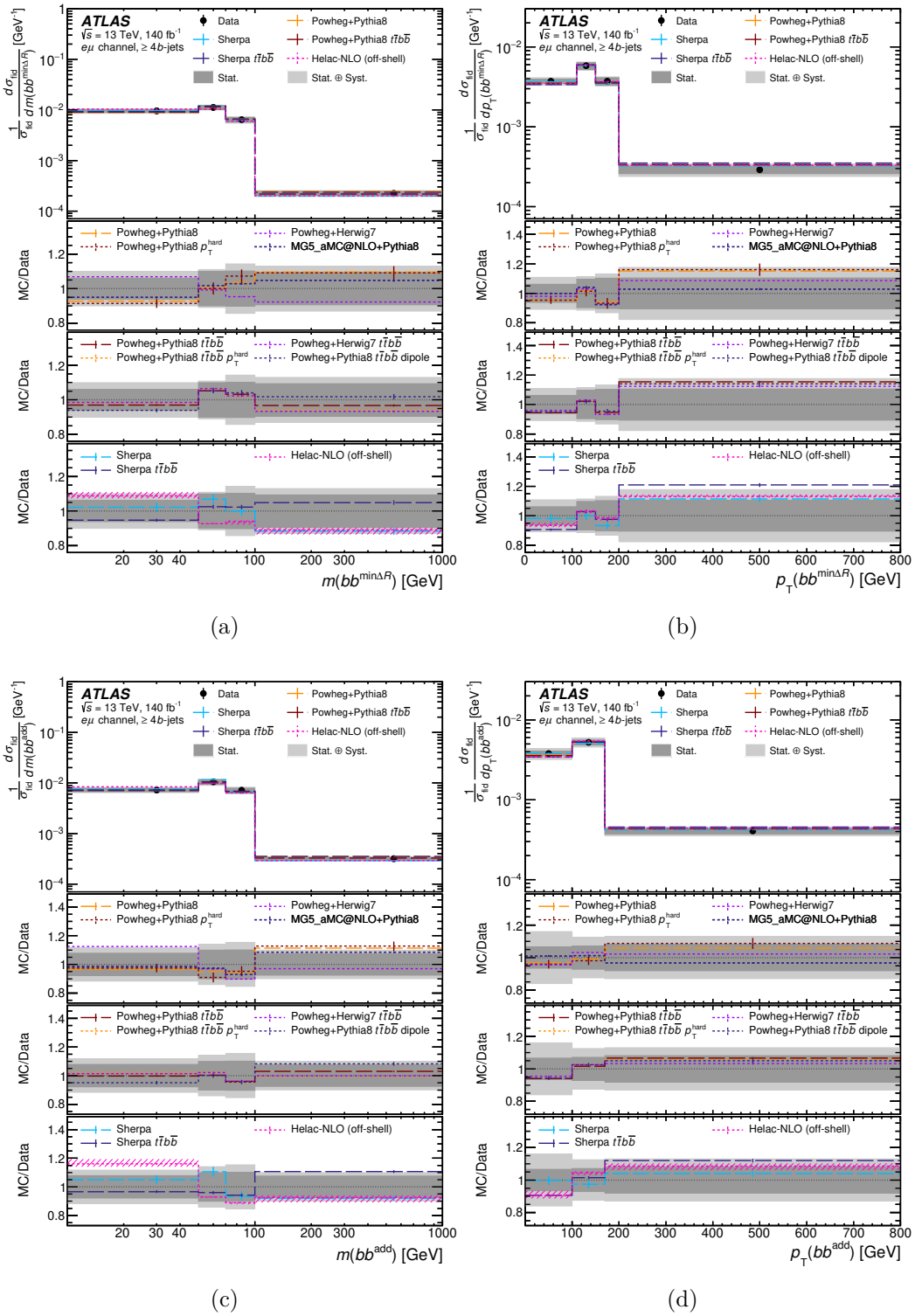

Figure 15. Measured normalised differential cross-section in the phase space with at least four b-jets as a function of (a) $m(bb^{\mathrm{min}\Delta R})$, (b) $p_{\mathrm{T}}(bb^{\mathrm{min}\Delta R})$, (c) $m(bb^{\mathrm{add}})$, and (d) $p_{\mathrm{T}}(bb^{\mathrm{add}})$ compared with predictions. The lower panels show the ratios of various predictions to the data. The hashed band around the HELAC-NLO $e\mu + 4b$ prediction represents the uncertainties obtained from the envelope of seven sets of μ_R, μ_F QCD scale variations. The shaded regions show the statistical (dark) and total uncertainties (light) in the measurement. The vertical line on the MC predictions represents the statistical uncertainty. The last bin contains the overflow, except in the case of HELAC-NLO (off-shell) $e\mu + 4b$ prediction.

JHEP01(2025)068

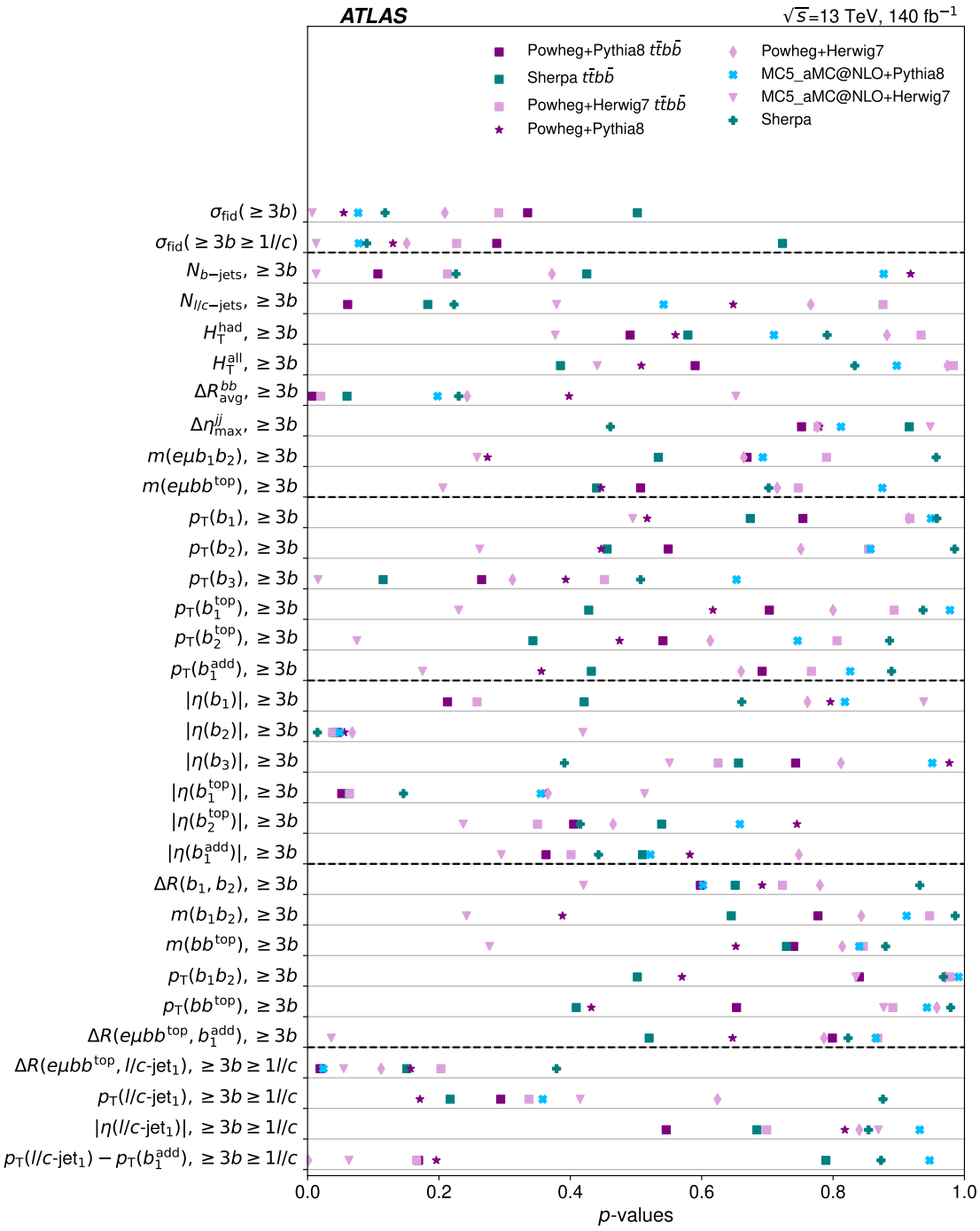

Figure 16. Summary of quantitative comparisons for each observable measurement to predictions in form of p-values. This summary refers to observables measured in the phase space with at least three b-jets. The theoretical uncertainties in the MC predictions are not taken into account when computing the p-values.

JHEP01(2025)068

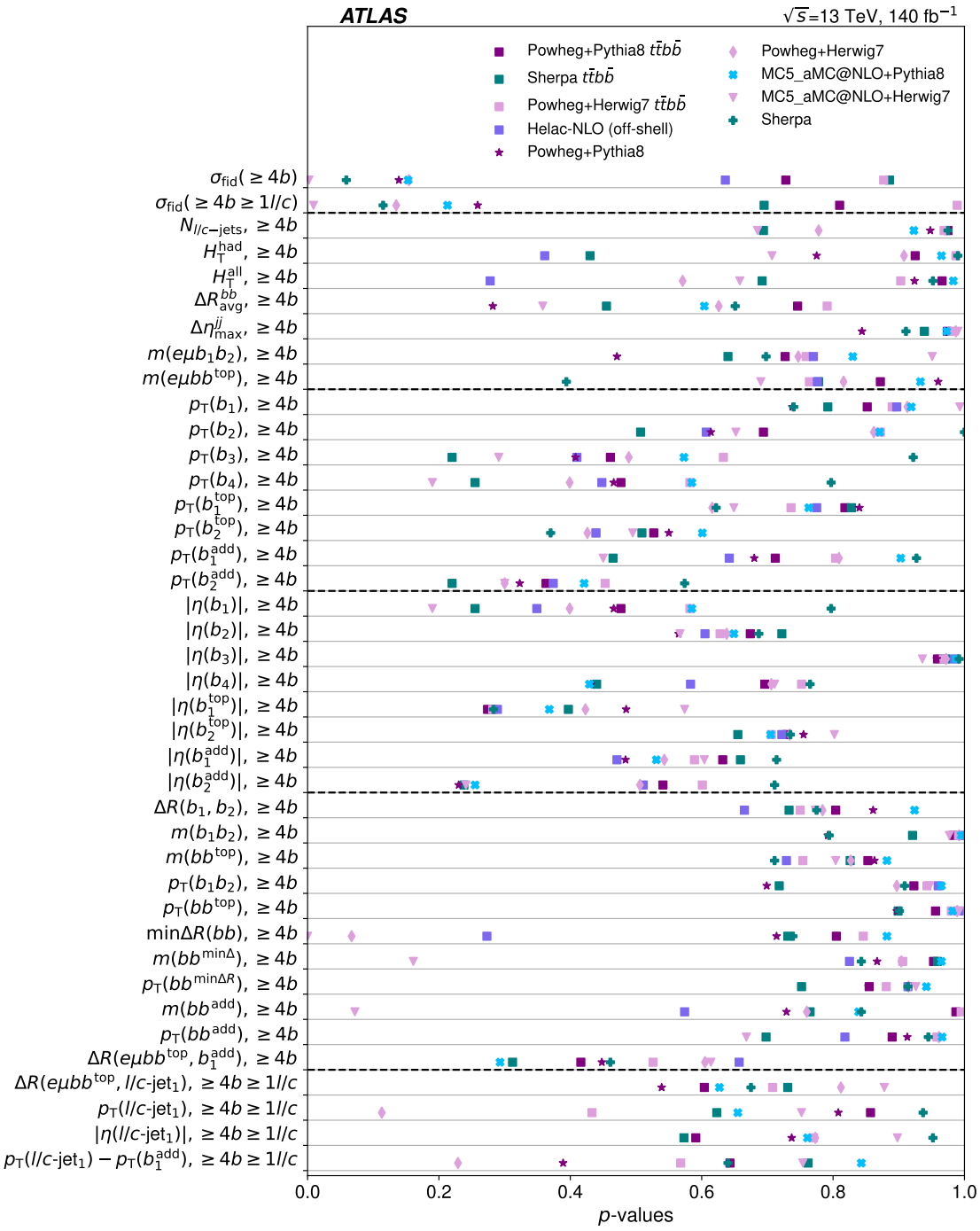

Figure 17. Summary of quantitative comparisons for each observable measurement to predictions in form of p-values. This summary refers to observables measured in the phase space with at least four b-jets. The theoretical uncertainties in the MC predictions are not taken into account when computing the p-values.

JHEP01(2025)068

or more. The SHERPA $t\bar{t}b\bar{b}$ simulation shows good consistency in the full spectrum of the b-jet multiplicity, while POWHEG+HERWIG 7 $t\bar{t}b\bar{b}$ describes the distributions of b-jet p_{T} and $H_{\mathrm{T}}^{\mathrm{had}}$ very well and performs better than POWHEG+PYTHIA 8 $t\bar{t}b\bar{b}$ in modelling b-jets and additional l/c-jets multiplicity spectra. Various predictions where the additional b-jets are generated mainly by the parton shower describe several differential measurements well, however, MADGRAPH5_aMC@NLO+HERWIG 7 $t\bar{t}$ has poor agreement in observables constructed from b-jet pairs originating from gluon emission. The kinematic distributions of b-jets assigned to top quark or gluons show similar level of compatibility to the data within uncertainties as those of the b-jets that are simply ordered in p_{T}.

Despite these overall agreements, differences between any two nominal predictions are often smaller than the QCD scale variations of the theory predictions and the uncertainty of the measurement. This highlights the need for further refinement in theoretical calculations and measurement techniques to better discriminate between models and improve our understanding of $t\bar{t}$ production in association with b-jets.

Acknowledgments

We thank CERN for the very successful operation of the LHC and its injectors, as well as the support staff at CERN and at our institutions worldwide without whom ATLAS could not be operated efficiently.

The crucial computing support from all WLCG partners is acknowledged gratefully, in particular from CERN, the ATLAS Tier-1 facilities at TRIUMF/SFU (Canada), NDGF (Denmark, Norway, Sweden), CC-IN2P3 (France), KIT/GridKA (Germany), INFN-CNAF (Italy), NL-T1 (Netherlands), PIC (Spain), RAL (UK) and BNL (USA), the Tier-2 facilities worldwide and large non-WLCG resource providers. Major contributors of computing resources are listed in ref. [124].

We gratefully acknowledge the support of ANPCyT, Argentina; YerPhI, Armenia; ARC, Australia; BMWFW and FWF, Austria; ANAS, Azerbaijan; CNPq and FAPESP, Brazil; NSERC, NRC and CFI, Canada; CERN; ANID, Chile; CAS, MOST and NSFC, China; Minciencias, Colombia; MEYS CR, Czech Republic; DNRF and DNSRC, Denmark; IN2P3-CNRS and CEA-DRF/IRFU, France; SRNSFG, Georgia; BMBF, HGF and MPG, Germany; GSRI, Greece; RGC and Hong Kong SAR, China; ISF and Benoziyo Center, Israel; INFN, Italy; MEXT and JSPS, Japan; CNRST, Morocco; NWO, Netherlands; RCN, Norway; MNiSW, Poland; FCT, Portugal; MNE/IFA, Romania; MSTDI, Serbia; MSSR, Slovakia; ARIS and MVZI, Slovenia; DSI/NRF, South Africa; MICIU/AEI, Spain; SRC and Wallenberg Foundation, Sweden; SERI, SNSF and Cantons of Bern and Geneva, Switzerland; NSTC, Taipei; TENMAK, Türkiye; STFC/UKRI, United Kingdom; DOE and NSF, United States of America.

Individual groups and members have received support from BCKDF, CANARIE, CRC and DRAC, Canada; CERN-CZ, FORTE and PRIMUS, Czech Republic; COST, ERC, ERDF, Horizon 2020, ICSC-NextGenerationEU and Marie Skłodowska-Curie Actions, European Union; Investissements d'Avenir Labex, Investissements d'Avenir Idex and ANR, France; DFG and AvH Foundation, Germany; Herakleitos, Thales and Aristeia programmes co-financed by EU-ESF and the Greek NSRF, Greece; BSF-NSF and MINERVA, Israel; NCN and NAWA,

JHEP01(2025)068

Poland; La Caixa Banking Foundation, CERCA Programme Generalitat de Catalunya and PROMETEO and GenT Programmes Generalitat Valenciana, Spain; Göran Gustafssons Stiftelse, Sweden; The Royal Society and Leverhulme Trust, United Kingdom.

In addition, individual members wish to acknowledge support from Armenia: Yerevan Physics Institute (FAPERJ); CERN: European Organization for Nuclear Research (CERN PJAS); Chile: Agencia Nacional de Investigación y Desarrollo (FONDECYT 1230812, FONDECYT 1230987, FONDECYT 1240864); China: Chinese Ministry of Science and Technology (MOST-2023YFA1605700), National Natural Science Foundation of China (NSFC - 12175119, NSFC 12275265, NSFC-12075060); Czech Republic: Czech Science Foundation (GACR - 24-11373S), Ministry of Education Youth and Sports (FORTE CZ.02.01.01/00/22_008/0004632), PRIMUS Research Programme (PRIMUS/21/SCI/017); EU: H2020 European Research Council (ERC - 101002463); European Union: European Research Council (ERC - 948254, ERC 101089007), Horizon 2020 Framework Programme (MUCCA - CHIST-ERA-19-XAI-00), European Union, Future Artificial Intelligence Research (FAIR-NextGenerationEU PE00000013), Italian Center for High Performance Computing, Big Data and Quantum Computing (ICSC, NextGenerationEU); France: Agence Nationale de la Recherche (ANR-20-CE31-0013, ANR-21-CE31-0013, ANR-21-CE31-0022, ANR-22-EDIR-0002), Investissements d'Avenir Labex (ANR-11-LABX-0012); Germany: Baden-Württemberg Stiftung (BW Stiftung-Postdoc Eliteprogramme), Deutsche Forschungsgemeinschaft (DFG - 469666862, DFG - CR 312/5-2); Italy: Istituto Nazionale di Fisica Nucleare (ICSC, NextGenerationEU), Ministero dell'Università e della Ricerca (PRIN - 20223N7F8K - PNRR M4.C2.1.1); Japan: Japan Society for the Promotion of Science (JSPS KAKENHI JP22H01227, JSPS KAKENHI JP22H04944, JSPS KAKENHI JP22KK0227, JSPS KAKENHI JP23KK0245); Netherlands: Netherlands Organisation for Scientific Research (NWO Veni 2020 - VI.Veni.202.179); Norway: Research Council of Norway (RCN-314472); Poland: Ministry of Science and Higher Education (IDUB AGH, POB8, D4 no 9722), Polish National Agency for Academic Exchange (PPN/PPO/2020/1/00002/U/00001), Polish National Science Centre (NCN 2021/42/E/ST2/00350, NCN OPUS nr 2022/47/B/ST2/03059, NCN UMO-2019/34/E/ST2/00393, NCN & H2020 MSCA 945339, UMO-2020/37/B/ST2/01043, UMO-2021/40/C/ST2/00187, UMO-2022/47/O/ST2/00148, UMO-2023/49/B/ST2/04085, UMO-2023/51/B/ST2/00920); Slovenia: Slovenian Research Agency (ARIS grant J1-3010); Spain: Generalitat Valenciana (Artemisa, FEDER, IDIFEDER/2018/048), Ministry of Science and Innovation (MCIN & NextGenEU PCI2022-135018-2, MICIN & FEDER PID2021-125273NB, RYC2019-028510-I, RYC2020-030254-I, RYC2021-031273-I, RYC2022-038164-I), PROMETEO and GenT Programmes Generalitat Valenciana (CIDEGENT/2019/027); Sweden: Carl Trygger Foundation (Carl Trygger Foundation CTS 22:2312), Swedish Research Council (Swedish Research Council 2023-04654, VR 2018-00482, VR 2022-03845, VR 2022-04683, VR 2023-03403, VR grant 2021-03651), Knut and Alice Wallenberg Foundation (KAW 2018.0157, KAW 2018.0458, KAW 2019.0447, KAW 2022.0358); Switzerland: Swiss National Science Foundation (SNSF - PCEFP2_194658); United Kingdom: Leverhulme Trust (Leverhulme Trust RPG-2020-004), Royal Society (NIF-R1-231091); United States of America: U.S. Department of Energy (ECA DE-AC02-76SF00515), Neubauer Family Foundation.

We thank the authors of refs. [75, 76], in particular G. Bevilacqua and M. Worek, for fruitful discussions and for providing dedicated theory predictions for our measurements.

JHEP01(2025)068

Data Availability Statement. This article has no associated data or the data will not be deposited.

Code Availability Statement. This article has no associated code or the code will not be deposited.

Open Access. This article is distributed under the terms of the Creative Commons Attribution License (CC-BY4.0), which permits any use, distribution and reproduction in any medium, provided the original author(s) and source are credited.

References

[1] ATLAS collaboration, *Observation of a new particle in the search for the Standard Model Higgs boson with the ATLAS detector at the LHC*, *Phys. Lett. B* **716** (2012) 1 [arXiv:1207.7214] [INSPIRE].

[2] CMS collaboration, *Observation of a New Boson at a Mass of 125 GeV with the CMS Experiment at the LHC*, *Phys. Lett. B* **716** (2012) 30 [arXiv:1207.7235] [INSPIRE].

[3] ATLAS collaboration, *Observation of Higgs boson production in association with a top quark pair at the LHC with the ATLAS detector*, *Phys. Lett. B* **784** (2018) 173 [arXiv:1806.00425] [INSPIRE].

[4] CMS collaboration, *Observation of* $\mathrm{t\bar{t}}H$ *production*, *Phys. Rev. Lett.* **120** (2018) 231801 [arXiv:1804.02610] [INSPIRE].

[5] CMS collaboration, *Observation of Higgs boson decay to bottom quarks*, *Phys. Rev. Lett.* **121** (2018) 121801 [arXiv:1808.08242] [INSPIRE].

[6] ATLAS collaboration, *Measurement of Higgs boson decay into b-quarks in associated production with a top-quark pair in pp collisions at* $\sqrt{s} = 13$ *TeV with the ATLAS detector*, *JHEP* **06** (2022) 097 [arXiv:2111.06712] [INSPIRE].

[7] S. Frixione, P. Nason and G. Ridolfi, *A Positive-weight next-to-leading-order Monte Carlo for heavy flavour hadroproduction*, *JHEP* **09** (2007) 126 [arXiv:0707.3088] [INSPIRE].

[8] P. Nason, *A new method for combining NLO QCD with shower Monte Carlo algorithms*, *JHEP* **11** (2004) 040 [hep-ph/0409146] [INSPIRE].

[9] S. Frixione, P. Nason and C. Oleari, *Matching NLO QCD computations with Parton Shower simulations: the POWHEG method*, *JHEP* **11** (2007) 070 [arXiv:0709.2092] [INSPIRE].

[10] S. Alioli, P. Nason, C. Oleari and E. Re, *A general framework for implementing NLO calculations in shower Monte Carlo programs: the POWHEG BOX*, *JHEP* **06** (2010) 043 [arXiv:1002.2581] [INSPIRE].

[11] SHERPA collaboration, *Event Generation with Sherpa 2.2*, *SciPost Phys.* **7** (2019) 034 [arXiv:1905.09127] [INSPIRE].

[12] J. Alwall et al., *The automated computation of tree-level and next-to-leading order differential cross sections, and their matching to parton shower simulations*, *JHEP* **07** (2014) 079 [arXiv:1405.0301] [INSPIRE].

[13] T. Ježo, J.M. Lindert, N. Moretti and S. Pozzorini, *New NLOPS predictions for* $t\bar{t} + b$*-jet production at the LHC*, *Eur. Phys. J. C* **78** (2018) 502 [arXiv:1802.00426] [INSPIRE].

JHEP01(2025)068

[14] F. Cascioli et al., *NLO matching for $t\bar{t}b\bar{b}$ production with massive b-quarks*, *Phys. Lett. B* **734** (2014) 210 [arXiv:1309.5912] [INSPIRE].

[15] L. Ferencz, S. Höche, J. Katzy and F. Siegert, *$t\bar{t}b\bar{b}$ at NLO precision in a variable flavor number scheme*, *JHEP* **07** (2024) 026 [arXiv:2402.15497] [INSPIRE].

[16] S. Hoeche et al., *Next-to-leading order QCD predictions for top-quark pair production with up to two jets merged with a parton shower*, *Phys. Lett. B* **748** (2015) 74 [arXiv:1402.6293] [INSPIRE].

[17] ATLAS collaboration, *Measurement of $t\bar{t}$ production with a veto on additional central jet activity in pp collisions at sqrt(s) = 7 TeV using the ATLAS detector*, *Eur. Phys. J. C* **72** (2012) 2043 [arXiv:1203.5015] [INSPIRE].

[18] ATLAS collaboration, *Measurement of the $t\bar{t}$ production cross-section as a function of jet multiplicity and jet transverse momentum in 7 TeV proton-proton collisions with the ATLAS detector*, *JHEP* **01** (2015) 020 [arXiv:1407.0891] [INSPIRE].

[19] ATLAS collaboration, *Measurement of jet activity in top quark events using the eμ final state with two b-tagged jets in pp collisions at $\sqrt{s} = 8$ TeV with the ATLAS detector*, *JHEP* **09** (2016) 074 [arXiv:1606.09490] [INSPIRE].

[20] ATLAS collaboration, *Measurements of differential cross sections of top quark pair production in association with jets in pp collisions at $\sqrt{s} = 13$ TeV using the ATLAS detector*, *JHEP* **10** (2018) 159 [arXiv:1802.06572] [INSPIRE].

[21] ATLAS collaboration, *Measurement of jet activity produced in top-quark events with an electron, a muon and two b-tagged jets in the final state in pp collisions at $\sqrt{s} = 13$ TeV with the ATLAS detector*, *Eur. Phys. J. C* **77** (2017) 220 [arXiv:1610.09978] [INSPIRE].

[22] ATLAS collaboration, *Study of heavy-flavor quarks produced in association with top-quark pairs at $\sqrt{s} = 7$ TeV using the ATLAS detector*, *Phys. Rev. D* **89** (2014) 072012 [arXiv:1304.6386] [INSPIRE].

[23] ATLAS collaboration, *Measurements of fiducial cross-sections for $t\bar{t}$ production with one or two additional b-jets in pp collisions at $\sqrt{s} = 8$ TeV using the ATLAS detector*, *Eur. Phys. J. C* **76** (2016) 11 [arXiv:1508.06868] [INSPIRE].

[24] ATLAS collaboration, *Measurements of inclusive and differential fiducial cross-sections of $t\bar{t}$ production with additional heavy-flavour jets in proton-proton collisions at $\sqrt{s} = 13$ TeV with the ATLAS detector*, *JHEP* **04** (2019) 046 [arXiv:1811.12113] [INSPIRE].

[25] CMS collaboration, *Measurement of jet multiplicity distributions in $\mathrm{t\bar{t}}$ production in pp collisions at $\sqrt{s} = 7$ TeV*, *Eur. Phys. J. C* **74** (2015) 3014 [*Erratum ibid.* **75** (2015) 216] [arXiv:1404.3171] [INSPIRE].

[26] CMS collaboration, *Measurement of $\mathrm{t\bar{t}}$ production with additional jet activity, including* b *quark jets, in the dilepton decay channel using pp collisions at $\sqrt{s} = 8$ TeV*, *Eur. Phys. J. C* **76** (2016) 379 [arXiv:1510.03072] [INSPIRE].

[27] CMS collaboration, *Measurement of differential cross sections for the production of top quark pairs and of additional jets in lepton+jets events from pp collisions at $\sqrt{s} = 13$ TeV*, *Phys. Rev. D* **97** (2018) 112003 [arXiv:1803.08856] [INSPIRE].

[28] CMS collaboration, *Measurement of the cross section for $t\bar{t}$ production with additional jets and b jets in pp collisions at $\sqrt{s} = 13$ TeV*, *JHEP* **07** (2020) 125 [arXiv:2003.06467] [INSPIRE].

JHEP01(2025)068

[29] CMS collaboration, *First measurement of the cross section for top quark pair production with additional charm jets using dileptonic final states in pp collisions at s=13TeV*, *Phys. Lett. B* **820** (2021) 136565 [arXiv:2012.09225] [INSPIRE].

[30] CMS collaboration, *Inclusive and differential cross section measurements of $t\bar{t}b\bar{b}$ production in the lepton+jets channel at $\sqrt{s} = 13$ TeV*, *JHEP* **05** (2024) 042 [arXiv:2309.14442] [INSPIRE].

[31] ATLAS collaboration, *The ATLAS Experiment at the CERN Large Hadron Collider*, 2008 *JINST* **3** S08003 [INSPIRE].

[32] ATLAS collaboration, *ATLAS Insertable B-Layer Technical Design Report*, CERN-LHCC-2010-013 (2010) [Addendum: CERN-LHCC-2012-009 (2012)].

[33] ATLAS IBL collaboration, *Production and Integration of the ATLAS Insertable B-Layer*, 2018 *JINST* **13** T05008 [arXiv:1803.00844] [INSPIRE].

[34] G. Avoni et al., *The new LUCID-2 detector for luminosity measurement and monitoring in ATLAS*, 2018 *JINST* **13** P07017 [INSPIRE].

[35] ATLAS collaboration, *Performance of the ATLAS Trigger System in 2015*, *Eur. Phys. J. C* **77** (2017) 317 [arXiv:1611.09661] [INSPIRE].

[36] ATLAS collaboration, *Software and computing for Run 3 of the ATLAS experiment at the LHC*, arXiv:2404.06335 [INSPIRE].

[37] ATLAS collaboration, *The ATLAS Simulation Infrastructure*, *Eur. Phys. J. C* **70** (2010) 823 [arXiv:1005.4568] [INSPIRE].

[38] GEANT4 collaboration, *GEANT4–a simulation toolkit*, *Nucl. Instrum. Meth. A* **506** (2003) 250 [INSPIRE].

[39] C. ATLAS et al., *The simulation principle and performance of the ATLAS fast calorimeter simulation FastCaloSim*, ATL-PHYS-PUB-2010-013, CERN, Geneva (2010).

[40] T. Sjostrand, S. Mrenna and P.Z. Skands, *A Brief Introduction to PYTHIA 8.1*, *Comput. Phys. Commun.* **178** (2008) 852 [arXiv:0710.3820] [INSPIRE].

[41] R.D. Ball et al., *Parton distributions with LHC data*, *Nucl. Phys. B* **867** (2013) 244 [arXiv:1207.1303] [INSPIRE].

[42] ATLAS collaboration, *The Pythia 8 A3 tune description of ATLAS minimum bias and inelastic measurements incorporating the Donnachie-Landshoff diffractive model*, ATL-PHYS-PUB-2016-017, CERN, Geneva (2016).

[43] D.J. Lange, *The EvtGen particle decay simulation package*, *Nucl. Instrum. Meth. A* **462** (2001) 152 [INSPIRE].

[44] NNPDF collaboration, *Parton distributions for the LHC Run II*, *JHEP* **04** (2015) 040 [arXiv:1410.8849] [INSPIRE].

[45] T. Sjöstrand et al., *An introduction to PYTHIA 8.2*, *Comput. Phys. Commun.* **191** (2015) 159 [arXiv:1410.3012] [INSPIRE].

[46] ATLAS collaboration, *Studies on top-quark Monte Carlo modelling for Top2016*, ATL-PHYS-PUB-2016-020, CERN, Geneva (2016).

[47] S. Höche et al., *A Study of QCD Radiation in VBF Higgs Production with Vincia and Pythia*, *SciPost Phys.* **12** (2022) 010 [arXiv:2106.10987] [INSPIRE].

[48] ATLAS Collaboration, *ATLAS Pythia 8 tunes to 7 TeV data*, ATL-PHYS-PUB-2014-021, CERN, Geneva (2014).

JHEP01(2025)068

[49] M. Beneke, P. Falgari, S. Klein and C. Schwinn, *Hadronic top-quark pair production with NNLL threshold resummation*, *Nucl. Phys. B* **855** (2012) 695 [arXiv:1109.1536] [INSPIRE].

[50] M. Cacciari et al., *Top-pair production at hadron colliders with next-to-next-to-leading logarithmic soft-gluon resummation*, *Phys. Lett. B* **710** (2012) 612 [arXiv:1111.5869] [INSPIRE].

[51] P. Bärnreuther, M. Czakon and A. Mitov, *Percent Level Precision Physics at the Tevatron: First Genuine NNLO QCD Corrections to $q\bar{q} \to t\bar{t} + X$*, *Phys. Rev. Lett.* **109** (2012) 132001 [arXiv:1204.5201] [INSPIRE].

[52] M. Czakon and A. Mitov, *NNLO corrections to top-pair production at hadron colliders: the all-fermionic scattering channels*, *JHEP* **12** (2012) 054 [arXiv:1207.0236] [INSPIRE].

[53] M. Czakon and A. Mitov, *NNLO corrections to top pair production at hadron colliders: the quark-gluon reaction*, *JHEP* **01** (2013) 080 [arXiv:1210.6832] [INSPIRE].

[54] M. Czakon, P. Fiedler and A. Mitov, *Total Top-Quark Pair-Production Cross Section at Hadron Colliders Through $O(\alpha_S^4)$*, *Phys. Rev. Lett.* **110** (2013) 252004 [arXiv:1303.6254] [INSPIRE].

[55] M. Czakon and A. Mitov, *Top++: A program for the Calculation of the Top-Pair Cross-Section at Hadron Colliders*, *Comput. Phys. Commun.* **185** (2014) 2930 [arXiv:1112.5675] [INSPIRE].

[56] J. Butterworth et al., *PDF4LHC recommendations for LHC Run II*, *J. Phys. G* **43** (2016) 023001 [arXiv:1510.03865] [INSPIRE].

[57] A.D. Martin, W.J. Stirling, R.S. Thorne and G. Watt, *Parton distributions for the LHC*, *Eur. Phys. J. C* **63** (2009) 189 [arXiv:0901.0002] [INSPIRE].

[58] A.D. Martin, W.J. Stirling, R.S. Thorne and G. Watt, *Uncertainties on alpha(S) in global PDF analyses and implications for predicted hadronic cross sections*, *Eur. Phys. J. C* **64** (2009) 653 [arXiv:0905.3531] [INSPIRE].

[59] H.-L. Lai et al., *New parton distributions for collider physics*, *Phys. Rev. D* **82** (2010) 074024 [arXiv:1007.2241] [INSPIRE].

[60] J. Gao et al., *CT10 next-to-next-to-leading order global analysis of QCD*, *Phys. Rev. D* **89** (2014) 033009 [arXiv:1302.6246] [INSPIRE].

[61] J. Bellm et al., *Herwig 7.1 Release Note*, arXiv:1705.06919 [INSPIRE].

[62] L.A. Harland-Lang, A.D. Martin, P. Motylinski and R.S. Thorne, *Parton distributions in the LHC era: MMHT 2014 PDFs*, *Eur. Phys. J. C* **75** (2015) 204 [arXiv:1412.3989] [INSPIRE].

[63] F. Buccioni et al., *OpenLoops 2*, *Eur. Phys. J. C* **79** (2019) 866 [arXiv:1907.13071] [INSPIRE].

[64] F. Cascioli, P. Maierhofer and S. Pozzorini, *Scattering Amplitudes with Open Loops*, *Phys. Rev. Lett.* **108** (2012) 111601 [arXiv:1111.5206] [INSPIRE].

[65] T. Gleisberg and S. Hoeche, *Comix, a new matrix element generator*, *JHEP* **12** (2008) 039 [arXiv:0808.3674] [INSPIRE].

[66] S. Schumann and F. Krauss, *A parton shower algorithm based on Catani-Seymour dipole factorisation*, *JHEP* **03** (2008) 038 [arXiv:0709.1027] [INSPIRE].

[67] S. Hoeche, F. Krauss, M. Schonherr and F. Siegert, *A critical appraisal of NLO+PS matching methods*, *JHEP* **09** (2012) 049 [arXiv:1111.1220] [INSPIRE].

[68] S. Catani, F. Krauss, R. Kuhn and B.R. Webber, *QCD matrix elements + parton showers*, *JHEP* **11** (2001) 063 [hep-ph/0109231] [INSPIRE].

JHEP01(2025)068

[69] S. Kallweit et al., *NLO electroweak automation and precise predictions for W+multijet production at the LHC*, *JHEP* **04** (2015) 012 [arXiv:1412.5157] [INSPIRE].

[70] S. Kallweit et al., *NLO QCD+EW predictions for V + jets including off-shell vector-boson decays and multijet merging*, *JHEP* **04** (2016) 021 [arXiv:1511.08692] [INSPIRE].

[71] C. Gütschow, J.M. Lindert and M. Schönherr, *Multi-jet merged top-pair production including electroweak corrections*, *Eur. Phys. J. C* **78** (2018) 317 [arXiv:1803.00950] [INSPIRE].

[72] L. Ferencz et al., *Study of $t\bar{t}b\bar{b}$ and $t\bar{t}W$ background modelling for $t\bar{t}H$ analyses*, arXiv:2301.11670 [INSPIRE].

[73] ATLAS collaboration, *Studies of Monte Carlo predictions for the $t\bar{t}b\bar{b}$ process*, ATL-PHYS-PUB-2022-006, CERN, Geneva (2022).

[74] G. Bevilacqua et al., *HELAC-NLO*, *Comput. Phys. Commun.* **184** (2013) 986 [arXiv:1110.1499] [INSPIRE].

[75] G. Bevilacqua et al., *$t\bar{t}b\bar{b}$ at the LHC: on the size of corrections and b-jet definitions*, *JHEP* **08** (2021) 008 [arXiv:2105.08404] [INSPIRE].

[76] G. Bevilacqua et al., *$t\bar{t}b\bar{b}$ at the LHC: On the size of off-shell effects and prompt b-jet identification*, *Phys. Rev. D* **107** (2023) 014028 [arXiv:2202.11186] [INSPIRE].

[77] NNPDF collaboration, *Parton distributions from high-precision collider data*, *Eur. Phys. J. C* **77** (2017) 663 [arXiv:1706.00428] [INSPIRE].

[78] E. Re, *Single-top Wt-channel production matched with parton showers using the POWHEG method*, *Eur. Phys. J. C* **71** (2011) 1547 [arXiv:1009.2450] [INSPIRE].

[79] S. Alioli, P. Nason, C. Oleari and E. Re, *NLO single-top production matched with shower in POWHEG: s- and t-channel contributions*, *JHEP* **09** (2009) 111 [*Erratum ibid.* **02** (2010) 011] [arXiv:0907.4076] [INSPIRE].

[80] R. Frederix, E. Re and P. Torrielli, *Single-top t-channel hadroproduction in the four-flavour scheme with POWHEG and aMC@NLO*, *JHEP* **09** (2012) 130 [arXiv:1207.5391] [INSPIRE].

[81] S. Frixione et al., *Single-top hadroproduction in association with a W boson*, *JHEP* **07** (2008) 029 [arXiv:0805.3067] [INSPIRE].

[82] M. Aliev et al., *HATHOR: HAdronic Top and Heavy quarks crOss section calculatoR*, *Comput. Phys. Commun.* **182** (2011) 1034 [arXiv:1007.1327] [INSPIRE].

[83] P. Kant et al., *HatHor for single top-quark production: Updated predictions and uncertainty estimates for single top-quark production in hadronic collisions*, *Comput. Phys. Commun.* **191** (2015) 74 [arXiv:1406.4403] [INSPIRE].

[84] N. Kidonakis, *Two-loop soft anomalous dimensions for single top quark associated production with a W^- or H^-*, *Phys. Rev. D* **82** (2010) 054018 [arXiv:1005.4451] [INSPIRE].

[85] C. Anastasiou, L.J. Dixon, K. Melnikov and F. Petriello, *High precision QCD at hadron colliders: Electroweak gauge boson rapidity distributions at NNLO*, *Phys. Rev. D* **69** (2004) 094008 [hep-ph/0312266] [INSPIRE].

[86] ATLAS Collaboration, *Vertex Reconstruction Performance of the ATLAS Detector at $\sqrt{s} = 13$ TeV*, ATL-PHYS-PUB-2015-026, CERN, Geneva (2015).

[87] ATLAS collaboration, *Electron and photon performance measurements with the ATLAS detector using the 2015–2017 LHC proton-proton collision data*, 2019 *JINST* **14** P12006 [arXiv:1908.00005] [INSPIRE].

JHEP01(2025)068

[88] ATLAS collaboration, *Muon reconstruction and identification efficiency in ATLAS using the full Run 2 pp collision data set at* $\sqrt{s} = 13$ *TeV*, *Eur. Phys. J. C* **81** (2021) 578 [arXiv:2012.00578] [INSPIRE].

[89] ATLAS collaboration, *Studies of the muon momentum calibration and performance of the ATLAS detector with pp collisions at* $\sqrt{s} = 13$ *TeV*, *Eur. Phys. J. C* **83** (2023) 686 [arXiv:2212.07338] [INSPIRE].

[90] ATLAS collaboration, *Jet reconstruction and performance using particle flow with the ATLAS Detector*, *Eur. Phys. J. C* **77** (2017) 466 [arXiv:1703.10485] [INSPIRE].

[91] M. Cacciari, G.P. Salam and G. Soyez, *The anti-*k_t *jet clustering algorithm*, *JHEP* **04** (2008) 063 [arXiv:0802.1189] [INSPIRE].

[92] M. Cacciari, G.P. Salam and G. Soyez, *FastJet User Manual*, *Eur. Phys. J. C* **72** (2012) 1896 [arXiv:1111.6097] [INSPIRE].

[93] ATLAS collaboration, *Jet energy scale and resolution measured in proton–proton collisions at* $\sqrt{s} = 13$ *TeV with the ATLAS detector*, *Eur. Phys. J. C* **81** (2021) 689 [arXiv:2007.02645] [INSPIRE].

[94] ATLAS collaboration, *Performance of pile-up mitigation techniques for jets in pp collisions at* $\sqrt{s} = 8$ *TeV using the ATLAS detector*, *Eur. Phys. J. C* **76** (2016) 581 [arXiv:1510.03823] [INSPIRE].

[95] ATLAS Collaboration, *Selection of jets produced in 13TeV proton-proton collisions with the ATLAS detector*, ATLAS-CONF-2015-029, CERN, Geneva (2015).

[96] ATLAS collaboration, *ATLAS flavour-tagging algorithms for the LHC Run 2 pp collision dataset*, *Eur. Phys. J. C* **83** (2023) 681 [arXiv:2211.16345] [INSPIRE].

[97] ATLAS collaboration, *ATLAS b-jet identification performance and efficiency measurement with* $t\bar{t}$ *events in pp collisions at* $\sqrt{s} = 13$ *TeV*, *Eur. Phys. J. C* **79** (2019) 970 [arXiv:1907.05120] [INSPIRE].

[98] ATLAS collaboration, *The performance of missing transverse momentum reconstruction and its significance with the ATLAS detector using* $140\,fb^{-1}$ *of* $\sqrt{s} = 13$ *TeV pp collisions*, arXiv:2402.05858 [INSPIRE].

[99] ATLAS collaboration, *Luminosity determination in pp collisions at* $\sqrt{s} = 13$ *TeV using the ATLAS detector at the LHC*, *Eur. Phys. J. C* **83** (2023) 982 [arXiv:2212.09379] [INSPIRE].

[100] ATLAS collaboration, *Performance of electron and photon triggers in ATLAS during LHC Run 2*, *Eur. Phys. J. C* **80** (2020) 47 [arXiv:1909.00761] [INSPIRE].

[101] ATLAS collaboration, *Performance of the ATLAS muon triggers in Run 2*, 2020 *JINST* **15** P09015 [arXiv:2004.13447] [INSPIRE].

[102] ATLAS Collaboration, *2015 start-up trigger menu and initial performance assessment of the ATLAS trigger using Run-2 data*, ATL-DAQ-PUB-2016-001, CERN, Geneva (2016).

[103] ATLAS collaboration, *Trigger Menu in 2016*, ATL-DAQ-PUB-2017-001, CERN, Geneva (2017).

[104] ATLAS collaboration, *Trigger Menu in 2017*, ATL-DAQ-PUB-2018-002, CERN, Geneva (2018).

[105] ATLAS collaboration, *Trigger menu in 2018*, ATL-DAQ-PUB-2019-001, CERN, Geneva (2019).

JHEP01(2025)068

[106] M. Cacciari, G.P. Salam and G. Soyez, *The Catchment Area of Jets*, *JHEP* **04** (2008) 005 [arXiv:0802.1188] [INSPIRE].

[107] ATLAS collaboration, *Measurement of the $t\bar{t}$ production cross-section using $e\mu$ events with b-tagged jets in pp collisions at $\sqrt{s} = 13$ TeV with the ATLAS detector*, *Phys. Lett. B* **761** (2016) 136 [arXiv:1606.02699] [INSPIRE].

[108] G. D'Agostini, *A multidimensional unfolding method based on Bayes' theorem*, *Nucl. Instrum. Meth. A* **362** (1995) 487 [INSPIRE].

[109] T. Adye, *Unfolding algorithms and tests using RooUnfold*, in the proceedings of the *Workshop on Statistical Issues Related to Discovery Claims in Search Experiments and Unfolding (PHYSTAT 2011)*, Geneva, Switzerland, January 17–20 (2011) [DOI:10.5170/CERN-2011-006.313] [arXiv:1105.1160] [INSPIRE].

[110] ATLAS collaboration, *Measurement of the c-jet mistagging efficiency in $t\bar{t}$ events using pp collision data at $\sqrt{s} = 13$ TeV collected with the ATLAS detector*, *Eur. Phys. J. C* **82** (2022) 95 [arXiv:2109.10627] [INSPIRE].

[111] ATLAS collaboration, *Calibration of the light-flavour jet mistagging efficiency of the b-tagging algorithms with Z+jets events using 139 fb^{-1} of ATLAS proton–proton collision data at $\sqrt{s} = 13$ TeV*, *Eur. Phys. J. C* **83** (2023) 728 [arXiv:2301.06319] [INSPIRE].

[112] M. Czakon et al., *Top-pair production at the LHC through NNLO QCD and NLO EW*, *JHEP* **10** (2017) 186 [arXiv:1705.04105] [INSPIRE].

[113] LHC Higgs Cross Section Working Group collaboration, *Handbook of LHC Higgs Cross Sections: 4. Deciphering the Nature of the Higgs Sector*, arXiv:1610.07922 [DOI:10.23731/CYRM-2017-002] [INSPIRE].

[114] ATLAS collaboration, *Measurements of the inclusive and differential production cross sections of a top-quark–antiquark pair in association with a Z boson at $\sqrt{s} = 13$ TeV with the ATLAS detector*, *Eur. Phys. J. C* **81** (2021) 737 [arXiv:2103.12603] [INSPIRE].

[115] ATLAS collaboration, *Inclusive and differential cross-section measurements of $t\bar{t}Z$ production in pp collisions at $\sqrt{s} = 13$ TeV with the ATLAS detector, including EFT and spin-correlation interpretations*, *JHEP* **07** (2024) 163 [arXiv:2312.04450] [INSPIRE].

[116] CMS collaboration, *Measurement of top quark pair production in association with a Z boson in proton-proton collisions at $\sqrt{s} = 13$ TeV*, *JHEP* **03** (2020) 056 [arXiv:1907.11270] [INSPIRE].

[117] ATLAS collaboration, *Measurement of the total and differential cross-sections of $t\bar{t}W$ production in pp collisions at $\sqrt{s} = 13$ TeV with the ATLAS detector*, *JHEP* **05** (2024) 131 [arXiv:2401.05299] [INSPIRE].

[118] ATLAS collaboration, *Search for pair production of third-generation leptoquarks decaying into a bottom quark and a τ-lepton with the ATLAS detector*, *Eur. Phys. J. C* **83** (2023) 1075 [arXiv:2303.01294] [INSPIRE].

[119] ATLAS collaboration, *Search for heavy resonances decaying into a Z or W boson and a Higgs boson in final states with leptons and b-jets in 139 fb^{-1} of pp collisions at $\sqrt{s} = 13$ TeV with the ATLAS detector*, *JHEP* **06** (2023) 016 [arXiv:2207.00230] [INSPIRE].

[120] ATLAS collaboration, *Studies on the improvement of the matching uncertainty definition in top-quark processes simulated with Powheg+Pythia 8*, ATL-PHYS-PUB-2023-029, CERN, Geneva (2023).

[121] ATLAS collaboration, *Studies of matrix element correction in $t\bar{t}$ events using MG5_aMC@NLO+Pythia8*, ATL-PHYS-PUB-2024-002, CERN, Geneva (2024).

JHEP01(2025)068

[122] ATLAS collaboration, *Study of top-quark pair modelling and uncertainties using ATLAS measurements at* $\sqrt{s} = 13$ *TeV*, ATL-PHYS-PUB-2020-023, CERN, Geneva (2020).

[123] E. Maguire, L. Heinrich and G. Watt, *HEPData: a repository for high energy physics data*, *J. Phys. Conf. Ser.* **898** (2017) 102006 [arXiv:1704.05473] [INSPIRE].

[124] ATLAS collaboration, *ATLAS Computing Acknowledgements*, ATL-SOFT-PUB-2023-001, CERN, Geneva (2023).

JHEP01(2025)068

The ATLAS collaboration

G. Aad[104], E. Aakvaag[17], B. Abbott[123], S. Abdelhameed[119a], K. Abeling[56], N.J. Abicht[50], S.H. Abidi[30], M. Aboelela[45], A. Aboulhorma[36e], H. Abramowicz[155], H. Abreu[154], Y. Abulaiti[120], B.S. Acharya[70a,70b,k], A. Ackermann[64a], C. Adam Bourdarios[4], L. Adamczyk[87a], S.V. Addepalli[27], M.J. Addison[103], J. Adelman[118], A. Adiguzel[22c], T. Adye[137], A.A. Affolder[139], Y. Afik[40], M.N. Agaras[13], J. Agarwala[74a,74b], A. Aggarwal[102], C. Agheorghiesei[28c], F. Ahmadov[39,y], W.S. Ahmed[106], S. Ahuja[97], X. Ai[63e], G. Aielli[77a,77b], A. Aikot[166], M. Ait Tamlihat[36e], B. Aitbenchikh[36a], M. Akbiyik[102], T.P.A. Åkesson[100], A.V. Akimov[38], D. Akiyama[171], N.N. Akolkar[25], S. Aktas[22a], K. Al Khoury[42], G.L. Alberghi[24b], J. Albert[168], P. Albicocco[54], G.L. Albouy[61], S. Alderweireldt[53], Z.L. Alegria[124], M. Aleksa[37], I.N. Aleksandrov[39], C. Alexa[28b], T. Alexopoulos[10], F. Alfonsi[24b], M. Algren[57], M. Alhroob[170], B. Ali[135], H.M.J. Ali[93,s], S. Ali[32], S.W. Alibocus[94], M. Aliev[34c], G. Alimonti[72a], W. Alkakhi[56], C. Allaire[67], B.M.M. Allbrooke[150], J.S. Allen[103], J.F. Allen[53], C.A. Allendes Flores[140f], P.P. Allport[21], A. Aloisio[73a,73b], F. Alonso[92], C. Alpigiani[142], Z.M.K. Alsolami[93], M. Alvarez Estevez[101], A. Alvarez Fernandez[102], M. Alves Cardoso[57], M.G. Alviggi[73a,73b], M. Aly[103], Y. Amaral Coutinho[84b], A. Ambler[106], C. Amelung[37], M. Amerl[103], C.G. Ames[111], D. Amidei[108], B. Amini[55], K.J. Amirie[158], S.P. Amor Dos Santos[133a], K.R. Amos[166], D. Amperiadou[156], S. An[85], V. Ananiev[128], C. Anastopoulos[143], T. Andeen[11], J.K. Anders[37], A.C. Anderson[60], S.Y. Andrean[48a,48b], A. Andreazza[72a,72b], S. Angelidakis[9], A. Angerami[42], A.V. Anisenkov[38], A. Annovi[75a], C. Antel[57], E. Antipov[149], M. Antonelli[54], F. Anulli[76a], M. Aoki[85], T. Aoki[157], M.A. Aparo[150], L. Aperio Bella[49], C. Appelt[19], A. Apyan[27], S.J. Arbiol Val[88], C. Arcangeletti[54], A.T.H. Arce[52], J-F. Arguin[110], S. Argyropoulos[55], J.-H. Arling[49], O. Arnaez[4], H. Arnold[149], G. Artoni[76a,76b], H. Asada[113], K. Asai[121], S. Asai[157], N.A. Asbah[37], R.A. Ashby Pickering[170], K. Assamagan[30], R. Astalos[29a], K.S.V. Astrand[100], S. Atashi[162], R.J. Atkin[34a], M. Atkinson[165], H. Atmani[36f], P.A. Atmasiddha[131], K. Augsten[135], S. Auricchio[73a,73b], A.D. Auriol[21], V.A. Austrup[103], G. Avolio[37], K. Axiotis[57], G. Azuelos[110,ad], D. Babal[29b], H. Bachacou[138], K. Bachas[156,o], A. Bachiu[35], F. Backman[48a,48b], A. Badea[40], T.M. Baer[108], P. Bagnaia[76a,76b], M. Bahmani[19], D. Bahner[55], K. Bai[126], J.T. Baines[137], L. Baines[96], O.K. Baker[175], E. Bakos[16], D. Bakshi Gupta[8], L.E. Balabram Filho[84b], V. Balakrishnan[123], R. Balasubramanian[4], E.M. Baldin[38], P. Balek[87a], E. Ballabene[24b,24a], F. Balli[138], L.M. Baltes[64a], W.K. Balunas[33], J. Balz[102], I. Bamwidhi[119b], E. Banas[88], M. Bandieramonte[132], A. Bandyopadhyay[25], S. Bansal[25], L. Barak[155], M. Barakat[49], E.L. Barberio[107], D. Barberis[58b,58a], M. Barbero[104], M.Z. Barel[117], T. Barillari[112], M-S. Barisits[37], T. Barklow[147], P. Baron[125], D.A. Baron Moreno[103], A. Baroncelli[63a], A.J. Barr[129], J.D. Barr[98], F. Barreiro[101], J. Barreiro Guimarães da Costa[14], U. Barron[155], M.G. Barros Teixeira[133a], S. Barsov[38], F. Bartels[64a], R. Bartoldus[147], A.E. Barton[93], P. Bartos[29a], A. Basan[102], M. Baselga[50], A. Bassalat[67,b], M.J. Basso[159a], S. Bataju[45], R. Bate[167], R.L. Bates[60], S. Batlamous[101], B. Batool[145], M. Battaglia[139], D. Battulga[19], M. Bauce[76a,76b], M. Bauer[80], P. Bauer[25], L.T. Bazzano Hurrell[31], J.B. Beacham[52], T. Beau[130], J.Y. Beaucamp[92], P.H. Beauchemin[161], P. Bechtle[25], H.P. Beck[20,n],

JHEP01(2025)068

K. Becker[170], A.J. Beddall[83], V.A. Bednyakov[39], C.P. Bee[149], L.J. Beemster[16], T.A. Beermann[37], M. Begalli[84d], M. Begel[30], A. Behera[149], J.K. Behr[49], J.F. Beirer[37], F. Beisiegel[25], M. Belfkir[119b], G. Bella[155], L. Bellagamba[24b], A. Bellerive[35], P. Bellos[21], K. Beloborodov[38], D. Benchekroun[36a], F. Bendebba[36a], Y. Benhammou[155], K.C. Benkendorfer[62], L. Beresford[49], M. Beretta[54], E. Bergeaas Kuutmann[164], N. Berger[4], B. Bergmann[135], J. Beringer[18a], G. Bernardi[5], C. Bernius[147], F.U. Bernlochner[25], F. Bernon[37], A. Berrocal Guardia[13], T. Berry[97], P. Berta[136], A. Berthold[51], S. Bethke[112], A. Betti[76a,76b], A.J. Bevan[96], N.K. Bhalla[55], S. Bhatta[149], D.S. Bhattacharya[169], P. Bhattarai[147], K.D. Bhide[55], V.S. Bhopatkar[124], R.M. Bianchi[132], G. Bianco[24b,24a], O. Biebel[111], R. Bielski[126], M. Biglietti[78a], C.S. Billingsley[45], Y. Bimgdi[36f], M. Bindi[56], A. Bingul[22b], C. Bini[76a,76b], G.A. Bird[33], M. Birman[172], M. Biros[136], S. Biryukov[150], T. Bisanz[50], E. Bisceglie[44b,44a], J.P. Biswal[137], D. Biswas[145], I. Bloch[49], A. Blue[60], U. Blumenschein[96], J. Blumenthal[102], V.S. Bobrovnikov[38], M. Boehler[55], B. Boehm[169], D. Bogavac[37], A.G. Bogdanchikov[38], L.S. Boggia[130], C. Bohm[48a], V. Boisvert[97], P. Bokan[37], T. Bold[87a], M. Bomben[5], M. Bona[96], M. Boonekamp[138], C.D. Booth[97], A.G. Borbély[60], I.S. Bordulev[38], G. Borissov[93], D. Bortoletto[129], D. Boscherini[24b], M. Bosman[13], J.D. Bossio Sola[37], K. Bouaouda[36a], N. Bouchhar[166], L. Boudet[4], J. Boudreau[132], E.V. Bouhova-Thacker[93], D. Boumediene[41], R. Bouquet[58b,58a], A. Boveia[122], J. Boyd[37], D. Boye[30], I.R. Boyko[39], L. Bozianu[57], J. Bracinik[21], N. Brahimi[4], G. Brandt[174], O. Brandt[33], F. Braren[49], B. Brau[105], J.E. Brau[126], R. Brener[172], L. Brenner[117], R. Brenner[164], S. Bressler[172], G. Brianti[79a,79b], D. Britton[60], D. Britzger[112], I. Brock[25], R. Brock[109], G. Brooijmans[42], E.M. Brooks[159b], E. Brost[30], L.M. Brown[168], L.E. Bruce[62], T.L. Bruckler[129], P.A. Bruckman de Renstrom[88], B. Brüers[49], A. Bruni[24b], G. Bruni[24b], M. Bruschi[24b], N. Bruscino[76a,76b], T. Buanes[17], Q. Buat[142], D. Buchin[112], A.G. Buckley[60], O. Bulekov[38], B.A. Bullard[147], S. Burdin[94], C.D. Burgard[50], A.M. Burger[37], B. Burghgrave[8], O. Burlayenko[55], J. Burleson[165], J.T.P. Burr[33], J.C. Burzynski[146], E.L. Busch[42], V. Büscher[102], P.J. Bussey[60], J.M. Butler[26], C.M. Buttar[60], J.M. Butterworth[98], W. Buttinger[137], C.J. Buxo Vazquez[109], A.R. Buzykaev[38], S. Cabrera Urbán[166], L. Cadamuro[67], D. Caforio[59], H. Cai[132], Y. Cai[14,114c], Y. Cai[114a], V.M.M. Cairo[37], O. Cakir[3a], N. Calace[37], P. Calafiura[18a], G. Calderini[130], P. Calfayan[69], G. Callea[60], L.P. Caloba[84b], D. Calvet[41], S. Calvet[41], M. Calvetti[75a,75b], R. Camacho Toro[130], S. Camarda[37], D. Camarero Munoz[27], P. Camarri[77a,77b], M.T. Camerlingo[73a,73b], D. Cameron[37], C. Camincher[168], M. Campanelli[98], A. Camplani[43], V. Canale[73a,73b], A.C. Canbay[3a], E. Canonero[97], J. Cantero[166], Y. Cao[165], F. Capocasa[27], M. Capua[44b,44a], A. Carbone[72a,72b], R. Cardarelli[77a], J.C.J. Cardenas[8], G. Carducci[44b,44a], T. Carli[37], G. Carlino[73a], J.I. Carlotto[13], B.T. Carlson[132,p], E.M. Carlson[168,159a], J. Carmignani[94], L. Carminati[72a,72b], A. Carnelli[138], M. Carnesale[37], S. Caron[116], E. Carquin[140f], I.B. Carr[107], S. Carrá[72a], G. Carratta[24b,24a], A.M. Carroll[126], M.P. Casado[13,h], M. Caspar[49], F.L. Castillo[4], L. Castillo Garcia[13], V. Castillo Gimenez[166], N.F. Castro[133a,133e], A. Catinaccio[37], J.R. Catmore[128], T. Cavaliere[4], V. Cavaliere[30], N. Cavalli[24b,24a], L.J. Caviedes Betancourt[23b], Y.C. Cekmecelioglu[49], E. Celebi[83], S. Cella[37],

JHEP01(2025)068

M.S. Centonze[71a,71b], V. Cepaitis[57], K. Cerny[125], A.S. Cerqueira[84a], A. Cerri[150], L. Cerrito[77a,77b], F. Cerutti[18a], B. Cervato[145], A. Cervelli[24b], G. Cesarini[54], S.A. Cetin[83], D. Chakraborty[118], J. Chan[18a], W.Y. Chan[157], J.D. Chapman[33], E. Chapon[138], B. Chargeishvili[153b], D.G. Charlton[21], M. Chatterjee[20], C. Chauhan[136], Y. Che[114a], S. Chekanov[6], S.V. Chekulaev[159a], G.A. Chelkov[39,a], A. Chen[108], B. Chen[155], B. Chen[168], H. Chen[114a], H. Chen[30], J. Chen[63c], J. Chen[146], M. Chen[129], S. Chen[89], S.J. Chen[114a], X. Chen[63c], X. Chen[15,ac], Y. Chen[63a], C.L. Cheng[173], H.C. Cheng[65a], S. Cheong[147], A. Cheplakov[39], E. Cheremushkina[49], E. Cherepanova[117], R. Cherkaoui El Moursli[36e], E. Cheu[7], K. Cheung[66], L. Chevalier[138], V. Chiarella[54], G. Chiarelli[75a], N. Chiedde[104], G. Chiodini[71a], A.S. Chisholm[21], A. Chitan[28b], M. Chitishvili[166], M.V. Chizhov[39,q], K. Choi[11], Y. Chou[142], E.Y.S. Chow[116], K.L. Chu[172], M.C. Chu[65a], X. Chu[14,114c], Z. Chubinidze[54], J. Chudoba[134], J.J. Chwastowski[88], D. Cieri[112], K.M. Ciesla[87a], V. Cindro[95], A. Ciocio[18a], F. Cirotto[73a,73b], Z.H. Citron[172], M. Citterio[72a], D.A. Ciubotaru[28b], A. Clark[57], P.J. Clark[53], N. Clarke Hall[98], C. Clarry[158], J.M. Clavijo Columbie[49], S.E. Clawson[49], C. Clement[48a,48b], Y. Coadou[104], M. Cobal[70a,70c], A. Coccaro[58b], R.F. Coelho Barrue[133a], R. Coelho Lopes De Sa[105], S. Coelli[72a], B. Cole[42], J. Collot[61], P. Conde Muiño[133a,133g], M.P. Connell[34c], S.H. Connell[34c], E.I. Conroy[129], F. Conventi[73a,ae], H.G. Cooke[21], A.M. Cooper-Sarkar[129], F.A. Corchia[24b,24a], A. Cordeiro Oudot Choi[130], L.D. Corpe[41], M. Corradi[76a,76b], F. Corriveau[106,x], A. Cortes-Gonzalez[19], M.J. Costa[166], F. Costanza[4], D. Costanzo[143], B.M. Cote[122], J. Couthures[4], G. Cowan[97], K. Cranmer[173], L. Cremer[50], D. Cremonini[24b,24a], S. Crépé-Renaudin[61], F. Crescioli[130], M. Cristinziani[145], M. Cristoforetti[79a,79b], V. Croft[117], J.E. Crosby[124], G. Crosetti[44b,44a], A. Cueto[101], H. Cui[98], Z. Cui[7], W.R. Cunningham[60], F. Curcio[166], J.R. Curran[53], P. Czodrowski[37], M.J. Da Cunha Sargedas De Sousa[58b,58a], J.V. Da Fonseca Pinto[84b], C. Da Via[103], W. Dabrowski[87a], T. Dado[37], S. Dahbi[152], T. Dai[108], D. Dal Santo[20], C. Dallapiccola[105], M. Dam[43], G. D'amen[30], V. D'Amico[111], J. Damp[102], J.R. Dandoy[35], D. Dannheim[37], M. Danninger[146], V. Dao[149], G. Darbo[58b], S.J. Das[30], F. Dattola[49], S. D'Auria[72a,72b], A. D'Avanzo[73a,73b], C. David[34a], T. Davidek[136], I. Dawson[96], H.A. Day-hall[135], K. De[8], R. De Asmundis[73a], N. De Biase[49], S. De Castro[24b,24a], N. De Groot[116], P. de Jong[117], H. De la Torre[118], A. De Maria[114a], A. De Salvo[76a], U. De Sanctis[77a,77b], F. De Santis[71a,71b], A. De Santo[150], J.B. De Vivie De Regie[61], J. Debevc[95], D.V. Dedovich[39], J. Degens[94], A.M. Deiana[45], F. Del Corso[24b,24a], J. Del Peso[101], L. Delagrange[130], F. Deliot[138], C.M. Delitzsch[50], M. Della Pietra[73a,73b], D. Della Volpe[57], A. Dell'Acqua[37], L. Dell'Asta[72a,72b], M. Delmastro[4], P.A. Delsart[61], S. Demers[175], M. Demichev[39], S.P. Denisov[38], L. D'Eramo[41], D. Derendarz[88], F. Derue[130], P. Dervan[94], K. Desch[25], C. Deutsch[25], F.A. Di Bello[58b,58a], A. Di Ciaccio[77a,77b], L. Di Ciaccio[4], A. Di Domenico[76a,76b], C. Di Donato[73a,73b], A. Di Girolamo[37], G. Di Gregorio[37], A. Di Luca[79a,79b], B. Di Micco[78a,78b], R. Di Nardo[78a,78b], K.F. Di Petrillo[40], M. Diamantopoulou[35], F.A. Dias[117], T. Dias Do Vale[146], M.A. Diaz[140a,140b], F.G. Diaz Capriles[25], A.R. Didenko[39], M. Didenko[166], E.B. Diehl[108], S. Díez Cornell[49], C. Diez Pardos[145], C. Dimitriadi[164], A. Dimitrievska[21], J. Dingfelder[25], T. Dingley[129], I-M. Dinu[28b], S.J. Dittmeier[64b], F. Dittus[37], M. Divisek[136], B. Dixit[94], F. Djama[104],

T. Djobava[153b], C. Doglioni[103,100], A. Dohnalova[29a], J. Dolejsi[136], Z. Dolezal[136], K. Domijan[87a], K.M. Dona[40], M. Donadelli[84d], B. Dong[109], J. Donini[41], A. D'Onofrio[73a,73b], M. D'Onofrio[94], J. Dopke[137], A. Doria[73a], N. Dos Santos Fernandes[133a], P. Dougan[103], M.T. Dova[92], A.T. Doyle[60], M.A. Draguet[129], M.P. Drescher[56], E. Dreyer[172], I. Drivas-koulouris[10], M. Drnevich[120], M. Drozdova[57], D. Du[63a], T.A. du Pree[117], F. Dubinin[38], M. Dubovsky[29a], E. Duchovni[172], G. Duckeck[111], O.A. Ducu[28b], D. Duda[53], A. Dudarev[37], E.R. Duden[27], M. D'uffizi[103], L. Duflot[67], M. Dührssen[37], I. Duminica[28g], A.E. Dumitriu[28b], M. Dunford[64a], S. Dungs[50], K. Dunne[48a,48b], A. Duperrin[104], H. Duran Yildiz[3a], M. Düren[59], A. Durglishvili[153b], D. Duvnjak[35], B.L. Dwyer[118], G.I. Dyckes[18a], M. Dyndal[87a], B.S. Dziedzic[37], Z.O. Earnshaw[150], G.H. Eberwein[129], B. Eckerova[29a], S. Eggebrecht[56], E. Egidio Purcino De Souza[84e], L.F. Ehrke[57], G. Eigen[17], K. Einsweiler[18a], T. Ekelof[164], P.A. Ekman[100], S. El Farkh[36b], Y. El Ghazali[63a], H. El Jarrari[37], A. El Moussaouy[36a], V. Ellajosyula[164], M. Ellert[164], F. Ellinghaus[174], N. Ellis[37], J. Elmsheuser[30], M. Elsawy[119a], M. Elsing[37], D. Emeliyanov[137], Y. Enari[85], I. Ene[18a], S. Epari[13], P.A. Erland[88], D. Ernani Martins Neto[88], M. Errenst[174], M. Escalier[67], C. Escobar[166], E. Etzion[155], G. Evans[133a], H. Evans[69], L.S. Evans[97], A. Ezhilov[38], S. Ezzarqtouni[36a], F. Fabbri[24b,24a], L. Fabbri[24b,24a], G. Facini[98], V. Fadeyev[139], R.M. Fakhrutdinov[38], D. Fakoudis[102], S. Falciano[76a], L.F. Falda Ulhoa Coelho[37], F. Fallavollita[112], G. Falsetti[44b,44a], J. Faltova[136], C. Fan[165], K.Y. Fan[65b], Y. Fan[14], Y. Fang[14,114c], M. Fanti[72a,72b], M. Faraj[70a,70b], Z. Farazpay[99], A. Farbin[8], A. Farilla[78a], T. Farooque[109], S.M. Farrington[53], F. Fassi[36e], D. Fassouliotis[9], M. Faucci Giannelli[77a,77b], W.J. Fawcett[33], L. Fayard[67], P. Federic[136], P. Federicova[134], O.L. Fedin[38,a], M. Feickert[173], L. Feligioni[104], D.E. Fellers[126], C. Feng[63b], Z. Feng[117], M.J. Fenton[162], L. Ferencz[49], R.A.M. Ferguson[93], S.I. Fernandez Luengo[140f], P. Fernandez Martinez[68], M.J.V. Fernoux[104], J. Ferrando[93], A. Ferrari[164], P. Ferrari[117,116], R. Ferrari[74a], D. Ferrere[57], C. Ferretti[108], D. Fiacco[76a,76b], F. Fiedler[102], P. Fiedler[135], S. Filimonov[38], A. Filipčič[95], E.K. Filmer[159a], F. Filthaut[116], M.C.N. Fiolhais[133a,133c,c], L. Fiorini[166], W.C. Fisher[109], T. Fitschen[103], P.M. Fitzhugh[138], I. Fleck[145], P. Fleischmann[108], T. Flick[174], M. Flores[34d,aa], L.R. Flores Castillo[65a], L. Flores Sanz De Acedo[37], F.M. Follega[79a,79b], N. Fomin[33], J.H. Foo[158], A. Formica[138], A.C. Forti[103], E. Fortin[37], A.W. Fortman[18a], M.G. Foti[18a], L. Fountas[9,i], D. Fournier[67], H. Fox[93], P. Francavilla[75a,75b], S. Francescato[62], S. Franchellucci[57], M. Franchini[24b,24a], S. Franchino[64a], D. Francis[37], L. Franco[116], V. Franco Lima[37], L. Franconi[49], M. Franklin[62], G. Frattari[27], Y.Y. Frid[155], J. Friend[60], N. Fritzsche[37], A. Froch[55], D. Froidevaux[37], J.A. Frost[129], Y. Fu[63a], S. Fuenzalida Garrido[140f], M. Fujimoto[104], K.Y. Fung[65a], E. Furtado De Simas Filho[84e], M. Furukawa[157], J. Fuster[166], A. Gaa[56], A. Gabrielli[24b,24a], A. Gabrielli[158], P. Gadow[37], G. Gagliardi[58b,58a], L.G. Gagnon[18a], S. Gaid[163], S. Galantzan[155], J. Gallagher[1], E.J. Gallas[129], B.J. Gallop[137], K.K. Gan[122], S. Ganguly[157], Y. Gao[53], F.M. Garay Walls[140a,140b], B. Garcia[30], C. García[166], A. Garcia Alonso[117], A.G. Garcia Caffaro[175], J.E. García Navarro[166], M. Garcia-Sciveres[18a], G.L. Gardner[131], R.W. Gardner[40], N. Garelli[161], D. Garg[81], R.B. Garg[147], J.M. Gargan[53], C.A. Garner[158], C.M. Garvey[34a], V.K. Gassmann[161], G. Gaudio[74a],

JHEP01(2025)068

V. Gautam[13], P. Gauzzi[76a,76b], J. Gavranovic[95], I.L. Gavrilenko[38], A. Gavrilyuk[38], C. Gay[167], G. Gaycken[126], E.N. Gazis[10], A.A. Geanta[28b], C.M. Gee[139], A. Gekow[122], C. Gemme[58b], M.H. Genest[61], A.D. Gentry[115], S. George[97], W.F. George[21], T. Geralis[47], P. Gessinger-Befurt[37], M.E. Geyik[174], M. Ghani[170], K. Ghorbanian[96], A. Ghosal[145], A. Ghosh[162], A. Ghosh[7], B. Giacobbe[24b], S. Giagu[76a,76b], T. Giani[117], A. Giannini[63a], S.M. Gibson[97], M. Gignac[139], D.T. Gil[87b], A.K. Gilbert[87a], B.J. Gilbert[42], D. Gillberg[35], G. Gilles[117], L. Ginabat[130], D.M. Gingrich[2,ad], M.P. Giordani[70a,70c], P.F. Giraud[138], G. Giugliarelli[70a,70c], D. Giugni[72a], F. Giuli[77a,77b], I. Gkialas[9,i], L.K. Gladilin[38], C. Glasman[101], G.R. Gledhill[126], G. Glemža[49], M. Glisic[126], I. Gnesi[44b], Y. Go[30], M. Goblirsch-Kolb[37], B. Gocke[50], D. Godin[110], B. Gokturk[22a], S. Goldfarb[107], T. Golling[57], M.G.D. Gololo[34g], D. Golubkov[38], J.P. Gombas[109], A. Gomes[133a,133b], G. Gomes Da Silva[145], A.J. Gomez Delegido[166], R. Gonçalo[133a], L. Gonella[21], A. Gongadze[153c], F. Gonnella[21], J.L. Gonski[147], R.Y. González Andana[53], S. González de la Hoz[166], R. Gonzalez Lopez[94], C. Gonzalez Renteria[18a], M.V. Gonzalez Rodrigues[49], R. Gonzalez Suarez[164], S. Gonzalez-Sevilla[57], L. Goossens[37], B. Gorini[37], E. Gorini[71a,71b], A. Gorišek[95], T.C. Gosart[131], A.T. Goshaw[52], M.I. Gostkin[39], S. Goswami[124], C.A. Gottardo[37], S.A. Gotz[111], M. Gouighri[36b], V. Goumarre[49], A.G. Goussiou[142], N. Govender[34c], R.P. Grabarczyk[129], I. Grabowska-Bold[87a], K. Graham[35], E. Gramstad[128], S. Grancagnolo[71a,71b], C.M. Grant[1,138], P.M. Gravila[28f], F.G. Gravili[71a,71b], H.M. Gray[18a], M. Greco[71a,71b], M.J. Green[1], C. Grefe[25], A.S. Grefsrud[17], I.M. Gregor[49], K.T. Greif[162], P. Grenier[147], S.G. Grewe[112], A.A. Grillo[139], K. Grimm[32], S. Grinstein[13,t], J.-F. Grivaz[67], E. Gross[172], J. Grosse-Knetter[56], L. Guan[108], J.G.R. Guerrero Rojas[166], G. Guerrieri[37], R. Gugel[102], J.A.M. Guhit[108], A. Guida[19], E. Guilloton[170], S. Guindon[37], F. Guo[14,114c], J. Guo[63c], L. Guo[49], Y. Guo[108], A. Gupta[50], R. Gupta[132], S. Gurbuz[25], S.S. Gurdasani[55], G. Gustavino[76a,76b], P. Gutierrez[123], L.F. Gutierrez Zagazeta[131], M. Gutsche[51], C. Gutschow[98], C. Gwenlan[129], C.B. Gwilliam[94], E.S. Haaland[128], A. Haas[120], M. Habedank[60], C. Haber[18a], H.K. Hadavand[8], A. Hadef[51], S. Hadzic[112], A.I. Hagan[93], J.J. Hahn[145], E.H. Haines[98], M. Haleem[169], J. Haley[124], G.D. Hallewell[104], L. Halser[20], K. Hamano[168], M. Hamer[25], E.J. Hampshire[97], J. Han[63b], L. Han[114a], L. Han[63a], S. Han[18a], Y.F. Han[158], K. Hanagaki[85], M. Hance[139], D.A. Hangal[42], H. Hanif[146], M.D. Hank[131], J.B. Hansen[43], P.H. Hansen[43], D. Harada[57], T. Harenberg[174], S. Harkusha[38], M.L. Harris[105], Y.T. Harris[25], J. Harrison[13], N.M. Harrison[122], P.F. Harrison[170], N.M. Hartman[112], N.M. Hartmann[111], R.Z. Hasan[97,137], Y. Hasegawa[144], F. Haslbeck[129], S. Hassan[17], R. Hauser[109], C.M. Hawkes[21], R.J. Hawkings[37], Y. Hayashi[157], D. Hayden[109], C. Hayes[108], R.L. Hayes[117], C.P. Hays[129], J.M. Hays[96], H.S. Hayward[94], F. He[63a], M. He[14,114c], Y. He[49], Y. He[98], N.B. Heatley[96], V. Hedberg[100], A.L. Heggelund[128], N.D. Hehir[96,*], C. Heidegger[55], K.K. Heidegger[55], J. Heilman[35], S. Heim[49], T. Heim[18a], J.G. Heinlein[131], J.J. Heinrich[126], L. Heinrich[112,ab], J. Hejbal[134], A. Held[173], S. Hellesund[17], C.M. Helling[167], S. Hellman[48a,48b], R.C.W. Henderson[93], L. Henkelmann[33], A.M. Henriques Correia[37], H. Herde[100], Y. Hernández Jiménez[149], L.M. Herrmann[25], T. Herrmann[51], G. Herten[55], R. Hertenberger[111], L. Hervas[37], M.E. Hesping[102], N.P. Hessey[159a], J. Hessler[112],

JHEP01(2025)068

M. Hidaoui[36b], N. Hidic[136], E. Hill[158], S.J. Hillier[21], J.R. Hinds[109], F. Hinterkeuser[25], M. Hirose[127], S. Hirose[160], D. Hirschbuehl[174], T.G. Hitchings[103], B. Hiti[95], J. Hobbs[149], R. Hobincu[28e], N. Hod[172], M.C. Hodgkinson[143], B.H. Hodkinson[129], A. Hoecker[37], D.D. Hofer[108], J. Hofer[166], T. Holm[25], M. Holzbock[37], L.B.A.H. Hommels[33], B.P. Honan[103], J.J. Hong[69], J. Hong[63c], T.M. Hong[132], B.H. Hooberman[165], W.H. Hopkins[6], M.C. Hoppesch[165], Y. Horii[113], M.E. Horstmann[112], S. Hou[152], A.S. Howard[95], J. Howarth[60], J. Hoya[6], M. Hrabovsky[125], A. Hrynevich[49], T. Hryn'ova[4], P.J. Hsu[66], S.-C. Hsu[142], T. Hsu[67], M. Hu[18a], Q. Hu[63a], S. Huang[65b], X. Huang[14,114c], Y. Huang[143], Y. Huang[102], Y. Huang[14], Z. Huang[103], Z. Hubacek[135], M. Huebner[25], F. Huegging[25], T.B. Huffman[129], M. Hufnagel Maranha De Faria[84a], C.A. Hugli[49], M. Huhtinen[37], S.K. Huiberts[17], R. Hulsken[106], N. Huseynov[12,f], J. Huston[109], J. Huth[62], R. Hyneman[147], G. Iacobucci[57], G. Iakovidis[30], L. Iconomidou-Fayard[67], J.P. Iddon[37], P. Iengo[73a,73b], R. Iguchi[157], Y. Iiyama[157], T. Iizawa[129], Y. Ikegami[85], N. Ilic[158], H. Imam[84c], G. Inacio Goncalves[84d], T. Ingebretsen Carlson[48a,48b], J.M. Inglis[96], G. Introzzi[74a,74b], M. Iodice[78a], V. Ippolito[76a,76b], R.K. Irwin[94], M. Ishino[157], W. Islam[173], C. Issever[19], S. Istin[22a,ah], H. Ito[171], R. Iuppa[79a,79b], A. Ivina[172], J.M. Izen[46], V. Izzo[73a], P. Jacka[134], P. Jackson[1], C.S. Jagfeld[111], G. Jain[159a], P. Jain[49], K. Jakobs[55], T. Jakoubek[172], J. Jamieson[60], W. Jang[157], M. Javurkova[105], P. Jawahar[103], L. Jeanty[126], J. Jejelava[153a,z], P. Jenni[55,e], C.E. Jessiman[35], C. Jia[63b], H. Jia[167], J. Jia[149], X. Jia[14,114c], Z. Jia[114a], C. Jiang[53], S. Jiggins[49], J. Jimenez Pena[13], S. Jin[114a], A. Jinaru[28b], O. Jinnouchi[141], P. Johansson[143], K.A. Johns[7], J.W. Johnson[139], F.A. Jolly[49], D.M. Jones[150], E. Jones[49], K.S. Jones[8], P. Jones[33], R.W.L. Jones[93], T.J. Jones[94], H.L. Joos[56,37], R. Joshi[122], J. Jovicevic[16], X. Ju[18a], J.J. Junggeburth[105], T. Junkermann[64a], A. Juste Rozas[13,t], M.K. Juzek[88], S. Kabana[140e], A. Kaczmarska[88], M. Kado[112], H. Kagan[122], M. Kagan[147], A. Kahn[131], C. Kahra[102], T. Kaji[157], E. Kajomovitz[154], N. Kakati[172], I. Kalaitzidou[55], C.W. Kalderon[30], N.J. Kang[139], D. Kar[34g], K. Karava[129], M.J. Kareem[159b], E. Karentzos[55], O. Karkout[117], S.N. Karpov[39], Z.M. Karpova[39], V. Kartvelishvili[93], A.N. Karyukhin[38], E. Kasimi[156], J. Katzy[49], S. Kaur[35], K. Kawade[144], M.P. Kawale[123], C. Kawamoto[89], T. Kawamoto[63a], E.F. Kay[37], F.I. Kaya[161], S. Kazakos[109], V.F. Kazanin[38], Y. Ke[149], J.M. Keaveney[34a], R. Keeler[168], G.V. Kehris[62], J.S. Keller[35], J.J. Kempster[150], O. Kepka[134], B.P. Kerridge[137], S. Kersten[174], B.P. Kerševan[95], L. Keszeghova[29a], S. Ketabchi Haghighat[158], R.A. Khan[132], A. Khanov[124], A.G. Kharlamov[38], T. Kharlamova[38], E.E. Khoda[142], M. Kholodenko[133a], T.J. Khoo[19], G. Khoriauli[169], J. Khubua[153b,*], Y.A.R. Khwaira[130], B. Kibirige[34g], D. Kim[6], D.W. Kim[48a,48b], Y.K. Kim[40], N. Kimura[98], M.K. Kingston[56], A. Kirchhoff[56], C. Kirfel[25], F. Kirfel[25], J. Kirk[137], A.E. Kiryunin[112], S. Kita[160], C. Kitsaki[10], O. Kivernyk[25], M. Klassen[161], C. Klein[35], L. Klein[169], M.H. Klein[45], S.B. Klein[57], U. Klein[94], A. Klimentov[30], T. Klioutchnikova[37], P. Kluit[117], S. Kluth[112], E. Kneringer[80], T.M. Knight[158], A. Knue[50], D. Kobylianskii[172], S.F. Koch[129], M. Kocian[147], P. Kodyš[136], D.M. Koeck[126], P.T. Koenig[25], T. Koffas[35], O. Kolay[51], I. Koletsou[4], T. Komarek[88], K. Köneke[55], A.X.Y. Kong[1], T. Kono[121], N. Konstantinidis[98], P. Kontaxakis[57], B. Konya[100], R. Kopeliansky[42], S. Koperny[87a],

JHEP01(2025)068

K. Korcyl[88], K. Kordas[156,d], A. Korn[98], S. Korn[56], I. Korolkov[13], N. Korotkova[38], B. Kortman[117], O. Kortner[112], S. Kortner[112], W.H. Kostecka[118], V.V. Kostyukhin[145], A. Kotsokechagia[37], A. Kotwal[52], A. Koulouris[37], A. Kourkoumeli-Charalampidi[74a,74b], C. Kourkoumelis[9], E. Kourlitis[112,ab], O. Kovanda[126], R. Kowalewski[168], W. Kozanecki[126], A.S. Kozhin[38], V.A. Kramarenko[38], G. Kramberger[95], P. Kramer[102], M.W. Krasny[130], A. Krasznahorkay[37], A.C. Kraus[118], J.W. Kraus[174], J.A. Kremer[49], T. Kresse[51], L. Kretschmann[174], J. Kretzschmar[94], K. Kreul[19], P. Krieger[158], M. Krivos[136], K. Krizka[21], K. Kroeninger[50], H. Kroha[112], J. Kroll[134], J. Kroll[131], K.S. Krowpman[109], U. Kruchonak[39], H. Krüger[25], N. Krumnack[82], M.C. Kruse[52], O. Kuchinskaia[38], S. Kuday[3a], S. Kuehn[37], R. Kuesters[55], T. Kuhl[49], V. Kukhtin[39], Y. Kulchitsky[38,a], S. Kuleshov[140d,140b], M. Kumar[34g], N. Kumari[49], P. Kumari[159b], A. Kupco[134], T. Kupfer[50], A. Kupich[38], O. Kuprash[55], H. Kurashige[86], L.L. Kurchaninov[159a], O. Kurdysh[67], Y.A. Kurochkin[38], A. Kurova[38], M. Kuze[141], A.K. Kvam[105], J. Kvita[125], T. Kwan[106], N.G. Kyriacou[108], L.A.O. Laatu[104], C. Lacasta[166], F. Lacava[76a,76b], H. Lacker[19], D. Lacour[130], N.N. Lad[98], E. Ladygin[39], A. Lafarge[41], B. Laforge[130], T. Lagouri[175], F.Z. Lahbabi[36a], S. Lai[56], J.E. Lambert[168], S. Lammers[69], W. Lampl[7], C. Lampoudis[156,d], G. Lamprinoudis[102], A.N. Lancaster[118], E. Lançon[30], U. Landgraf[55], M.P.J. Landon[96], V.S. Lang[55], O.K.B. Langrekken[128], A.J. Lankford[162], F. Lanni[37], K. Lantzsch[25], A. Lanza[74a], M. Lanzac Berrocal[166], J.F. Laporte[138], T. Lari[72a], F. Lasagni Manghi[24b], M. Lassnig[37], V. Latonova[134], A. Laurier[154], S.D. Lawlor[143], Z. Lawrence[103], R. Lazaridou[170], M. Lazzaroni[72a,72b], B. Le[103], H.D.M. Le[109], E.M. Le Boulicaut[175], L.T. Le Pottier[18a], B. Leban[24b,24a], A. Lebedev[82], M. LeBlanc[103], F. Ledroit-Guillon[61], S.C. Lee[152], S. Lee[48a,48b], T.F. Lee[94], L.L. Leeuw[34c], H.P. Lefebvre[97], M. Lefebvre[168], C. Leggett[18a], G. Lehmann Miotto[37], M. Leigh[57], W.A. Leight[105], W. Leinonen[116], A. Leisos[156,r], M.A.L. Leite[84c], C.E. Leitgeb[19], R. Leitner[136], K.J.C. Leney[45], T. Lenz[25], S. Leone[75a], C. Leonidopoulos[53], A. Leopold[148], R. Les[109], C.G. Lester[33], M. Levchenko[38], J. Levêque[4], L.J. Levinson[172], G. Levrini[24b,24a], M.P. Lewicki[88], C. Lewis[142], D.J. Lewis[4], L. Lewitt[143], A. Li[30], B. Li[63b], C. Li[63a], C-Q. Li[112], H. Li[63a], H. Li[63b], H. Li[114a], H. Li[15], H. Li[63b], J. Li[63c], K. Li[14], L. Li[63c], M. Li[14,114c], S. Li[14,114c], S. Li[63d,63c], T. Li[5], X. Li[106], Y. Li[49], Z. Li[157], Z. Li[14,114c], Z. Li[63a], S. Liang[14,114c], Z. Liang[14], M. Liberatore[138], B. Liberti[77a], K. Lie[65c], J. Lieber Marin[84e], H. Lien[69], H. Lin[108], K. Lin[109], R.E. Lindley[7], J.H. Lindon[2], J. Ling[62], E. Lipeles[131], A. Lipniacka[17], A. Lister[167], J.D. Little[69], B. Liu[14], B.X. Liu[114b], D. Liu[63d,63c], E.H.L. Liu[21], J.B. Liu[63a], J.K.K. Liu[33], K. Liu[63d], K. Liu[63d,63c], M. Liu[63a], M.Y. Liu[63a], P. Liu[14], Q. Liu[63d,142,63c], X. Liu[63a], X. Liu[63b], Y. Liu[114b,114c], Y.L. Liu[63b], Y.W. Liu[63a], S.L. Lloyd[96], E.M. Lobodzinska[49], P. Loch[7], E. Lodhi[158], T. Lohse[19], K. Lohwasser[143], E. Loiacono[49], M. Lokajicek[134,*], J.D. Lomas[21], J.D. Long[42], I. Longarini[162], R. Longo[165], I. Lopez Paz[68], A. Lopez Solis[49], N.A. Lopez-canelas[7], N. Lorenzo Martinez[4], A.M. Lory[111], M. Losada[119a], G. Löschcke Centeno[150], O. Loseva[38], X. Lou[48a,48b], X. Lou[14,114c], A. Lounis[67], P.A. Love[93], G. Lu[14,114c], M. Lu[67], S. Lu[131], Y.J. Lu[66], H.J. Lubatti[142], C. Luci[76a,76b], F.L. Lucio Alves[114a], F. Luehring[69], O. Lukianchuk[67], B.S. Lunday[131], O. Lundberg[148], B. Lund-Jensen[148,*], N.A. Luongo[6], M.S. Lutz[37],

JHEP01(2025)068

A.B. Lux[26], D. Lynn[30], R. Lysak[134], E. Lytken[100], V. Lyubushkin[39], T. Lyubushkina[39], M.M. Lyukova[149], M.Firdaus M. Soberi[53], H. Ma[30], K. Ma[63a], L.L. Ma[63b], W. Ma[63a], Y. Ma[124], J.C. MacDonald[102], P.C. Machado De Abreu Farias[84e], R. Madar[41], T. Madula[98], J. Maeda[86], T. Maeno[30], H. Maguire[143], V. Maiboroda[138], A. Maio[133a,133b,133d], K. Maj[87a], O. Majersky[49], S. Majewski[126], N. Makovec[67], V. Maksimovic[16], B. Malaescu[130], Pa. Malecki[88], V.P. Maleev[38], F. Malek[61,m], M. Mali[95], D. Malito[97], U. Mallik[81,*], S. Maltezos[10], S. Malyukov[39], J. Mamuzic[13], G. Mancini[54], M.N. Mancini[27], G. Manco[74a,74b], J.P. Mandalia[96], S.S. Mandarry[150], I. Mandić[95], L. Manhaes de Andrade Filho[84a], I.M. Maniatis[172], J. Manjarres Ramos[91], D.C. Mankad[172], A. Mann[111], S. Manzoni[37], L. Mao[63c], X. Mapekula[34c], A. Marantis[156,r], G. Marchiori[5], M. Marcisovsky[134], C. Marcon[72a], M. Marinescu[21], S. Marium[49], M. Marjanovic[123], A. Markhoos[55], M. Markovitch[67], E.J. Marshall[93], Z. Marshall[18a], S. Marti-Garcia[166], J. Martin[98], T.A. Martin[137], V.J. Martin[53], B. Martin dit Latour[17], L. Martinelli[76a,76b], M. Martinez[13,t], P. Martinez Agullo[166], V.I. Martinez Outschoorn[105], P. Martinez Suarez[13], S. Martin-Haugh[137], G. Martinovicova[136], V.S. Martoiu[28b], A.C. Martyniuk[98], A. Marzin[37], D. Mascione[79a,79b], L. Masetti[102], J. Masik[103], A.L. Maslennikov[38], S.L. Mason[42], P. Massarotti[73a,73b], P. Mastrandrea[75a,75b], A. Mastroberardino[44b,44a], T. Masubuchi[127], T.T. Mathew[126], T. Mathisen[164], J. Matousek[136], D.M. Mattern[50], J. Maurer[28b], T. Maurin[60], A.J. Maury[67], B. Maček[95], D.A. Maximov[38], A.E. May[103], R. Mazini[152], I. Maznas[118], M. Mazza[109], S.M. Mazza[139], E. Mazzeo[72a,72b], C. Mc Ginn[30], J.P. Mc Gowan[168], S.P. Mc Kee[108], C.A. Mc Lean[6], C.C. McCracken[167], E.F. McDonald[107], A.E. McDougall[117], J.A. Mcfayden[150], R.P. McGovern[131], R.P. Mckenzie[34g], T.C. Mclachlan[49], D.J. Mclaughlin[98], S.J. McMahon[137], C.M. Mcpartland[94], R.A. McPherson[168,x], S. Mehlhase[111], A. Mehta[94], D. Melini[166], B.R. Mellado Garcia[34g], A.H. Melo[56], F. Meloni[49], A.M. Mendes Jacques Da Costa[103], H.Y. Meng[158], L. Meng[93], S. Menke[112], M. Mentink[37], E. Meoni[44b,44a], G. Mercado[118], S. Merianos[156], C. Merlassino[70a,70c], L. Merola[73a,73b], C. Meroni[72a,72b], J. Metcalfe[6], A.S. Mete[6], E. Meuser[102], C. Meyer[69], J-P. Meyer[138], R.P. Middleton[137], L. Mijović[53], G. Mikenberg[172], M. Mikestikova[134], M. Mikuž[95], H. Mildner[102], A. Milic[37], D.W. Miller[40], E.H. Miller[147], L.S. Miller[35], A. Milov[172], D.A. Milstead[48a,48b], T. Min[114a], A.A. Minaenko[38], I.A. Minashvili[153b], L. Mince[60], A.I. Mincer[120], B. Mindur[87a], M. Mineev[39], Y. Mino[89], L.M. Mir[13], M. Miralles Lopez[60], M. Mironova[18a], M.C. Missio[116], A. Mitra[170], V.A. Mitsou[166], Y. Mitsumori[113], O. Miu[158], P.S. Miyagawa[96], T. Mkrtchyan[64a], M. Mlinarevic[98], T. Mlinarevic[98], M. Mlynarikova[37], S. Mobius[20], P. Mogg[111], M.H. Mohamed Farook[115], A.F. Mohammed[14,114c], S. Mohapatra[42], G. Mokgatitswane[34g], L. Moleri[172], B. Mondal[145], S. Mondal[135], K. Mönig[49], E. Monnier[104], L. Monsonis Romero[166], J. Montejo Berlingen[13], A. Montella[48a,48b], M. Montella[122], F. Montereali[78a,78b], F. Monticelli[92], S. Monzani[70a,70c], A. Morancho Tarda[43], N. Morange[67], A.L. Moreira De Carvalho[49], M. Moreno Llácer[166], C. Moreno Martinez[57], J.M. Moreno Perez[23b], P. Morettini[58b], S. Morgenstern[37], M. Morii[62], M. Morinaga[157], M. Moritsu[90], F. Morodei[76a,76b], P. Moschovakos[37], B. Moser[129], M. Mosidze[153b], T. Moskalets[45], P. Moskvitina[116], J. Moss[32,j], P. Moszkowicz[87a],

JHEP01(2025)068

A. Moussa[36d], E.J.W. Moyse[105], O. Mtintsilana[34g], S. Muanza[104], J. Mueller[132], D. Muenstermann[93], R. Müller[37], G.A. Mullier[164], A.J. Mullin[33], J.J. Mullin[131], A.E. Mulski[62], D.P. Mungo[158], D. Munoz Perez[166], F.J. Munoz Sanchez[103], M. Murin[103], W.J. Murray[170,137], M. Muškinja[95], C. Mwewa[30], A.G. Myagkov[38,a], A.J. Myers[8], G. Myers[108], M. Myska[135], B.P. Nachman[18a], O. Nackenhorst[50], K. Nagai[129], K. Nagano[85], R. Nagasaka[157], J.L. Nagle[30,af], E. Nagy[104], A.M. Nairz[37], Y. Nakahama[85], K. Nakamura[85], K. Nakkalil[5], H. Nanjo[127], E.A. Narayanan[45], I. Naryshkin[38], L. Nasella[72a,72b], M. Naseri[35], S. Nasri[119b], C. Nass[25], G. Navarro[23a], J. Navarro-Gonzalez[166], R. Nayak[155], A. Nayaz[19], P.Y. Nechaeva[38], S. Nechaeva[24b,24a], F. Nechansky[134], L. Nedic[129], T.J. Neep[21], A. Negri[74a,74b], M. Negrini[24b], C. Nellist[117], C. Nelson[106], K. Nelson[108], S. Nemecek[134], M. Nessi[37,g], M.S. Neubauer[165], F. Neuhaus[102], J. Neundorf[49], J. Newell[94], P.R. Newman[21], C.W. Ng[132], Y.W.Y. Ng[49], B. Ngair[119a], H.D.N. Nguyen[110], R.B. Nickerson[129], R. Nicolaidou[138], J. Nielsen[139], M. Niemeyer[56], J. Niermann[56], N. Nikiforou[37], V. Nikolaenko[38,a], I. Nikolic-Audit[130], K. Nikolopoulos[21], P. Nilsson[30], I. Ninca[49], G. Ninio[155], A. Nisati[76a], N. Nishu[2], R. Nisius[112], J-E. Nitschke[51], E.K. Nkadimeng[34g], T. Nobe[157], T. Nommensen[151], M.B. Norfolk[143], B.J. Norman[35], M. Noury[36a], J. Novak[95], T. Novak[95], L. Novotny[135], R. Novotny[115], L. Nozka[125], K. Ntekas[162], N.M.J. Nunes De Moura Junior[84b], J. Ocariz[130], A. Ochi[86], I. Ochoa[133a], S. Oerdek[49,u], J.T. Offermann[40], A. Ogrodnik[136], A. Oh[103], C.C. Ohm[148], H. Oide[85], R. Oishi[157], M.L. Ojeda[37], Y. Okumura[157], L.F. Oleiro Seabra[133a], I. Oleksiyuk[57], S.A. Olivares Pino[140d], G. Oliveira Correa[13], D. Oliveira Damazio[30], J.L. Oliver[162], Ö.O. Öncel[55], A.P. O'Neill[20], A. Onofre[133a,133e], P.U.E. Onyisi[11], M.J. Oreglia[40], G.E. Orellana[92], D. Orestano[78a,78b], N. Orlando[13], R.S. Orr[158], L.M. Osojnak[131], R. Ospanov[63a], Y. Osumi[113], G. Otero y Garzon[31], H. Otono[90], P.S. Ott[64a], G.J. Ottino[18a], M. Ouchrif[36d], F. Ould-Saada[128], T. Ovsiannikova[142], M. Owen[60], R.E. Owen[137], V.E. Ozcan[22a], F. Ozturk[88], N. Ozturk[8], S. Ozturk[83], H.A. Pacey[129], A. Pacheco Pages[13], C. Padilla Aranda[13], G. Padovano[76a,76b], S. Pagan Griso[18a], G. Palacino[69], A. Palazzo[71a,71b], J. Pampel[25], J. Pan[175], T. Pan[65a], D.K. Panchal[11], C.E. Pandini[117], J.G. Panduro Vazquez[137], H.D. Pandya[1], H. Pang[15], P. Pani[49], G. Panizzo[70a,70c], L. Panwar[130], L. Paolozzi[57], S. Parajuli[165], A. Paramonov[6], C. Paraskevopoulos[54], D. Paredes Hernandez[65b], A. Pareti[74a,74b], K.R. Park[42], T.H. Park[158], M.A. Parker[33], F. Parodi[58b,58a], E.W. Parrish[118], V.A. Parrish[53], J.A. Parsons[42], U. Parzefall[55], B. Pascual Dias[110], L. Pascual Dominguez[101], E. Pasqualucci[76a], S. Passaggio[58b], F. Pastore[97], P. Patel[88], U.M. Patel[52], J.R. Pater[103], T. Pauly[37], F. Pauwels[136], C.I. Pazos[161], M. Pedersen[128], R. Pedro[133a], S.V. Peleganchuk[38], O. Penc[37], E.A. Pender[53], S. Peng[15], G.D. Penn[175], K.E. Penski[111], M. Penzin[38], B.S. Peralva[84d], A.P. Pereira Peixoto[142], L. Pereira Sanchez[147], D.V. Perepelitsa[30,af], G. Perera[105], E. Perez Codina[159a], M. Perganti[10], H. Pernegger[37], S. Perrella[76a,76b], O. Perrin[41], K. Peters[49], R.F.Y. Peters[103], B.A. Petersen[37], T.C. Petersen[43], E. Petit[104], V. Petousis[135], C. Petridou[156,d], T. Petru[136], A. Petrukhin[145], M. Pettee[18a], A. Petukhov[38], K. Petukhova[37], R. Pezoa[140f], L. Pezzotti[37], G. Pezzullo[175], A.J. Pfleger[37], T.M. Pham[173], T. Pham[107], P.W. Phillips[137], G. Piacquadio[149], E. Pianori[18a], F. Piazza[126], R. Piegaia[31],

JHEP01(2025)068

D. Pietreanu[28b], A.D. Pilkington[103], M. Pinamonti[70a,70c], J.L. Pinfold[2], B.C. Pinheiro Pereira[133a], J. Pinol Bel[13], A.E. Pinto Pinoargote[138,138], L. Pintucci[70a,70c], K.M. Piper[150], A. Pirttikoski[57], D.A. Pizzi[35], L. Pizzimento[65b], A. Pizzini[117], M.-A. Pleier[30], V. Pleskot[136], E. Plotnikova[39], G. Poddar[96], R. Poettgen[100], L. Poggioli[130], I. Pokharel[56], S. Polacek[136], G. Polesello[74a], A. Poley[146,159a], A. Polini[24b], C.S. Pollard[170], Z.B. Pollock[122], E. Pompa Pacchi[76a,76b], N.I. Pond[98], D. Ponomarenko[69], L. Pontecorvo[37], S. Popa[28a], G.A. Popeneciu[28d], A. Poreba[37], D.M. Portillo Quintero[159a], S. Pospisil[135], M.A. Postill[143], P. Postolache[28c], K. Potamianos[170], P.A. Potepa[87a], I.N. Potrap[39], C.J. Potter[33], H. Potti[151], J. Poveda[166], M.E. Pozo Astigarraga[37], A. Prades Ibanez[77a,77b], J. Pretel[168], D. Price[103], M. Primavera[71a], L. Primomo[70a,70c], M.A. Principe Martin[101], R. Privara[125], T. Procter[60], M.L. Proffitt[142], N. Proklova[131], K. Prokofiev[65c], G. Proto[112], J. Proudfoot[6], M. Przybycien[87a], W.W. Przygoda[87b], A. Psallidas[47], J.E. Puddefoot[143], D. Pudzha[55], D. Pyatiizbyantseva[38], J. Qian[108], D. Qichen[103], Y. Qin[13], T. Qiu[53], A. Quadt[56], M. Queitsch-Maitland[103], G. Quetant[57], R.P. Quinn[167], G. Rabanal Bolanos[62], D. Rafanoharana[55], F. Raffaeli[77a,77b], F. Ragusa[72a,72b], J.L. Rainbolt[40], J.A. Raine[57], S. Rajagopalan[30], E. Ramakoti[38], L. Rambelli[58b,58a], I.A. Ramirez-Berend[35], K. Ran[49,114c], D.S. Rankin[131], N.P. Rapheeha[34g], H. Rasheed[28b], V. Raskina[130], D.F. Rassloff[64a], A. Rastogi[18a], S. Rave[102], S. Ravera[58b,58a], B. Ravina[56], I. Ravinovich[172], M. Raymond[37], A.L. Read[128], N.P. Readioff[143], D.M. Rebuzzi[74a,74b], G. Redlinger[30], A.S. Reed[112], K. Reeves[27], J.A. Reidelsturz[174], D. Reikher[126], A. Rej[50], C. Rembser[37], M. Renda[28b], F. Renner[49], A.G. Rennie[162], A.L. Rescia[49], S. Resconi[72a], M. Ressegotti[58b,58a], S. Rettie[37], J.G. Reyes Rivera[109], E. Reynolds[18a], O.L. Rezanova[38], P. Reznicek[136], H. Riani[36d], N. Ribaric[52], E. Ricci[79a,79b], R. Richter[112], S. Richter[48a,48b], E. Richter-Was[87b], M. Ridel[130], S. Ridouani[36d], P. Rieck[120], P. Riedler[37], E.M. Riefel[48a,48b], J.O. Rieger[117], M. Rijssenbeek[149], M. Rimoldi[37], L. Rinaldi[24b,24a], P. Rincke[56,164], T.T. Rinn[30], M.P. Rinnagel[111], G. Ripellino[164], I. Riu[13], J.C. Rivera Vergara[168], F. Rizatdinova[124], E. Rizvi[96], B.R. Roberts[18a], S.S. Roberts[139], S.H. Robertson[106,x], M. Robin[19], D. Robinson[33], M. Robles Manzano[102], A. Robson[60], A. Rocchi[77a,77b], C. Roda[75a,75b], S. Rodriguez Bosca[37], Y. Rodriguez Garcia[23a], A. Rodriguez Rodriguez[55], A.M. Rodríguez Vera[118], S. Roe[37], J.T. Roemer[37], A.R. Roepe-Gier[139], O. Røhne[128], R.A. Rojas[105], C.P.A. Roland[130], J. Roloff[30], A. Romaniouk[80], E. Romano[74a,74b], M. Romano[24b], A.C. Romero Hernandez[165], N. Rompotis[94], L. Roos[130], S. Rosati[76a], B.J. Rosser[40], E. Rossi[129], E. Rossi[73a,73b], L.P. Rossi[62], L. Rossini[55], R. Rosten[122], M. Rotaru[28b], B. Rottler[55], C. Rougier[91], D. Rousseau[67], D. Rousso[49], A. Roy[165], S. Roy-Garand[158], A. Rozanov[104], Z.M.A. Rozario[60], Y. Rozen[154], A. Rubio Jimenez[166], A.J. Ruby[94], V.H. Ruelas Rivera[19], T.A. Ruggeri[1], A. Ruggiero[129], A. Ruiz-Martinez[166], A. Rummler[37], Z. Rurikova[55], N.A. Rusakovich[39], H.L. Russell[168], G. Russo[76a,76b], J.P. Rutherfoord[7], S. Rutherford Colmenares[33], M. Rybar[136], E.B. Rye[128], A. Ryzhov[45], J.A. Sabater Iglesias[57], H.F-W. Sadrozinski[139], F. Safai Tehrani[76a], B. Safarzadeh Samani[137], S. Saha[1], M. Sahinsoy[83], A. Saibel[166], M. Saimpert[138], M. Saito[157], T. Saito[157], A. Sala[72a,72b], D. Salamani[37], A. Salnikov[147], J. Salt[166], A. Salvador Salas[155],

JHEP01(2025)068

D. Salvatore[44b,44a], F. Salvatore[150], A. Salzburger[37], D. Sammel[55], E. Sampson[93], D. Sampsonidis[156,d], D. Sampsonidou[126], J. Sánchez[166], V. Sanchez Sebastian[166], H. Sandaker[128], C.O. Sander[49], J.A. Sandesara[105], M. Sandhoff[174], C. Sandoval[23b], L. Sanfilippo[64a], D.P.C. Sankey[137], T. Sano[89], A. Sansoni[54], L. Santi[37,76b], C. Santoni[41], H. Santos[133a,133b], A. Santra[172], E. Sanzani[24b,24a], K.A. Saoucha[163], J.G. Saraiva[133a,133d], J. Sardain[7], O. Sasaki[85], K. Sato[160], C. Sauer[64b], E. Sauvan[4], P. Savard[158,ad], R. Sawada[157], C. Sawyer[137], L. Sawyer[99], C. Sbarra[24b], A. Sbrizzi[24b,24a], T. Scanlon[98], J. Schaarschmidt[142], U. Schäfer[102], A.C. Schaffer[67,45], D. Schaile[111], R.D. Schamberger[149], C. Scharf[19], M.M. Schefer[20], V.A. Schegelsky[38], D. Scheirich[136], M. Schernau[162], C. Scheulen[56], C. Schiavi[58b,58a], M. Schioppa[44b,44a], B. Schlag[147], S. Schlenker[37], J. Schmeing[174], M.A. Schmidt[174], K. Schmieden[102], C. Schmitt[102], N. Schmitt[102], S. Schmitt[49], L. Schoeffel[138], A. Schoening[64b], P.G. Scholer[35], E. Schopf[129], M. Schott[25], J. Schovancova[37], S. Schramm[57], T. Schroer[57], H-C. Schultz-Coulon[64a], M. Schumacher[55], B.A. Schumm[139], Ph. Schune[138], A.J. Schuy[142], H.R. Schwartz[139], A. Schwartzman[147], T.A. Schwarz[108], Ph. Schwemling[138], R. Schwienhorst[109], F.G. Sciacca[20], A. Sciandra[30], G. Sciolla[27], F. Scuri[75a], C.D. Sebastiani[94], K. Sedlaczek[118], S.C. Seidel[115], A. Seiden[139], B.D. Seidlitz[42], C. Seitz[49], J.M. Seixas[84b], G. Sekhniaidze[73a], L. Selem[61], N. Semprini-Cesari[24b,24a], D. Sengupta[57], V. Senthilkumar[166], L. Serin[67], M. Sessa[77a,77b], H. Severini[123], F. Sforza[58b,58a], A. Sfyrla[57], Q. Sha[14], E. Shabalina[56], A.H. Shah[33], R. Shaheen[148], J.D. Shahinian[131], D. Shaked Renous[172], L.Y. Shan[14], M. Shapiro[18a], A. Sharma[37], A.S. Sharma[167], P. Sharma[81], P.B. Shatalov[38], K. Shaw[150], S.M. Shaw[103], Q. Shen[63c], D.J. Sheppard[146], P. Sherwood[98], L. Shi[98], X. Shi[14], S. Shimizu[85], C.O. Shimmin[175], J.D. Shinner[97], I.P.J. Shipsey[129,*], S. Shirabe[90], M. Shiyakova[39,v], M.J. Shochet[40], D.R. Shope[128], B. Shrestha[123], S. Shrestha[122,ag], I. Shreyber[38], M.J. Shroff[168], P. Sicho[134], A.M. Sickles[165], E. Sideras Haddad[34g], A.C. Sidley[117], A. Sidoti[24b], F. Siegert[51], Dj. Sijacki[16], F. Sili[92], J.M. Silva[53], I. Silva Ferreira[84b], M.V. Silva Oliveira[30], S.B. Silverstein[48a], S. Simion[67], R. Simoniello[37], E.L. Simpson[103], H. Simpson[150], L.R. Simpson[108], S. Simsek[83], S. Sindhu[56], P. Sinervo[158], S. Singh[158], S. Sinha[49], S. Sinha[103], M. Sioli[24b,24a], I. Siral[37], E. Sitnikova[49], J. Sjölin[48a,48b], A. Skaf[56], E. Skorda[21], P. Skubic[123], M. Slawinska[88], V. Smakhtin[172], B.H. Smart[137], S.Yu. Smirnov[38], Y. Smirnov[38], L.N. Smirnova[38,a], O. Smirnova[100], A.C. Smith[42], D.R. Smith[162], E.A. Smith[40], J.L. Smith[103], R. Smith[147], M. Smizanska[93], K. Smolek[135], A.A. Snesarev[38], H.L. Snoek[117], S. Snyder[30], R. Sobie[168,x], A. Soffer[155], C.A. Solans Sanchez[37], E.Yu. Soldatov[38], U. Soldevila[166], A.A. Solodkov[38], S. Solomon[27], A. Soloshenko[39], K. Solovieva[55], O.V. Solovyanov[41], P. Sommer[51], A. Sonay[13], W.Y. Song[159b], A. Sopczak[135], A.L. Sopio[53], F. Sopkova[29b], J.D. Sorenson[115], I.R. Sotarriva Alvarez[141], V. Sothilingam[64a], O.J. Soto Sandoval[140c,140b], S. Sottocornola[69], R. Soualah[163], Z. Soumaimi[36e], D. South[49], N. Soybelman[172], S. Spagnolo[71a,71b], M. Spalla[112], D. Sperlich[55], G. Spigo[37], B. Spisso[73a,73b], D.P. Spiteri[60], M. Spousta[136], E.J. Staats[35], R. Stamen[64a], A. Stampekis[21], E. Stanecka[88], W. Stanek-Maslouska[49], M.V. Stange[51], B. Stanislaus[18a], M.M. Stanitzki[49], B. Stapf[49], E.A. Starchenko[38], G.H. Stark[139], J. Stark[91], P. Staroba[134], P. Starovoitov[64a], S. Stärz[106], R. Staszewski[88], G. Stavropoulos[47], A. Stefl[37], P. Steinberg[30], B. Stelzer[146,159a], H.J. Stelzer[132],

JHEP01(2025)068

O. Stelzer-Chilton[159a], H. Stenzel[59], T.J. Stevenson[150], G.A. Stewart[37], J.R. Stewart[124], M.C. Stockton[37], G. Stoicea[28b], M. Stolarski[133a], S. Stonjek[112], A. Straessner[51], J. Strandberg[148], S. Strandberg[48a,48b], M. Stratmann[174], M. Strauss[123], T. Strebler[104], P. Strizenec[29b], R. Ströhmer[169], D.M. Strom[126], R. Stroynowski[45], A. Strubig[48a,48b], S.A. Stucci[30], B. Stugu[17], J. Stupak[123], N.A. Styles[49], D. Su[147], S. Su[63a], W. Su[63d], X. Su[63a], D. Suchy[29a], K. Sugizaki[157], V.V. Sulin[38], M.J. Sullivan[94], D.M.S. Sultan[129], L. Sultanaliyeva[38], S. Sultansoy[3b], T. Sumida[89], S. Sun[173], O. Sunneborn Gudnadottir[164], N. Sur[104], M.R. Sutton[150], H. Suzuki[160], M. Svatos[134], M. Swiatlowski[159a], T. Swirski[169], I. Sykora[29a], M. Sykora[136], T. Sykora[136], D. Ta[102], K. Tackmann[49,u], A. Taffard[162], R. Tafirout[159a], J.S. Tafoya Vargas[67], Y. Takubo[85], M. Talby[104], A.A. Talyshev[38], K.C. Tam[65b], N.M. Tamir[155], A. Tanaka[157], J. Tanaka[157], R. Tanaka[67], M. Tanasini[149], Z. Tao[167], S. Tapia Araya[140f], S. Tapprogge[102], A. Tarek Abouelfadl Mohamed[109], S. Tarem[154], K. Tariq[14], G. Tarna[28b], G.F. Tartarelli[72a], M.J. Tartarin[91], P. Tas[136], M. Tasevsky[134], E. Tassi[44b,44a], A.C. Tate[165], G. Tateno[157], Y. Tayalati[36e,w], G.N. Taylor[107], W. Taylor[159b], R. Teixeira De Lima[147], P. Teixeira-Dias[97], J.J. Teoh[158], K. Terashi[157], J. Terron[101], S. Terzo[13], M. Testa[54], R.J. Teuscher[158,x], A. Thaler[80], O. Theiner[57], T. Theveneaux-Pelzer[104], O. Thielmann[174], D.W. Thomas[97], J.P. Thomas[21], E.A. Thompson[18a], P.D. Thompson[21], E. Thomson[131], R.E. Thornberry[45], C. Tian[63a], Y. Tian[57], V. Tikhomirov[38,a], Yu.A. Tikhonov[38], S. Timoshenko[38], D. Timoshyn[136], E.X.L. Ting[1], P. Tipton[175], A. Tishelman-Charny[30], S.H. Tlou[34g], K. Todome[141], S. Todorova-Nova[136], S. Todt[51], L. Toffolin[70a,70c], M. Togawa[85], J. Tojo[90], S. Tokár[29a], K. Tokushuku[85], O. Toldaiev[69], M. Tomoto[85,113], L. Tompkins[147,l], K.W. Topolnicki[87b], E. Torrence[126], H. Torres[91], E. Torró Pastor[166], M. Toscani[31], C. Tosciri[40], M. Tost[11], D.R. Tovey[143], I.S. Trandafir[28b], T. Trefzger[169], A. Tricoli[30], I.M. Trigger[159a], S. Trincaz-Duvoid[130], D.A. Trischuk[27], B. Trocmé[61], A. Tropina[39], L. Truong[34c], M. Trzebinski[88], A. Trzupek[88], F. Tsai[149], M. Tsai[108], A. Tsiamis[156], P.V. Tsiareshka[38], S. Tsigaridas[159a], A. Tsirigotis[156,r], V. Tsiskaridze[158], E.G. Tskhadadze[153a], M. Tsopoulou[156], Y. Tsujikawa[89], I.I. Tsukerman[38], V. Tsulaia[18a], S. Tsuno[85], K. Tsuri[121], D. Tsybychev[149], Y. Tu[65b], A. Tudorache[28b], V. Tudorache[28b], A.N. Tuna[62], S. Turchikhin[58b,58a], I. Turk Cakir[3a], R. Turra[72a], T. Turtuvshin[39], P.M. Tuts[42], S. Tzamarias[156,d], E. Tzovara[102], F. Ukegawa[160], P.A. Ulloa Poblete[140c,140b], E.N. Umaka[30], G. Unal[37], A. Undrus[30], G. Unel[162], J. Urban[29b], P. Urrejola[140a], G. Usai[8], R. Ushioda[141], M. Usman[110], F. Ustuner[53], Z. Uysal[83], V. Vacek[135], B. Vachon[106], T. Vafeiadis[37], A. Vaitkus[98], C. Valderanis[111], E. Valdes Santurio[48a,48b], M. Valente[159a], S. Valentinetti[24b,24a], A. Valero[166], E. Valiente Moreno[166], A. Vallier[91], J.A. Valls Ferrer[166], D.R. Van Arneman[117], T.R. Van Daalen[142], A. Van Der Graaf[50], P. Van Gemmeren[6], M. Van Rijnbach[37], S. Van Stroud[98], I. Van Vulpen[117], P. Vana[136], M. Vanadia[77a,77b], U.M. Vande Voorde[148], W. Vandelli[37], E.R. Vandewall[124], D. Vannicola[155], L. Vannoli[54], R. Vari[76a], E.W. Varnes[7], C. Varni[18b], T. Varol[152], D. Varouchas[67], L. Varriale[166], K.E. Varvell[151], M.E. Vasile[28b], L. Vaslin[85], G.A. Vasquez[168], A. Vasyukov[39], L.M. Vaughan[124], R. Vavricka[102], T. Vazquez Schroeder[37], J. Veatch[32], V. Vecchio[103], M.J. Veen[105], I. Veliscek[30], L.M. Veloce[158], F. Veloso[133a,133c], S. Veneziano[76a], A. Ventura[71a,71b], S. Ventura Gonzalez[138], A. Verbytskyi[112],

JHEP01(2025)068

M. Verducci[75a,75b], C. Vergis[96], M. Verissimo De Araujo[84b], W. Verkerke[117], J.C. Vermeulen[117], C. Vernieri[147], M. Vessella[105], M.C. Vetterli[146,ad], A. Vgenopoulos[102], N. Viaux Maira[140f], T. Vickey[143], O.E. Vickey Boeriu[143], G.H.A. Viehhauser[129], L. Vigani[64b], M. Vigl[112], M. Villa[24b,24a], M. Villaplana Perez[166], E.M. Villhauer[53], E. Vilucchi[54], M.G. Vincter[35], A. Visibile[117], C. Vittori[37], I. Vivarelli[24b,24a], E. Voevodina[112], F. Vogel[111], J.C. Voigt[51], P. Vokac[135], Yu. Volkotrub[87b], E. Von Toerne[25], B. Vormwald[37], V. Vorobel[136], K. Vorobev[38], M. Vos[166], K. Voss[145], M. Vozak[117], L. Vozdecky[123], N. Vranjes[16], M. Vranjes Milosavljevic[16], M. Vreeswijk[117], N.K. Vu[63d,63c], R. Vuillermet[37], O. Vujinovic[102], I. Vukotic[40], I.K. Vyas[35], S. Wada[160], C. Wagner[147], J.M. Wagner[18a], W. Wagner[174], S. Wahdan[174], H. Wahlberg[92], J. Walder[137], R. Walker[111], W. Walkowiak[145], A. Wall[131], E.J. Wallin[100], T. Wamorkar[6], A.Z. Wang[139], C. Wang[102], C. Wang[11], H. Wang[18a], J. Wang[65c], P. Wang[98], R. Wang[62], R. Wang[6], S.M. Wang[152], S. Wang[63b], S. Wang[14], T. Wang[63a], W.T. Wang[81], W. Wang[14], X. Wang[114a], X. Wang[165], X. Wang[63c], Y. Wang[63d], Y. Wang[114a], Y. Wang[63a], Z. Wang[108], Z. Wang[63d,52,63c], Z. Wang[108], A. Warburton[106], R.J. Ward[21], N. Warrack[60], S. Waterhouse[97], A.T. Watson[21], H. Watson[53], M.F. Watson[21], E. Watton[60,137], G. Watts[142], B.M. Waugh[98], J.M. Webb[55], C. Weber[30], H.A. Weber[19], M.S. Weber[20], S.M. Weber[64a], C. Wei[63a], Y. Wei[55], A.R. Weidberg[129], E.J. Weik[120], J. Weingarten[50], C. Weiser[55], C.J. Wells[49], T. Wenaus[30], B. Wendland[50], T. Wengler[37], N.S. Wenke[112], N. Wermes[25], M. Wessels[64a], A.M. Wharton[93], A.S. White[62], A. White[8], M.J. White[1], D. Whiteson[162], L. Wickremasinghe[127], W. Wiedenmann[173], M. Wielers[137], C. Wiglesworth[43], D.J. Wilbern[123], H.G. Wilkens[37], J.J.H. Wilkinson[33], D.M. Williams[42], H.H. Williams[131], S. Williams[33], S. Willocq[105], B.J. Wilson[103], P.J. Windischhofer[40], F.I. Winkel[31], F. Winklmeier[126], B.T. Winter[55], J.K. Winter[103], M. Wittgen[147], M. Wobisch[99], T. Wojtkowski[61], Z. Wolffs[117], J. Wollrath[162], M.W. Wolter[88], H. Wolters[133a,133c], M.C. Wong[139], E.L. Woodward[42], S.D. Worm[49], B.K. Wosiek[88], K.W. Woźniak[88], S. Wozniewski[56], K. Wraight[60], C. Wu[21], M. Wu[114b], M. Wu[116], S.L. Wu[173], X. Wu[57], Y. Wu[63a], Z. Wu[4], J. Wuerzinger[112,ab], T.R. Wyatt[103], B.M. Wynne[53], S. Xella[43], L. Xia[114a], M. Xia[15], M. Xie[63a], S. Xin[14,114c], A. Xiong[126], J. Xiong[18a], D. Xu[14], H. Xu[63a], L. Xu[63a], R. Xu[131], T. Xu[108], Y. Xu[15], Z. Xu[53], Z. Xu[114a], B. Yabsley[151], S. Yacoob[34a], Y. Yamaguchi[85], E. Yamashita[157], H. Yamauchi[160], T. Yamazaki[18a], Y. Yamazaki[86], S. Yan[60], Z. Yan[105], H.J. Yang[63c,63d], H.T. Yang[63a], S. Yang[63a], T. Yang[65c], X. Yang[37], X. Yang[14], Y. Yang[45], Y. Yang[63a], Z. Yang[63a], W-M. Yao[18a], H. Ye[114a], H. Ye[56], J. Ye[14], S. Ye[30], X. Ye[63a], Y. Yeh[98], I. Yeletskikh[39], B. Yeo[18b], M.R. Yexley[98], T.P. Yildirim[129], P. Yin[42], K. Yorita[171], S. Younas[28b], C.J.S. Young[37], C. Young[147], C. Yu[14,114c], Y. Yu[63a], J. Yuan[14,114c], M. Yuan[108], R. Yuan[63d,63c], L. Yue[98], M. Zaazoua[63a], B. Zabinski[88], E. Zaid[53], Z.K. Zak[88], T. Zakareishvili[166], S. Zambito[57], J.A. Zamora Saa[140d,140b], J. Zang[157], D. Zanzi[55], O. Zaplatilek[135], C. Zeitnitz[174], H. Zeng[14], J.C. Zeng[165], D.T. Zenger Jr[27], O. Zenin[38], T. Ženiš[29a], S. Zenz[96], S. Zerradi[36a], D. Zerwas[67], M. Zhai[14,114c], D.F. Zhang[143], J. Zhang[63b], J. Zhang[6], K. Zhang[14,114c], L. Zhang[63a], L. Zhang[114a], P. Zhang[14,114c], R. Zhang[173], S. Zhang[108], S. Zhang[91], T. Zhang[157], X. Zhang[63c], X. Zhang[63b], Y. Zhang[63c], Y. Zhang[98],

JHEP01(2025)068

Y. Zhang[114a], Z. Zhang[18a], Z. Zhang[63b], Z. Zhang[67], H. Zhao[142], T. Zhao[63b], Y. Zhao[139], Z. Zhao[63a], Z. Zhao[63a], A. Zhemchugov[39], J. Zheng[114a], K. Zheng[165], X. Zheng[63a], Z. Zheng[147], D. Zhong[165], B. Zhou[108], H. Zhou[7], N. Zhou[63c], Y. Zhou[15], Y. Zhou[114a], Y. Zhou[7], C.G. Zhu[63b], J. Zhu[108], X. Zhu[63d], Y. Zhu[63c], Y. Zhu[63a], X. Zhuang[14], K. Zhukov[69], N.I. Zimine[39], J. Zinsser[64b], M. Ziolkowski[145], L. Živković[16], A. Zoccoli[24b,24a], K. Zoch[62], T.G. Zorbas[143], O. Zormpa[47], W. Zou[42], L. Zwalinski[37]

[1] *Department of Physics, University of Adelaide, Adelaide; Australia*
[2] *Department of Physics, University of Alberta, Edmonton AB; Canada*
[3] [(a)] *Department of Physics, Ankara University, Ankara;* [(b)] *Division of Physics, TOBB University of Economics and Technology, Ankara; Türkiye*
[4] *LAPP, Université Savoie Mont Blanc, CNRS/IN2P3, Annecy; France*
[5] *APC, Université Paris Cité, CNRS/IN2P3, Paris; France*
[6] *High Energy Physics Division, Argonne National Laboratory, Argonne IL; United States of America*
[7] *Department of Physics, University of Arizona, Tucson AZ; United States of America*
[8] *Department of Physics, University of Texas at Arlington, Arlington TX; United States of America*
[9] *Physics Department, National and Kapodistrian University of Athens, Athens; Greece*
[10] *Physics Department, National Technical University of Athens, Zografou; Greece*
[11] *Department of Physics, University of Texas at Austin, Austin TX; United States of America*
[12] *Institute of Physics, Azerbaijan Academy of Sciences, Baku; Azerbaijan*
[13] *Institut de Física d'Altes Energies (IFAE), Barcelona Institute of Science and Technology, Barcelona; Spain*
[14] *Institute of High Energy Physics, Chinese Academy of Sciences, Beijing; China*
[15] *Physics Department, Tsinghua University, Beijing; China*
[16] *Institute of Physics, University of Belgrade, Belgrade; Serbia*
[17] *Department for Physics and Technology, University of Bergen, Bergen; Norway*
[18] [(a)] *Physics Division, Lawrence Berkeley National Laboratory, Berkeley CA;* [(b)] *University of California, Berkeley CA; United States of America*
[19] *Institut für Physik, Humboldt Universität zu Berlin, Berlin; Germany*
[20] *Albert Einstein Center for Fundamental Physics and Laboratory for High Energy Physics, University of Bern, Bern; Switzerland*
[21] *School of Physics and Astronomy, University of Birmingham, Birmingham; United Kingdom*
[22] [(a)] *Department of Physics, Bogazici University, Istanbul;* [(b)] *Department of Physics Engineering, Gaziantep University, Gaziantep;* [(c)] *Department of Physics, Istanbul University, Istanbul; Türkiye*
[23] [(a)] *Facultad de Ciencias y Centro de Investigaciónes, Universidad Antonio Nariño, Bogotá;* [(b)] *Departamento de Física, Universidad Nacional de Colombia, Bogotá; Colombia*
[24] [(a)] *Dipartimento di Fisica e Astronomia A. Righi, Università di Bologna, Bologna;* [(b)] *INFN Sezione di Bologna; Italy*
[25] *Physikalisches Institut, Universität Bonn, Bonn; Germany*
[26] *Department of Physics, Boston University, Boston MA; United States of America*
[27] *Department of Physics, Brandeis University, Waltham MA; United States of America*
[28] [(a)] *Transilvania University of Brasov, Brasov;* [(b)] *Horia Hulubei National Institute of Physics and Nuclear Engineering, Bucharest;* [(c)] *Department of Physics, Alexandru Ioan Cuza University of Iasi, Iasi;* [(d)] *National Institute for Research and Development of Isotopic and Molecular Technologies, Physics Department, Cluj-Napoca;* [(e)] *National University of Science and Technology Politechnica, Bucharest;* [(f)] *West University in Timisoara, Timisoara;* [(g)] *Faculty of Physics, University of Bucharest, Bucharest; Romania*
[29] [(a)] *Faculty of Mathematics, Physics and Informatics, Comenius University, Bratislava;* [(b)] *Department of Subnuclear Physics, Institute of Experimental Physics of the Slovak Academy of Sciences, Kosice; Slovak Republic*
[30] *Physics Department, Brookhaven National Laboratory, Upton NY; United States of America*
[31] *Universidad de Buenos Aires, Facultad de Ciencias Exactas y Naturales, Departamento de Física, y CONICET, Instituto de Física de Buenos Aires (IFIBA), Buenos Aires; Argentina*

JHEP01(2025)068

[32] California State University, CA; United States of America
[33] Cavendish Laboratory, University of Cambridge, Cambridge; United Kingdom
[34] [(a)] Department of Physics, University of Cape Town, Cape Town; [(b)] iThemba Labs, Western Cape; [(c)] Department of Mechanical Engineering Science, University of Johannesburg, Johannesburg; [(d)] National Institute of Physics, University of the Philippines Diliman (Philippines); [(e)] University of South Africa, Department of Physics, Pretoria; [(f)] University of Zululand, KwaDlangezwa; [(g)] School of Physics, University of the Witwatersrand, Johannesburg; South Africa
[35] Department of Physics, Carleton University, Ottawa ON; Canada
[36] [(a)] Faculté des Sciences Ain Chock, Université Hassan II de Casablanca; [(b)] Faculté des Sciences, Université Ibn-Tofail, Kénitra; [(c)] Faculté des Sciences Semlalia, Université Cadi Ayyad, LPHEA-Marrakech; [(d)] LPMR, Faculté des Sciences, Université Mohamed Premier, Oujda; [(e)] Faculté des sciences, Université Mohammed V, Rabat; [(f)] Institute of Applied Physics, Mohammed VI Polytechnic University, Ben Guerir; Morocco
[37] CERN, Geneva; Switzerland
[38] Affiliated with an institute covered by a cooperation agreement with CERN
[39] Affiliated with an international laboratory covered by a cooperation agreement with CERN
[40] Enrico Fermi Institute, University of Chicago, Chicago IL; United States of America
[41] LPC, Université Clermont Auvergne, CNRS/IN2P3, Clermont-Ferrand; France
[42] Nevis Laboratory, Columbia University, Irvington NY; United States of America
[43] Niels Bohr Institute, University of Copenhagen, Copenhagen; Denmark
[44] [(a)] Dipartimento di Fisica, Università della Calabria, Rende; [(b)] INFN Gruppo Collegato di Cosenza, Laboratori Nazionali di Frascati; Italy
[45] Physics Department, Southern Methodist University, Dallas TX; United States of America
[46] Physics Department, University of Texas at Dallas, Richardson TX; United States of America
[47] National Centre for Scientific Research "Demokritos", Agia Paraskevi; Greece
[48] [(a)] Department of Physics, Stockholm University; [(b)] Oskar Klein Centre, Stockholm; Sweden
[49] Deutsches Elektronen-Synchrotron DESY, Hamburg and Zeuthen; Germany
[50] Fakultät Physik, Technische Universität Dortmund, Dortmund; Germany
[51] Institut für Kern- und Teilchenphysik, Technische Universität Dresden, Dresden; Germany
[52] Department of Physics, Duke University, Durham NC; United States of America
[53] SUPA - School of Physics and Astronomy, University of Edinburgh, Edinburgh; United Kingdom
[54] INFN e Laboratori Nazionali di Frascati, Frascati; Italy
[55] Physikalisches Institut, Albert-Ludwigs-Universität Freiburg, Freiburg; Germany
[56] II. Physikalisches Institut, Georg-August-Universität Göttingen, Göttingen; Germany
[57] Département de Physique Nucléaire et Corpusculaire, Université de Genève, Genève; Switzerland
[58] [(a)] Dipartimento di Fisica, Università di Genova, Genova; [(b)] INFN Sezione di Genova; Italy
[59] II. Physikalisches Institut, Justus-Liebig-Universität Giessen, Giessen; Germany
[60] SUPA — School of Physics and Astronomy, University of Glasgow, Glasgow; United Kingdom
[61] LPSC, Université Grenoble Alpes, CNRS/IN2P3, Grenoble INP, Grenoble; France
[62] Laboratory for Particle Physics and Cosmology, Harvard University, Cambridge MA; United States of America
[63] [(a)] Department of Modern Physics and State Key Laboratory of Particle Detection and Electronics, University of Science and Technology of China, Hefei; [(b)] Institute of Frontier and Interdisciplinary Science and Key Laboratory of Particle Physics and Particle Irradiation (MOE), Shandong University, Qingdao; [(c)] School of Physics and Astronomy, Shanghai Jiao Tong University, Key Laboratory for Particle Astrophysics and Cosmology (MOE), SKLPPC, Shanghai; [(d)] Tsung-Dao Lee Institute, Shanghai; [(e)] School of Physics, Zhengzhou University; China
[64] [(a)] Kirchhoff-Institut für Physik, Ruprecht-Karls-Universität Heidelberg, Heidelberg; [(b)] Physikalisches Institut, Ruprecht-Karls-Universität Heidelberg, Heidelberg; Germany
[65] [(a)] Department of Physics, Chinese University of Hong Kong, Shatin, N.T., Hong Kong; [(b)] Department of Physics, University of Hong Kong, Hong Kong; [(c)] Department of Physics and Institute for Advanced Study, Hong Kong University of Science and Technology, Clear Water Bay, Kowloon, Hong Kong; China
[66] Department of Physics, National Tsing Hua University, Hsinchu; Taiwan
[67] IJCLab, Université Paris-Saclay, CNRS/IN2P3, 91405, Orsay; France

JHEP01(2025)068

[68] Centro Nacional de Microelectrónica (IMB-CNM-CSIC), Barcelona; Spain
[69] Department of Physics, Indiana University, Bloomington IN; United States of America
[70] [(a)] INFN Gruppo Collegato di Udine, Sezione di Trieste, Udine; [(b)] ICTP, Trieste; [(c)] Dipartimento Politecnico di Ingegneria e Architettura, Università di Udine, Udine; Italy
[71] [(a)] INFN Sezione di Lecce; [(b)] Dipartimento di Matematica e Fisica, Università del Salento, Lecce; Italy
[72] [(a)] INFN Sezione di Milano; [(b)] Dipartimento di Fisica, Università di Milano, Milano; Italy
[73] [(a)] INFN Sezione di Napoli; [(b)] Dipartimento di Fisica, Università di Napoli, Napoli; Italy
[74] [(a)] INFN Sezione di Pavia; [(b)] Dipartimento di Fisica, Università di Pavia, Pavia; Italy
[75] [(a)] INFN Sezione di Pisa; [(b)] Dipartimento di Fisica E. Fermi, Università di Pisa, Pisa; Italy
[76] [(a)] INFN Sezione di Roma; [(b)] Dipartimento di Fisica, Sapienza Università di Roma, Roma; Italy
[77] [(a)] INFN Sezione di Roma Tor Vergata; [(b)] Dipartimento di Fisica, Università di Roma Tor Vergata, Roma; Italy
[78] [(a)] INFN Sezione di Roma Tre; [(b)] Dipartimento di Matematica e Fisica, Università Roma Tre, Roma; Italy
[79] [(a)] INFN-TIFPA; [(b)] Università degli Studi di Trento, Trento; Italy
[80] Universität Innsbruck, Department of Astro and Particle Physics, Innsbruck; Austria
[81] University of Iowa, Iowa City IA; United States of America
[82] Department of Physics and Astronomy, Iowa State University, Ames IA; United States of America
[83] Istinye University, Sariyer, Istanbul; Türkiye
[84] [(a)] Departamento de Engenharia Elétrica, Universidade Federal de Juiz de Fora (UFJF), Juiz de Fora; [(b)] Universidade Federal do Rio De Janeiro COPPE/EE/IF, Rio de Janeiro; [(c)] Instituto de Física, Universidade de São Paulo, São Paulo; [(d)] Rio de Janeiro State University, Rio de Janeiro; [(e)] Federal University of Bahia, Bahia; Brazil
[85] KEK, High Energy Accelerator Research Organization, Tsukuba; Japan
[86] Graduate School of Science, Kobe University, Kobe; Japan
[87] [(a)] AGH University of Krakow, Faculty of Physics and Applied Computer Science, Krakow; [(b)] Marian Smoluchowski Institute of Physics, Jagiellonian University, Krakow; Poland
[88] Institute of Nuclear Physics Polish Academy of Sciences, Krakow; Poland
[89] Faculty of Science, Kyoto University, Kyoto; Japan
[90] Research Center for Advanced Particle Physics and Department of Physics, Kyushu University, Fukuoka; Japan
[91] L2IT, Université de Toulouse, CNRS/IN2P3, UPS, Toulouse; France
[92] Instituto de Física La Plata, Universidad Nacional de La Plata and CONICET, La Plata; Argentina
[93] Physics Department, Lancaster University, Lancaster; United Kingdom
[94] Oliver Lodge Laboratory, University of Liverpool, Liverpool; United Kingdom
[95] Department of Experimental Particle Physics, Jožef Stefan Institute and Department of Physics, University of Ljubljana, Ljubljana; Slovenia
[96] School of Physics and Astronomy, Queen Mary University of London, London; United Kingdom
[97] Department of Physics, Royal Holloway University of London, Egham; United Kingdom
[98] Department of Physics and Astronomy, University College London, London; United Kingdom
[99] Louisiana Tech University, Ruston LA; United States of America
[100] Fysiska institutionen, Lunds universitet, Lund; Sweden
[101] Departamento de Física Teorica C-15 and CIAFF, Universidad Autónoma de Madrid, Madrid; Spain
[102] Institut für Physik, Universität Mainz, Mainz; Germany
[103] School of Physics and Astronomy, University of Manchester, Manchester; United Kingdom
[104] CPPM, Aix-Marseille Université, CNRS/IN2P3, Marseille; France
[105] Department of Physics, University of Massachusetts, Amherst MA; United States of America
[106] Department of Physics, McGill University, Montreal QC; Canada
[107] School of Physics, University of Melbourne, Victoria; Australia
[108] Department of Physics, University of Michigan, Ann Arbor MI; United States of America
[109] Department of Physics and Astronomy, Michigan State University, East Lansing MI; United States of America
[110] Group of Particle Physics, University of Montreal, Montreal QC; Canada
[111] Fakultät für Physik, Ludwig-Maximilians-Universität München, München; Germany

JHEP01(2025)068

[112] Max-Planck-Institut für Physik (Werner-Heisenberg-Institut), München; Germany
[113] Graduate School of Science and Kobayashi-Maskawa Institute, Nagoya University, Nagoya; Japan
[114] [(a)] Department of Physics, Nanjing University, Nanjing;[(b)] School of Science, Shenzhen Campus of Sun Yat-sen University;[(c)] University of Chinese Academy of Science (UCAS), Beijing; China
[115] Department of Physics and Astronomy, University of New Mexico, Albuquerque NM; United States of America
[116] Institute for Mathematics, Astrophysics and Particle Physics, Radboud University/Nikhef, Nijmegen; Netherlands
[117] Nikhef National Institute for Subatomic Physics and University of Amsterdam, Amsterdam; Netherlands
[118] Department of Physics, Northern Illinois University, DeKalb IL; United States of America
[119] [(a)] New York University Abu Dhabi, Abu Dhabi;[(b)] United Arab Emirates University, Al Ain; United Arab Emirates
[120] Department of Physics, New York University, New York NY; United States of America
[121] Ochanomizu University, Otsuka, Bunkyo-ku, Tokyo; Japan
[122] Ohio State University, Columbus OH; United States of America
[123] Homer L. Dodge Department of Physics and Astronomy, University of Oklahoma, Norman OK; United States of America
[124] Department of Physics, Oklahoma State University, Stillwater OK; United States of America
[125] Palacký University, Joint Laboratory of Optics, Olomouc; Czech Republic
[126] Institute for Fundamental Science, University of Oregon, Eugene, OR; United States of America
[127] Graduate School of Science, Osaka University, Osaka; Japan
[128] Department of Physics, University of Oslo, Oslo; Norway
[129] Department of Physics, Oxford University, Oxford; United Kingdom
[130] LPNHE, Sorbonne Université, Université Paris Cité, CNRS/IN2P3, Paris; France
[131] Department of Physics, University of Pennsylvania, Philadelphia PA; United States of America
[132] Department of Physics and Astronomy, University of Pittsburgh, Pittsburgh PA; United States of America
[133] [(a)] Laboratório de Instrumentação e Física Experimental de Partículas - LIP, Lisboa;[(b)] Departamento de Física, Faculdade de Ciências, Universidade de Lisboa, Lisboa;[(c)] Departamento de Física, Universidade de Coimbra, Coimbra;[(d)] Centro de Física Nuclear da Universidade de Lisboa, Lisboa;[(e)] Departamento de Física, Universidade do Minho, Braga;[(f)] Departamento de Física Teórica y del Cosmos, Universidad de Granada, Granada (Spain);[(g)] Departamento de Física, Instituto Superior Técnico, Universidade de Lisboa, Lisboa; Portugal
[134] Institute of Physics of the Czech Academy of Sciences, Prague; Czech Republic
[135] Czech Technical University in Prague, Prague; Czech Republic
[136] Charles University, Faculty of Mathematics and Physics, Prague; Czech Republic
[137] Particle Physics Department, Rutherford Appleton Laboratory, Didcot; United Kingdom
[138] IRFU, CEA, Université Paris-Saclay, Gif-sur-Yvette; France
[139] Santa Cruz Institute for Particle Physics, University of California Santa Cruz, Santa Cruz CA; United States of America
[140] [(a)] Departamento de Física, Pontificia Universidad Católica de Chile, Santiago;[(b)] Millennium Institute for Subatomic physics at high energy frontier (SAPHIR), Santiago;[(c)] Instituto de Investigación Multidisciplinario en Ciencia y Tecnología, y Departamento de Física, Universidad de La Serena;[(d)] Universidad Andres Bello, Department of Physics, Santiago;[(e)] Instituto de Alta Investigación, Universidad de Tarapacá, Arica;[(f)] Departamento de Física, Universidad Técnica Federico Santa María, Valparaíso; Chile
[141] Department of Physics, Institute of Science, Tokyo; Japan
[142] Department of Physics, University of Washington, Seattle WA; United States of America
[143] Department of Physics and Astronomy, University of Sheffield, Sheffield; United Kingdom
[144] Department of Physics, Shinshu University, Nagano; Japan
[145] Department Physik, Universität Siegen, Siegen; Germany
[146] Department of Physics, Simon Fraser University, Burnaby BC; Canada
[147] SLAC National Accelerator Laboratory, Stanford CA; United States of America
[148] Department of Physics, Royal Institute of Technology, Stockholm; Sweden

JHEP01(2025)068

[149] Departments of Physics and Astronomy, Stony Brook University, Stony Brook NY; United States of America
[150] Department of Physics and Astronomy, University of Sussex, Brighton; United Kingdom
[151] School of Physics, University of Sydney, Sydney; Australia
[152] Institute of Physics, Academia Sinica, Taipei; Taiwan
[153] [(a)] E. Andronikashvili Institute of Physics, Iv. Javakhishvili Tbilisi State University, Tbilisi;[(b)] High Energy Physics Institute, Tbilisi State University, Tbilisi;[(c)] University of Georgia, Tbilisi; Georgia
[154] Department of Physics, Technion, Israel Institute of Technology, Haifa; Israel
[155] Raymond and Beverly Sackler School of Physics and Astronomy, Tel Aviv University, Tel Aviv; Israel
[156] Department of Physics, Aristotle University of Thessaloniki, Thessaloniki; Greece
[157] International Center for Elementary Particle Physics and Department of Physics, University of Tokyo, Tokyo; Japan
[158] Department of Physics, University of Toronto, Toronto ON; Canada
[159] [(a)] TRIUMF, Vancouver BC;[(b)] Department of Physics and Astronomy, York University, Toronto ON; Canada
[160] Division of Physics and Tomonaga Center for the History of the Universe, Faculty of Pure and Applied Sciences, University of Tsukuba, Tsukuba; Japan
[161] Department of Physics and Astronomy, Tufts University, Medford MA; United States of America
[162] Department of Physics and Astronomy, University of California Irvine, Irvine CA; United States of America
[163] University of Sharjah, Sharjah; United Arab Emirates
[164] Department of Physics and Astronomy, University of Uppsala, Uppsala; Sweden
[165] Department of Physics, University of Illinois, Urbana IL; United States of America
[166] Instituto de Física Corpuscular (IFIC), Centro Mixto Universidad de Valencia - CSIC, Valencia; Spain
[167] Department of Physics, University of British Columbia, Vancouver BC; Canada
[168] Department of Physics and Astronomy, University of Victoria, Victoria BC; Canada
[169] Fakultät für Physik und Astronomie, Julius-Maximilians-Universität Würzburg, Würzburg; Germany
[170] Department of Physics, University of Warwick, Coventry; United Kingdom
[171] Waseda University, Tokyo; Japan
[172] Department of Particle Physics and Astrophysics, Weizmann Institute of Science, Rehovot; Israel
[173] Department of Physics, University of Wisconsin, Madison WI; United States of America
[174] Fakultät für Mathematik und Naturwissenschaften, Fachgruppe Physik, Bergische Universität Wuppertal, Wuppertal; Germany
[175] Department of Physics, Yale University, New Haven CT; United States of America

[a] Also Affiliated with an institute covered by a cooperation agreement with CERN
[b] Also at An-Najah National University, Nablus; Palestine
[c] Also at Borough of Manhattan Community College, City University of New York, New York NY; United States of America
[d] Also at Center for Interdisciplinary Research and Innovation (CIRI-AUTH), Thessaloniki; Greece
[e] Also at CERN, Geneva; Switzerland
[f] Also at CMD-AC UNEC Research Center, Azerbaijan State University of Economics (UNEC); Azerbaijan
[g] Also at Département de Physique Nucléaire et Corpusculaire, Université de Genève, Genève; Switzerland
[h] Also at Departament de Fisica de la Universitat Autonoma de Barcelona, Barcelona; Spain
[i] Also at Department of Financial and Management Engineering, University of the Aegean, Chios; Greece
[j] Also at Department of Physics, California State University, Sacramento; United States of America
[k] Also at Department of Physics, King's College London, London; United Kingdom
[l] Also at Department of Physics, Stanford University, Stanford CA; United States of America
[m] Also at Department of Physics, Stellenbosch University; South Africa
[n] Also at Department of Physics, University of Fribourg, Fribourg; Switzerland
[o] Also at Department of Physics, University of Thessaly; Greece
[p] Also at Department of Physics, Westmont College, Santa Barbara; United States of America
[q] Also at Faculty of Physics, Sofia University, 'St. Kliment Ohridski', Sofia; Bulgaria
[r] Also at Hellenic Open University, Patras; Greece

JHEP01(2025)068

[s] Also at Imam Mohammad Ibn Saud Islamic University; Saudi Arabia
[t] Also at Institucio Catalana de Recerca i Estudis Avancats, ICREA, Barcelona; Spain
[u] Also at Institut für Experimentalphysik, Universität Hamburg, Hamburg; Germany
[v] Also at Institute for Nuclear Research and Nuclear Energy (INRNE) of the Bulgarian Academy of Sciences, Sofia; Bulgaria
[w] Also at Institute of Applied Physics, Mohammed VI Polytechnic University, Ben Guerir; Morocco
[x] Also at Institute of Particle Physics (IPP); Canada
[y] Also at Institute of Physics, Azerbaijan Academy of Sciences, Baku; Azerbaijan
[z] Also at Institute of Theoretical Physics, Ilia State University, Tbilisi; Georgia
[aa] Also at National Institute of Physics, University of the Philippines Diliman (Philippines); Philippines
[ab] Also at Technical University of Munich, Munich; Germany
[ac] Also at The Collaborative Innovation Center of Quantum Matter (CICQM), Beijing; China
[ad] Also at TRIUMF, Vancouver BC; Canada
[ae] Also at Università di Napoli Parthenope, Napoli; Italy
[af] Also at University of Colorado Boulder, Department of Physics, Colorado; United States of America
[ag] Also at Washington College, Chestertown, MD; United States of America
[ah] Also at Yeditepe University, Physics Department, Istanbul; Türkiye
[*] Deceased

JHEP01(2025)068